N 69 27029
NASA CR 72392

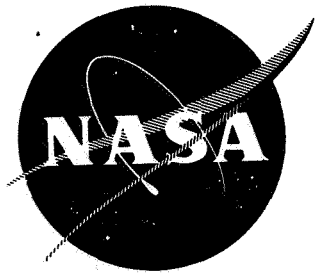

ANALYTIC DESIGN OF A 2.0 GHz SPACE BORNE LINEAR INJECTED BEAM CROSSED FIELD AMPLIFIER

by

C.L. Jones and J.E. Orr

prepared for

NATIONAL AERONAUTICS AND SPACE ADMINISTRATION

CONTRACT NAS 3-11513

LITTON INDUSTRIES
ELECTRON TUBE DIVISION

NOTICE

This report was prepared as an account of Government sponsored work. Neither the United States, nor the National Aeronautics and Space Administration (NASA), nor any person acting on behalf of NASA:

A) Makes any warranty or representation, expressed or implied, with respect to the accuracy, completeness, or usefulness of the information contained in this report, or that the use of any information, apparatus, method, or process disclosed in this report may not infringe privately owned rights; or

B) Assumes any liabilities with respect to the use of, or for damages resulting from the use of any information, apparatus, method or process disclosed in this report.

As used above, "person acting on behalf of NASA" includes any employee or contractor of NASA, or employees of such contractor, to the extent that such employee or contractor of NASA, or employee of such contractor prepares, disseminates, or provides access to, any information pursuant to his employment or contract with NASA, or his employment with such contractor.

Requests for copies of this report should be referred to

National Aeronautics and Space Administration
Office of Scientific and Technical Information
Attention: AFSS-A
Washington, D. C. 20546

NASA CR-72392

FINAL REPORT

ANALYTIC DESIGN OF A 2.0 GHz SPACE BORNE LINEAR INJECTED BEAM CROSSED FIELD AMPLIFIER

by

C. L. Jones and J. E. Orr

Prepared for

NATIONAL AERONAUTICS AND SPACE ADMINISTRATION

27 October 1968

CONTRACT NAS 3-11513

TECHNICAL MANAGEMENT
NASA LEWIS RESEARCH CENTER
CLEVELAND, OHIO
Peter Ramins

LITTON INDUSTRIES
ELECTRON TUBE DIVISION
960 INDUSTRIAL ROAD
SAN CARLOS, CALIF.

ABSTRACT

This final report describes the theoretical design of a high efficiency injected beam crossed-field amplifier suitable for space borne applications. The CFA is intended to serve as the output stage aboard a synchronous satellite which broadcasts FM television signals at a power level of 5 kw and a frequency of 2 GHz. The design emphasizes maximum overall efficiency and an expected life of at least two years.

Experimental and analytic studies were performed with variations of the Karp interaction circuit. These results were used with small-signal and large-signal computer analyses to optimize interaction efficiency for the narrow (30 MHz) bandwidth requirements of the intended application. Multi-element depressed collectors were analyzed using electron energy distributions from the large-signal interaction studies. Overall efficiencies in excess of 80% were computed for the output amplifier stage using a conventional crossed-field interaction region.

Less conventional efficiency enhancement techniques were evaluated in order to obtain even higher device ef-

ficiency. Phase focusing and negative line pre-bunching are particular techniques which should result in the attainment of amplifier efficiencies greater than 85%.

TABLE OF CONTENTS

TABLE OF CONTENTS (Continued)

FIGURES

FIGURES (CON"T)

FIGURES (CON"T)

SECTION 1
INTRODUCTION

This report describes an analytic study program to develop the theoretical design of an injected-beam crossed-field amplifier. The intended application is for a high power space borne FM television transmitter. Long life, high reliability and very high conversion efficiency are parameters of prime importance for this application.

Injected-beam crossed-field amplifiers which are currently available or in development are designed for instantaneous bandwidths of 10% to an octave or more. Airborne applications have heretofore emphasized reasonably high efficiency consistent with the requirement of power supply simplicity. As a result multi-segment collector geometries have not been considered practical in broadband amplifiers. The most common CFA collector consists of one element operated at anode potential and one element operated at cathode potential (100% depression). An internal tube connection generally provides the path for recirculating current and additional collector power supplies are not required.

This study focused on exploring new techniques and design concepts which should advance the present state of the art of the injected-beam crossed-field amplifier. The particular areas of investigation included:

1. New methods of multi-segment beam collection at depressed potentials.
2. Improved interaction efficiency with electron beam phase focusing and prebunching.
3. A study of interaction circuits in order to optimize tradeoffs between efficiency and bandwidth.

SECTION 2
PROGRAM OBJECTIVES

The prime objective of this program is to obtain an optimized analytic design of an advanced injected-beam crossed-field amplifier for use as an orbiting television transmitter. This application requires a lightweight amplifier which will operate reliably at very high overall efficiency for a period of at least two years.

2.1 DEVICE SPECIFICATIONS

The major specifications for this design include the following:

1.	CW Output Power	5000 watts
2.	Center Frequency	2000 MHz
3.	Instantaneous Bandwidth	30 MHz
4.	Modulation Type	FM
5.	Signal to Noise Ratio (Min)	32 db
	(Desired)	45 db
6.	Second Derivative Phase Response (Min)	$0.05°/MHz^2$
	(Desired)	$0.015°/MHz^2$
7.	Gain - Amplifier Chain	40 db
8.	VSWR, Input and Output	1.05
9.	Vibration	
	a) Sinusoidal (20-400 Hz)	5 g peak
	(400-3000 Hz)	15 g peak

10.	Shock (8 millisecond duration)	30 g
11.	Cooling	Radiation
12.	Life	20,000 Hrs

2.2 BACKGROUND

The injected-beam crossed-field amplifier (IBCFA) is one member of a family of high efficiency dc to microwave energy converters. Other crossed-field devices include the magnetron oscillator. M-type backward-wave oscillator, crossed-field backward-wave amplifier and distributed-emission CFA. Crossed-field devices differ from linear beam (O-type) devices in the basic mechanism of energy exchange.

A crossed-field amplifier converts potential energy directly into rf energy. Figure 1 illustrates the concept of a CFA energy box. Only a small fraction of the total beam power is represented by the electron beam velocity. Synchronous voltage is typically 5-15% of the total cathode to circuit potential for high efficiency designs. The major portion of beam energy is potential energy. Interaction of this low velocity beam with a nearly synchronous rf wave results in a net conversion of beam potential energy into rf energy of the amplified wave without any intermediate kinetic energy power transfer. Throughout the crossed-field interaction region beam kinetic energy remains nearly constant. Electrons are

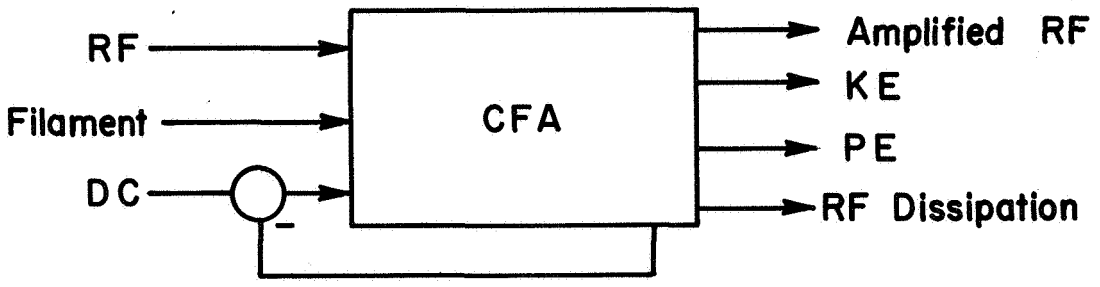

Energy Box Representation Of CFA
Fig. 1

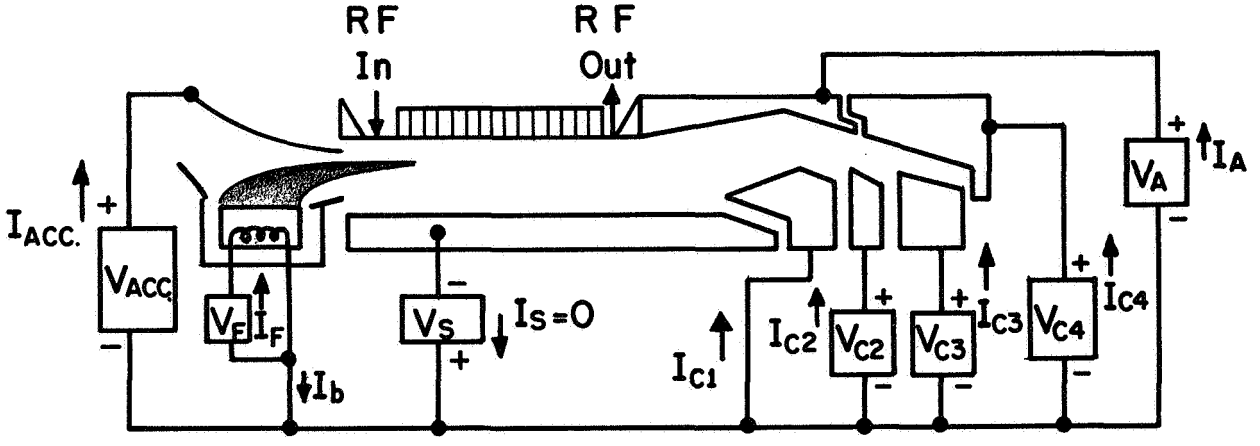

$$P_{IN} = V_A I_A + \sum_{1}^{N} V_{CN} I_{CN} + V_S I_S + V_{ACC} I_{ACC} + V_F I_F + \rho_{RF\,IN}$$

Schematic Representation Of CFA
Fig. 2

phase focused and are constrained to stay locked into synchronism with the rf wave. Fully interacted electrons are collected along the interaction circuit with only their low kinetic energy corresponding to synchronous velocity.

Figure 2 shows the schematic representation of an injected-beam crossed-field amplifier. Neither electron beam nor rf circuit is re-entrant. After a beam has traveled the length of an interaction region it is possible to recover a major portion of the remaining energy at depressed potential levels. Kinetic energy can be readily converted into potential energy in the collector region by simply reducing the ratio of dc electric to magnetic field. Energy sorting is a built-in feature of crossed-field collectors since the potential energy of each electron is a function of its position between a negative sole electrode and a positive anode.

2.3 STATEMENT OF PROBLEM AND GENERAL APPROACH

Space borne applications impose severe restrictions on the design and performance of a high power transmitter. High systems efficiency and long life are absolute requirements for a successful mission.

Crossed-field devices are well established as high efficiency sources of microwave power. Conventional crossed-field tubes have demonstrated conversion efficiencies in

excess of 70%[1]. Previous injected-beam crossed-field amplifiers have been designed for bandwidths several times the bandwidth required for a satellite television transmitter.

A tradeoff between bandwidth and efficiency exists in the design of many microwave devices. This tradeoff as it applies to a conventional injected-beam CFA was thoroughly examined throughout this program. Analytic and experimental studies were conducted to develop an optimum high impedance interaction circuit. The resultant circuit is a modified Karp structure. Electrical, thermal and mechanical design considerations were integrated into the circuit optimization study so that the final design was consistent with the objective specifications.

Recovery of a major portion of the electron beam energy with a multi-potential depressed collector was analyzed for many interim designs. Output stage efficiencies in excess of 80% were computed for the final composite design.

Other less conventional techniques for efficiency enhancement were studied. Those which require additional analytic and experimental verification are discussed in detail.

2.4 METHOD OF ANALYSIS AND COMPUTATION

Figure 3 illustrates in block form the principal steps leading to an optimized overall design of a high efficiency injected-beam crossed-field amplifier. A design study of this type necessarily involved extensive calculation of many parameters. Whenever these calculations became sufficiently involved, so that manual solutions were not practical, use was made of digital computer programs to aid in the analyses. These programs can be classified as:

1. existing programs used in original form
2. existing programs modified for the problem under consideration
3. new programs developed for a particular problem when no existing programs were available

Another classification will distinguish between two types of program processing. Batch programs are those which are processed with outside computer facilities. Timeshare programs are those which are processed with in-house facilities. The particular timeshare computer used in this study was a GE-265, coupled to a remote teletype terminal. Timeshare computation provides low-cost program de-bugging of individual portions of large batch programs or complete short programs. The timeshare system is engineer-oriented and highly interactive.

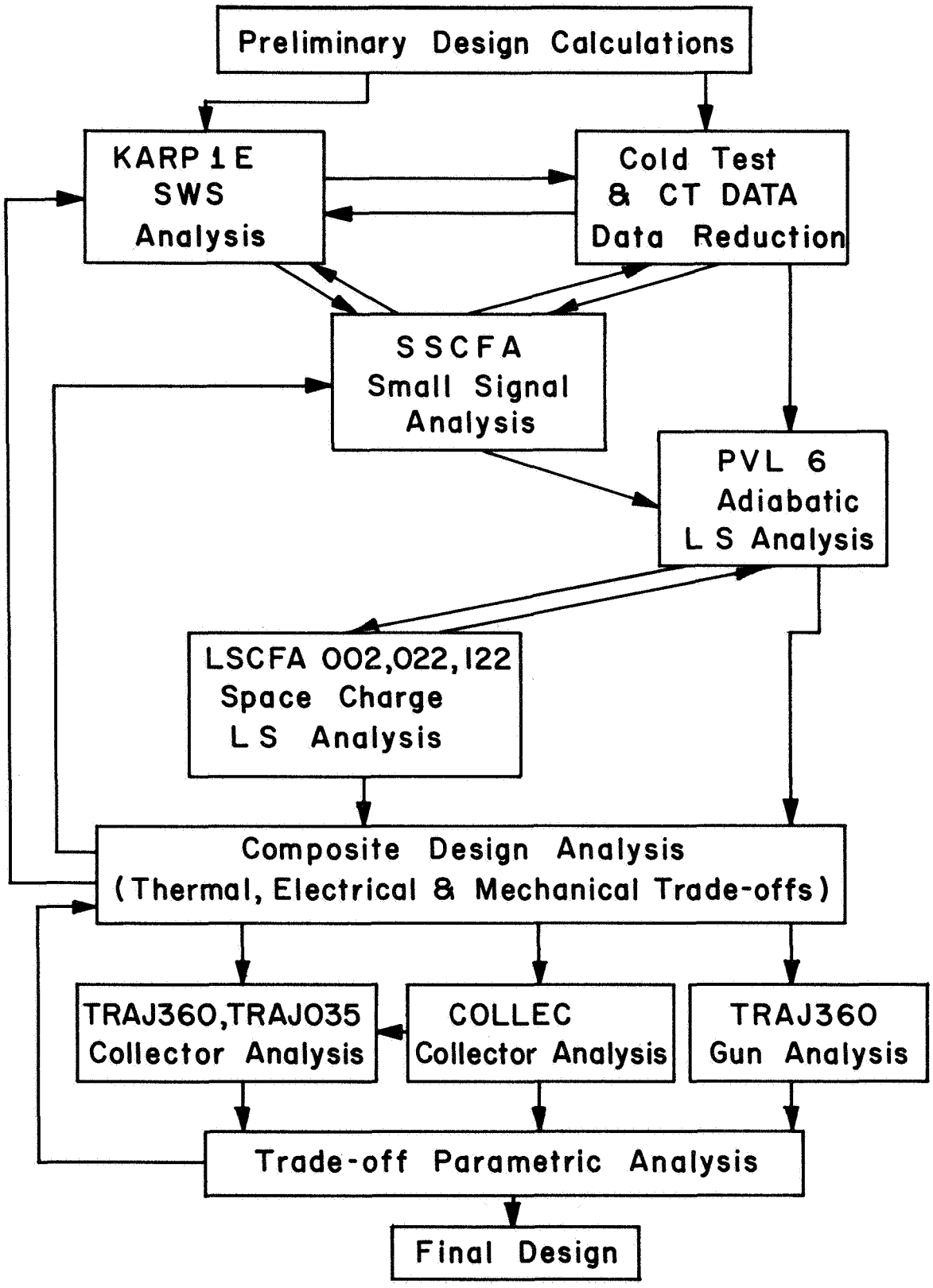

General Design Flow Diagram

Fig. 3

It eliminates much of the need for constant availability of a programmer. It also provides iterative solutions with nearly real-time output. This allows for rapid program modification without delay and useless computation when program errors exist.

Using outside facilities for batch processing one can generally use a longer program with a more complete and accurate model. For example, acceleration and space charge terms can be included in large-signal interaction programs if batch processing is used. Also long programs do not require constant monitoring by an engineer or programmer. In addition the print and plotter capabilities of batch processing are significantly greater than those of timeshare.

The following brief description of the computer programs which were used in this design study is expanded in Appendix A.

1. SSCFA - is an algebraic solution for crossed-field amplifier interaction parameters and dimensions using the notations of Gould[2] and Pierce[3]. It is useful for determining the basic electrical design tradeoffs for a wide range of design parameters.

2. KARPlE - is a slow-wave structure analysis program particularly designed for analyzing the Karp circuit. It is based upon the theory of bar lines developed by Fletcher[4], and later extended by Walling[5]. This program considers three distinct regions across the circuit and includes the effect of a sole electrode as well as the Karp structure loading geometry.

3. CTDATA - is a program used to reduce slow-wave circuit data obtained at cold test. It computes and prints such quantities as phase velocity, group velocity, phase shift, interaction impedance, etc.

The Litton large-signal interaction and electron trajectory analysis programs are discussed in greater detail in Section 3.4.

Each collector analysis requires a realistic charge and electron velocity distribution for setting-up initial conditions. The large signal space-charge interaction programs provide this information in the form of punched cards at specified interaction lengths.

SECTION 3
DETAILED DESIGN ANALYSIS

3.1 SLOW WAVE STRUCTURE CHARACTERISTICS

The electrical properties of a slow-wave structure may be characterized by three quantities:

1. Brillouin (dispersion or ω-β) diagram
2. Interaction impedance
3. Attenuation

An ω-β diagram is commonly drawn with values of frequency on the ordinate axis and phase shift per period on the abscissa. Figure 4 illustrates the general form of a Brillouin diagram for fundamental forward-wave and fundamental backward-wave circuits.

Phase velocity of a traveling wave ($v_p=\omega/\beta$) is represented by the slope of a straight line extending through the origin and a point on the ω-β curve. Group velocity ($v_g=\partial\omega/\partial\beta$) is represented by the slope of the ω-β curve at any point on the curve.

Several passbands and stopbands are shown in the figure. The frequency band from A to B represents a forward wave region of the fundamental passband of a forward-wave circuit. The ω-β diagram for a fundamental backward wave circuit shows the region C to D as the first forward-wave space harmonic. Either region is suitable for forward-wave interaction between an electron beam and an rf wave in a traveling wave amplifier (TWA).

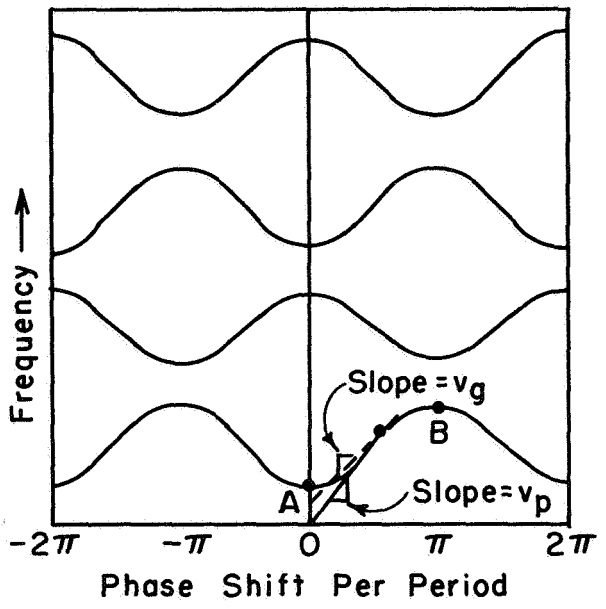

General ω-β Diagram For Fundamental Forward-Wave Interaction Circuit.

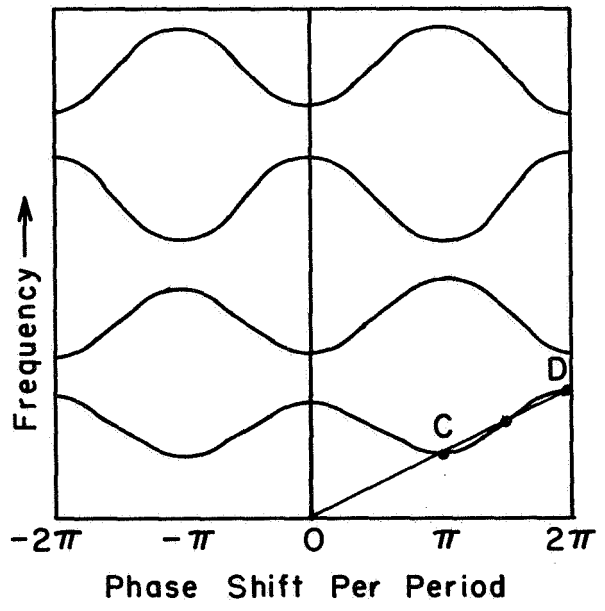

General ω-β Diagram For Fundamental Backward-Wave Interaction Circuit.

Fig. 4

The ω-β diagram also provides information related to the potential amplification bandwidth of a circuit. Dispersion ($d=\partial v_p/\partial\omega$) defines the frequency range over which an electron beam and a traveling wave remains in near synchronism. The bandwidth of a particular amplifier design also depends upon large signal interaction parameters, nevertheless the dispersion curve is useful for evaluating each slow-wave structure.

Interaction impedance is defined by:

$$Z_i = \frac{E^2}{2\beta^2 P} \qquad (3\text{-}1)$$

where E is the magnitude of the rf electric field component which interacts with the electron beam, β is the circuit phase shift and P is the total power flow in the circuit. Z_i defines the degree of coupling between beam and wave. High interaction impedance is desired for high gain per unit length. This implies shorter interaction length for a given gain requirement, hence less circuit loss and higher efficiency.

Circuit attenuation is a complex function of circuit geometry, frequency and mode(s) of propagation. Low attenuation per cell, α_c, also results in higher gain per unit length, consequently lower circuit loss and higher device efficiency. These concepts, as well as impedance-dispersion-attenuation tradeoffs are discussed in greater detail in Section 3.4.

3.2 SLOW-WAVE STRUCTURE TYPES

Any attempt to classify the large number of existing and proposed interaction circuits will result in an arbitrary tabulation. Many circuits can shift from one classification into another by simple geometric modification.

Interaction circuits suitable for use in a forward-wave crossed-field traveling wave amplifier may be classified as:

1. Fundamental backward-wave circuits designed for operation in the first space harmonic mode.
2. Fundamental forward-wave circuits designed for operation in the fundamental mode.
   a. Helix derived circuits
   b. Periodically loaded transmission lines

3.2.1 Fundamental Backward-Wave Circuits

Many microwave amplifiers and oscillators use fundamental backward-wave interaction circuits. For backward-wave interaction in either O or M type devices the phase velocity and group velocity are oppositely directed. Interaction is generally with the fundamental backward-wave symmetric mode, as in an M-BWO with an inter-digital line.

Forward-wave interaction occurs when beam velocity is approximately equal to the phase velocity of one of the forward-wave space harmonics propagating on the slow-wave structure. The split-folded waveguide circuit (SFWG) is a useful high power delay line. CFA's frequently use this circuit for bandwidths less than 40%, particularly at frequencies above C band.

A backward-wave circuit is generally two to three times the size of a forward wave circuit with equivalent phase velocity. Interaction impedance at the circuit plane (K_o) is lower than for a similar forward-wave circuit since space-harmonic operation implies values of phase shift per period (βp) greater than π. Another factor which reduces the effective interaction impedance (Z_i) at the electron beam position is the exponential decay in rf field strength proportional to $e^{\beta x}$. Typical values of K_o are 5 to 20 ohms for useful SFWG circuits. Since high interaction efficiency requires high interaction impedance, fundamental backward-wave circuits are not compatible with the requirements of this design study.

3.2.2 Circuits Derived from the Simple Helix

The first delay line used in an injected-beam CFA was a rectangular helix[6]. The simple helix is an excellent interaction circuit for broad bandwidth applications. Linear beam traveling wave tubes (O-TWT) have used this cir-

cuit successfully for several years in low power devices, and its electrical characteristics are well understood. Recent advances in materials technology have improved the helix thermal capability. Average power output in excess of 1 KW has been demonstrated in an X-band TWT[7] and in a broadband CFA[8]. In each device a helix was brazed to high thermal conductivity beryllium oxide supports.

A practical crossed-field electron beam is in the form of a ribbon of finite thickness. For this reason a rectangular helix is generally used in broadband CFA's below C-band. One or more planar faces of the helix, in conjunction with a sole electrode, are used to establish the static dc electric field. Interaction takes place with rf fields outside the helix perimeter rather than with internal fields as in the O-TWT.

In a conventional crossed-field tube the beam width is limited to the length of a single face of the total helix peripheral length. Figure 5 shows typical ω-β curves for a rectangular helix supported and unsupported. The free-space helix exhibits π phase shift per turn when the peripheral length is approximately one-half wavelength ($l_\pi = \lambda/2$) at the π mode frequency. As the helix thermal capability is increased (i.e., smaller loading factor, F) length is decreased for a fixed value of frequency.

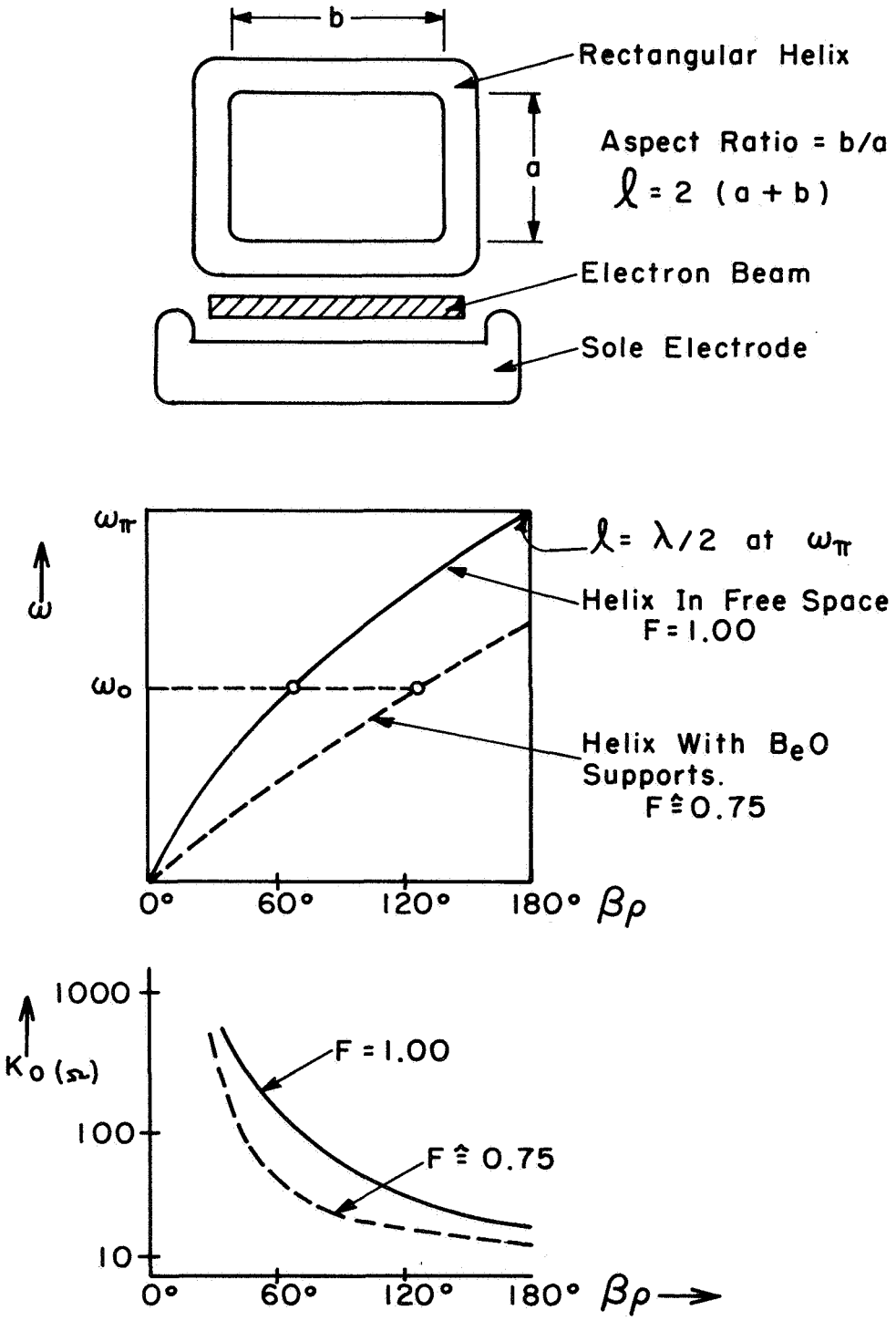

Electrical Characteristics Of Rectangular Helix.
Fig. 5

Interaction impedance at the helix beam face, K_o, increases for lower values of phase shift and decreases with increasing thermal capability. A high impedance SWS results in higher interaction impedance, hence a typical design is limited to $\beta p \leq 60°$. This corresponds to a maximum helix perimeter of approximately F * ($\lambda/6$).

Thermal and electrical requirements impose limits on the helix aspect ratio. Values ranging from 1 to 5 appear to be feasible. Maximum beam width varies from $F\lambda/24$ to $F\lambda/14$. This corresponds to a width of 6.3 to 10.3 mm at a frequency of 2 GHz for an unsupported helix. This width is reduced to 4.7 to 7.7 mm for a thermally adequate helix with F = 0.75.

The relationship between beam width, cathode loading and other design parameter trade-offs is discussed in greater detail in Section 3.4. For the present discussion one must conclude that a simple rectangular helix provides a limited interaction width which constrains the optimization of other design parameters.

3.2.3 Modified Helix Circuits

This general category includes many slow-wave structures. Those which are currently used in crossed-field devices include the helix coupled vane circuit (HCV), the stub supported helix (SSH) and the helix coupled bar line (HCBL).

Bandwidths of the available circuits range from 10% to greater than an octave. A tradeoff of bandwidth for impedance is possible with the modified helix circuits, particularly for low values of phase shift. Figures 6 and 7 illustrate analytic and experimental results of several modified helix circuits which were obtained on a previous contract.[9] Since interaction impedance generally decreases for high values of phase shift a high impedance circuit is relatively narrow. This characteristic limits the available interaction width in a conventional, single beam crossed-field device. Attempts to optimize interaction efficiency for those modified helix circuits which were studied indicated the desirability of a wider interaction region with high impedance at high values of phase shift.

3.2.4 Periodically-Loaded Transmission Lines

Included in this classification of interaction circuits are coaxial lines, strip lines, planar conductors and waveguide. Each transmission line can become a useful slow-wave structure by periodic loading with stubs, vanes, slots or fins.

Two variations of the loaded coaxial line are shown in figure 8. Included in the figure are experimental ω-β and interaction impedance curves for several variations of the familiar disc-loaded rod circuit (DLR)[9]. Structure

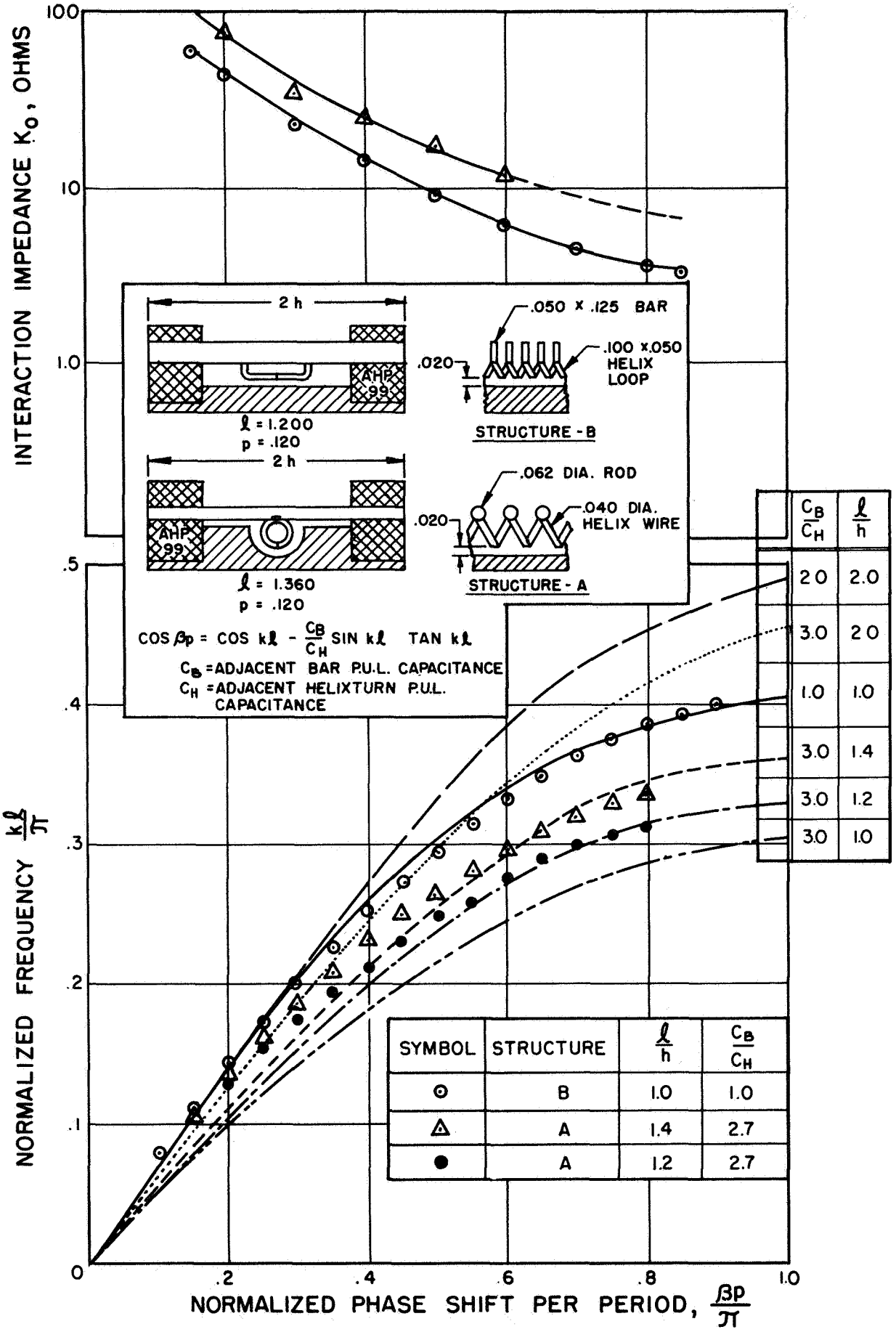

DISPERSION AND INTERACTION IMPEDANCE OF VARIOUS HELIX-COUPLED BAR LINES

Fig. 6

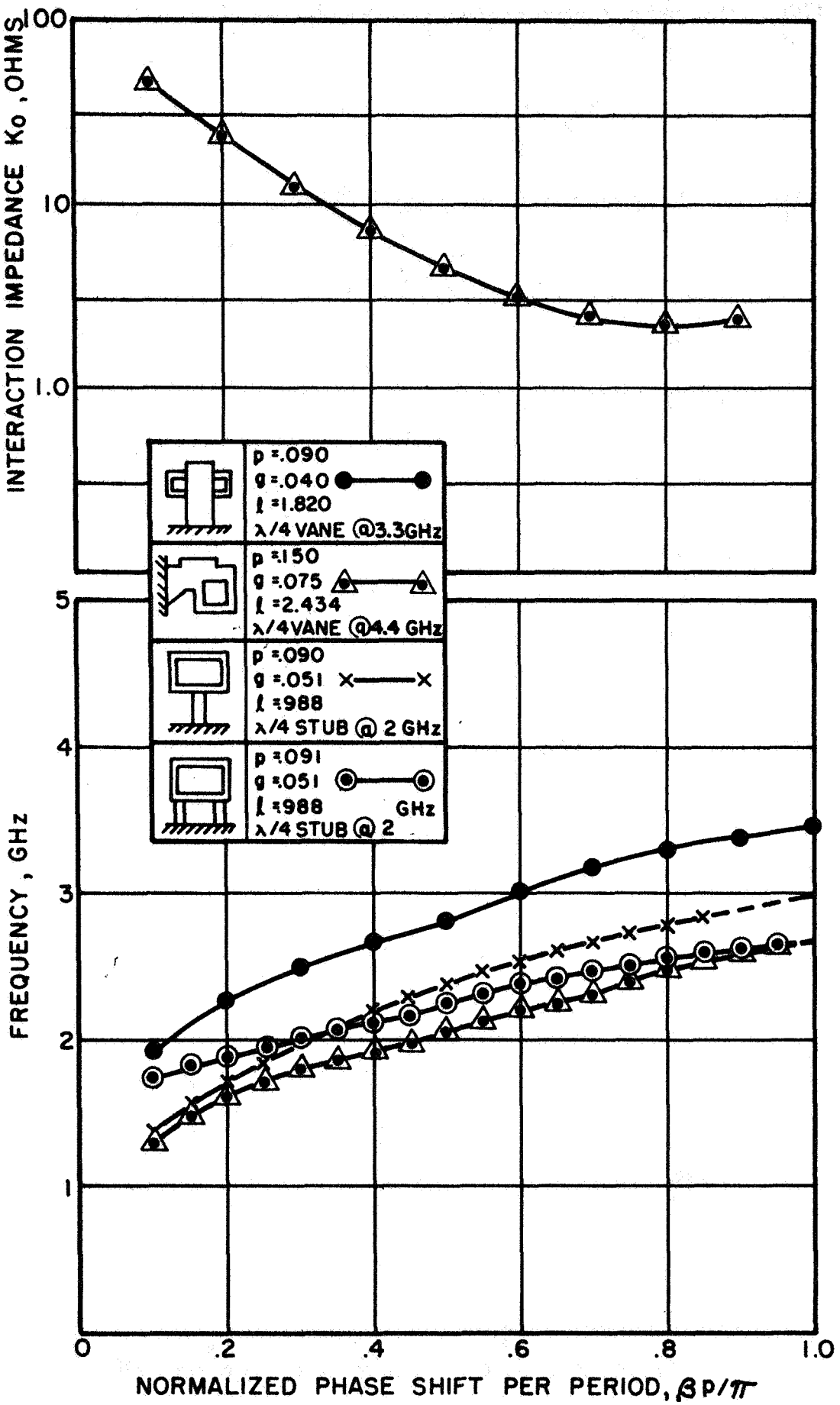

DISPERSION AND INTERACTION IMPEDANCE OF VARIOUS RECTANGULAR HELICES WITH VANE AND STUB SUPPORTS

Fig. 7

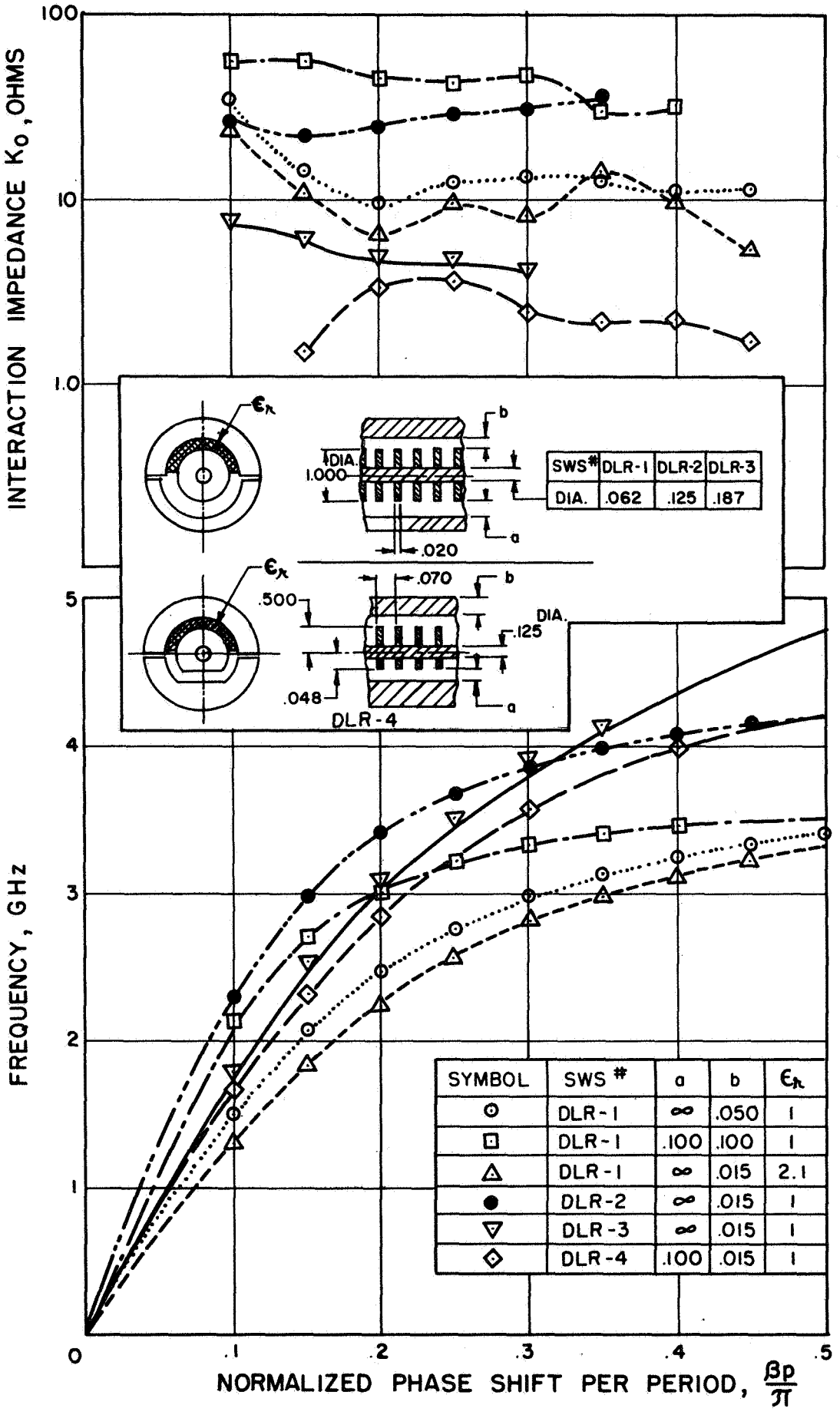

DISPERSION AND INTERACTION IMPEDANCE OF VARIOUS DISC-LOADED-ROD SLOW-WAVE STRUCTURES

Fig. 8

DLR-4 is particularly interesting for crossed-field applications since it provides a planar beam face opposite the sole electrode. Other variations are more suitable for hollow beam TWT circuits when dielectric loading materials are moved from the location shown to the area between adjacent discs.

Reasonably high impedance can be maintained at high values of phase shift, primarily because of decreasing group velocity (additional stored energy) at high frequencies. Dispersion and bandwidth are directly related to group velocity deviation. The obvious impedance-bandwidth tradeoff is characteristic of periodically-loaded transmission lines.

The loaded strip line includes the comb line commonly used in masers, and the meander line used in many microwave devices including broadband crossed-field amplifiers. The experimental data in figure 9 show typical electrical characteristics of two practical meander lines.[9] Bandwidth can be varied from a few per cent to more than an octave by modifying certain structure and ground plane dimensions. In general the thermal capability of this circuit increases as bandwidth and impedance decrease. Energy storage in a dielectric support medium tends to reduce the useful interaction impedance, particularly in a high power structure.

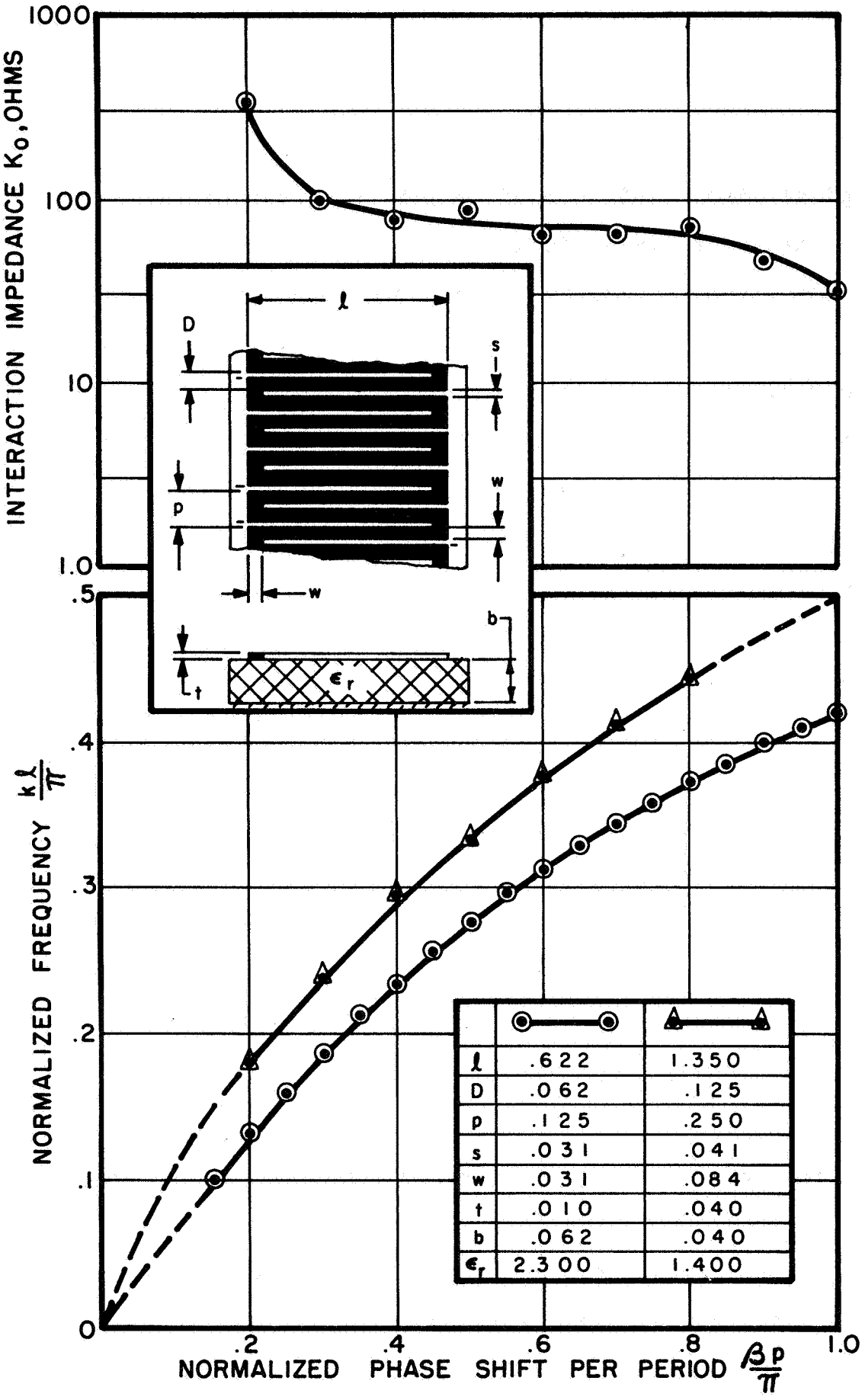

DISPERSION AND INTERACTION IMPEDANCE OF TWO MEANDER LINES SUPPORTED BY DIELECTRIC.

Fig. 9

Another common strip line circuit is the interdigital line. This circuit exhibits a fundamental backward-wave symmetric mode, and is currently used in most M-BWO's. Many attempts have been made to use this circuit for space harmonic forward-wave operation. However, the unperturbed circuit propagates an antisymmetric forward mode with zero electric field along the center of each bar. Misregister, offset bars and other multi-periodic techniques have been used to suppress this undesirable mode. Interaction impedance for space harmonic operation is considerably lower than for other fundamental forward-wave slow-wave structure.

Loaded waveguide interaction circuits can be designed to have high power capability and exhibit high impedance for values of phase shift per period greater than 100°c. Three slow-wave structures which belong to this group are the Karp [10,11] circuit, the Feinstein[12] circuit and the Millman[13] circuit.

The Karp circuit is a ridged waveguide coupled to a ladder circuit which forms one broad waveguide wall. The Feinstein circuit is also a ridged waveguide, but the ladder circuit is replaced by a vane circuit with coupling through a series of slots. The simplest of the loaded waveguide structures, the Millman circuit, consists of a serrated ridge in the waveguide.

Loaded-waveguide circuits offer a definite advantage in structure width. With minimal loading each structure propagates a single frequency which has a wavelength equal to twice the circuit width. Useful structures, when loaded to obtain the desired passband, retain a circuit width of nearly $\lambda/2$. Early interest in these circuits was to utilize the relatively large dimensions to minimize the fabrication problems associated with millimeter tubes. Each circuit was originally used with a ribbon electron beam, although subsequent modifications resulted in circuits which were also suitable for solid or hollow O-type beams.[14]

This general circuit evaluation phase resulted in a decision to expand existing knowledge of periodically-loaded transmission lines. The Karp circuit, in particular, appeared to offer the greatest potential for design optimization of a higher power, high efficiency amplifier.

3.3 ANALYTIC AND EXPERIMENTAL OPTIMIZATION OF A KARP CIRCUIT

In the simplest form the Karp circuit consists of a ridged rectangular waveguide whose broad wall contains an array of transverse slots (figure 10a). Without ridge loading a slotted array or ladder line acts as a zero-passband circuit. Each slot is a half-wave aperture with

π phase shift between adjacent slots at the resonant frequency. Ridge loading in the center of a structure adds shunt capacitance to unbalance the resonant inductive and capacitive susceptances.

Figure 10b illustrates an approximate equivalent circuit which neglects coupling between slots. Capacitive loading due to the ridge creates a fundamental forward-wave circuit which propagates a delayed rf wave in a frequency band which is above the cutoff frequency of the unperturbed ridged waveguide and below the slot resonant frequency.

Coupling between adjacent slots can be included in the equivalent circuit analysis by adding elements. However the resulting ladder network becomes quite complicated.

An alternate analytical approach was applied to the Karp circuit with excellent results. The method was originally studied by Fletcher[4] and later extended by Walling[5]. Circuit properties are determined by considering an array of parallel conductors which support one or more TEM waves propagating in the direction of the conductors. Details of the analysis and a digital computer program developed around the analysis are contained in Appendix A.

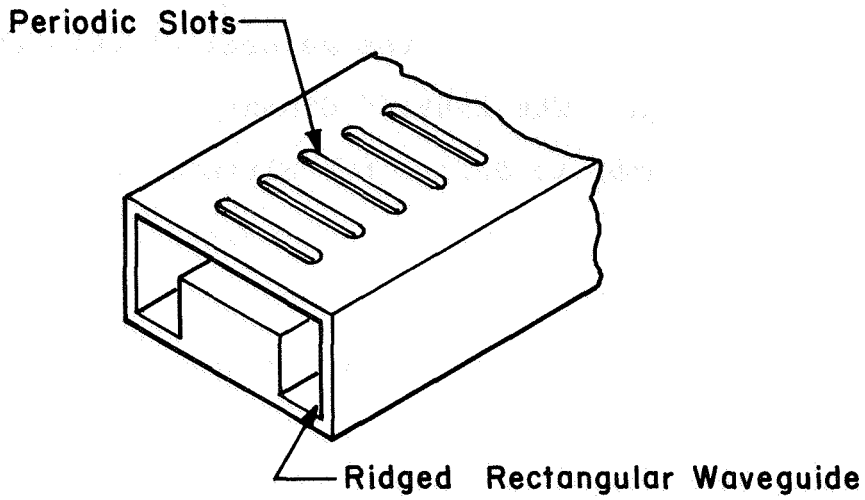

(a) General Form

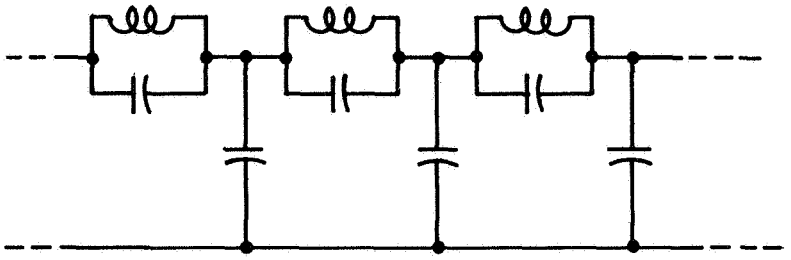

(b) Approximate Equivalent Circuit
For Widely Separated Slots.

General Form And Equivalent Circuit Of Karp Slow-Wave Structure.

Fig. 10

Figure 11 is a sketch of the general circuit type under consideration. The labeled dimensions are used in subsequent figures to define the circuit variations which were studied. Preliminary electrical design calculations indicated the importance of accurate dispersion and impedance data. Cold test structures were fabricated to obtain these measured values, and to determine the limits of the analytic circuit model.

As the composite thermal, electrical and mechanical design was optimized it was necessary to return to the analytic circuit model. Circuit design calculations were performed to avoid fabricating a large number of slow-wave structures. New circuits were fabricated only when the desired circuit quantities deviated significantly from the established limits of the model, or when accurate attenuation data were required.

A total of twelve bar lines and two ground plane-sole assemblies were fabricated. Eleven cold test structures were designed with the slot resonant frequency in low S band. One larger circuit was designed with a slot resonant frequency in L band. S band circuits were chosen to minimize fabrication and measurement problems, and because very little scaling would be required for the final design at 2GHz. The L band circuit was used to study field distribution and mode configuration in the fundamental and higher passbands. Most of the cold test circuits contained ten periodic cells, an

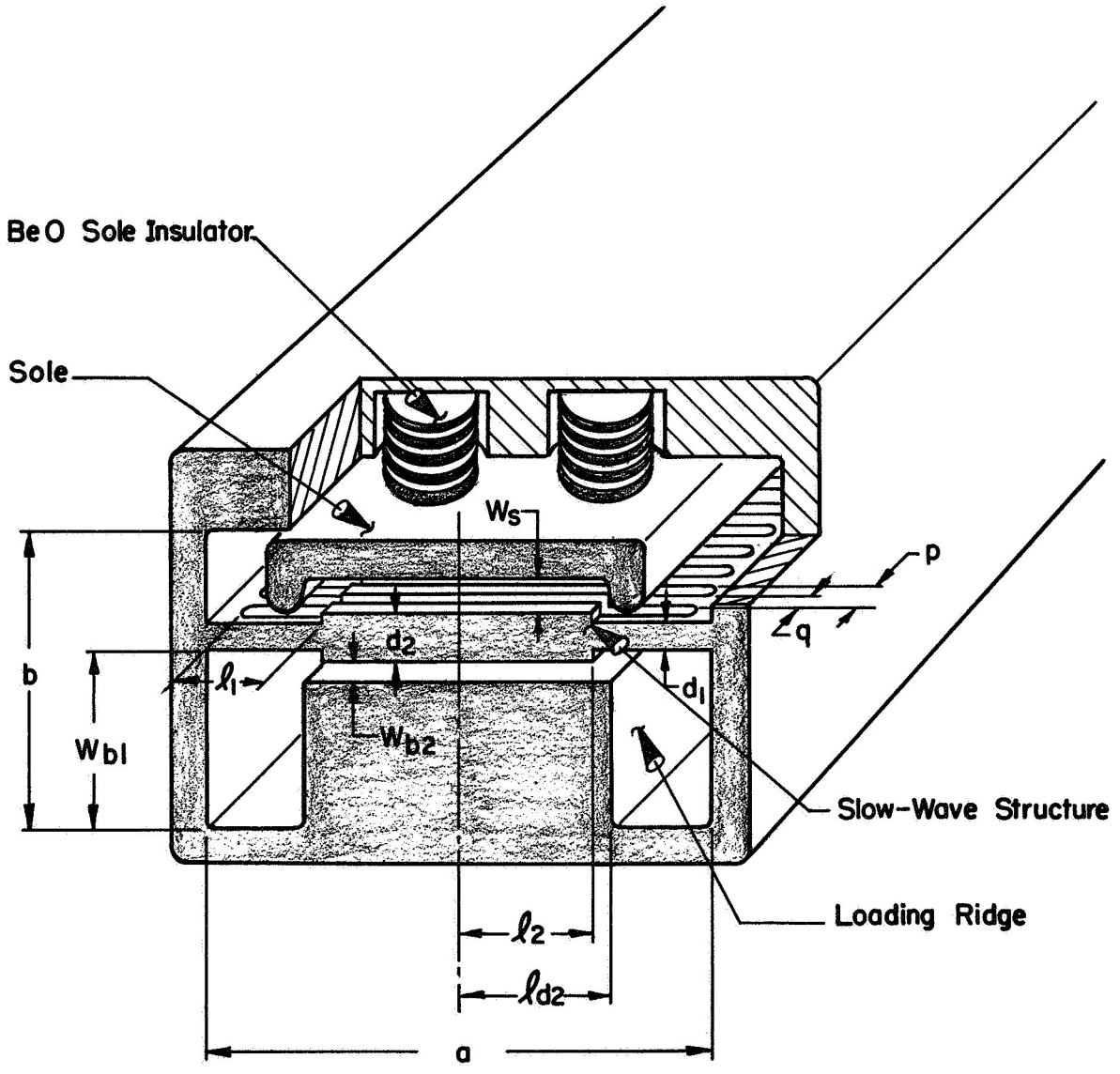

$$l = l_1 + l_2$$

Sketch of A Karp Circuit With Body, Sole Assembly And Ground Planes

Fig. 11

ideal number for measuring phase and impedance. Two circuits containing 24 and 30 cells were used to obtain more accurate circuit attenuation data.

Figure 12 shows the electrical characteristics of four representative cold test structures. Certain dimensions were varied in a systematic manner with those circuits which were of particular interest to this design. Independent variables included:

p	circuit pitch
q/p	gap to pitch ratio
d_1	bar thickness outside the interaction region
d_2	bar thickness in the interaction region
w_{b2}	ridge to bar spacing
l_2/l	ratio of interaction width to total bar length

The most obvious characteristic of the Karp circuit is high impedance with large phase shift. The trade-off between interaction impedance and bandwidth is controlled by the energy stored per unit length, W_s

$$v_g = P/W_s \qquad (3\text{-}2)$$

where P is the total power propagating on the circuit, and v_g is the group or energy velocity of the wave. The qualitative tradeoffs in the region of interest for this design are illustrated in figure 13. With each dimension

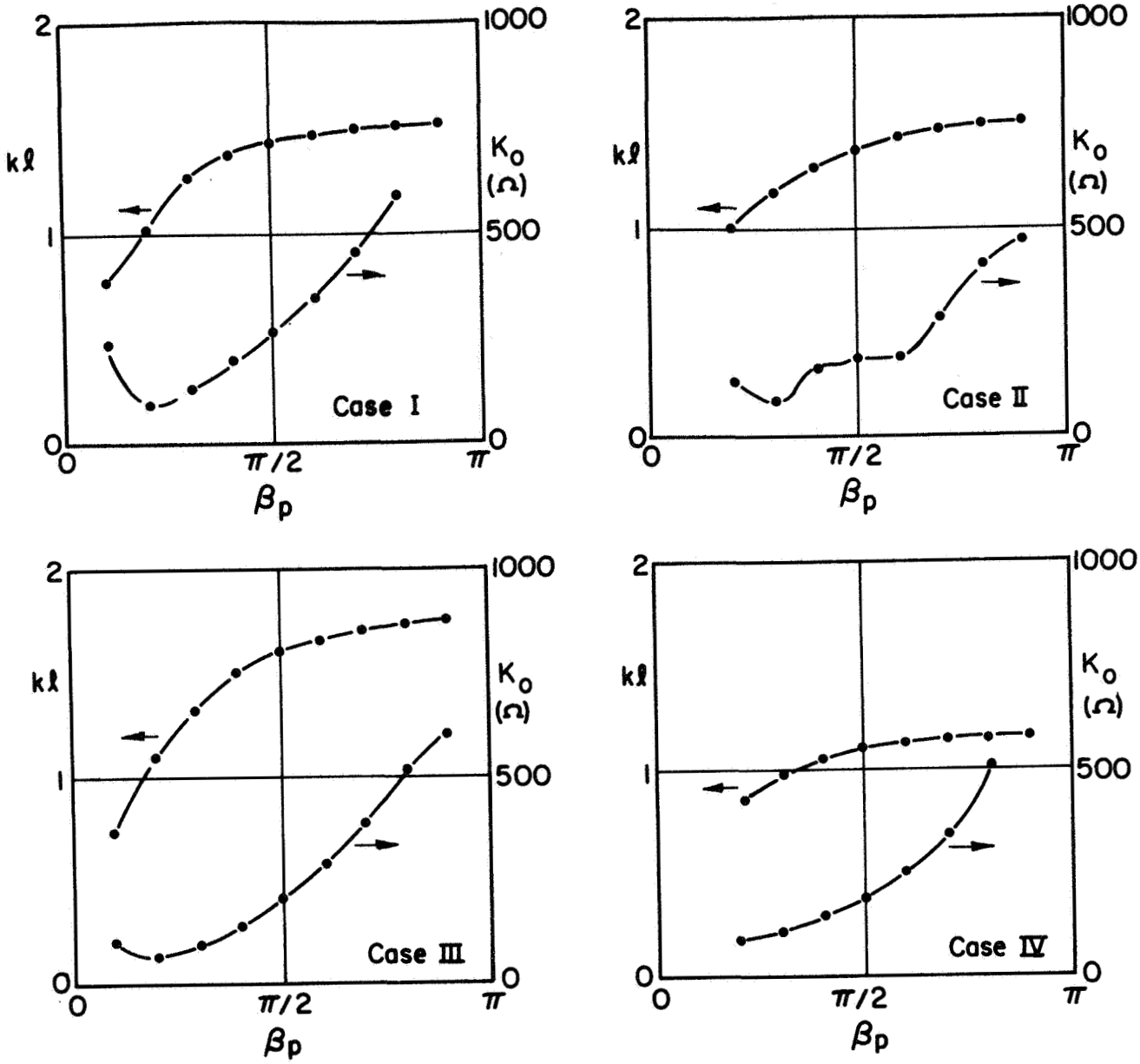

Case	SWS	p	q	d_1	d_2	ℓ_1	ℓ_2	ℓ_{d2}	wb1	wb2	ws
I	K5	.125	.062	.062	.062	.458	.852	.852	1.340	.040	.125
II	K1	.300	.156	.256	.256	.458	.852	.852	1.340	.060	.300
III	K11	.300	.156	.256	.080	.760	.550	.852	1.340	.040	—
IV	K10	.300	.156	.256	.375	.760	.550	.852	1.340	.040	.300

Experimental Dispersion And Interaction Impedance For Circuits With Dimensions As Specified In Fig.-11

Fig. 12

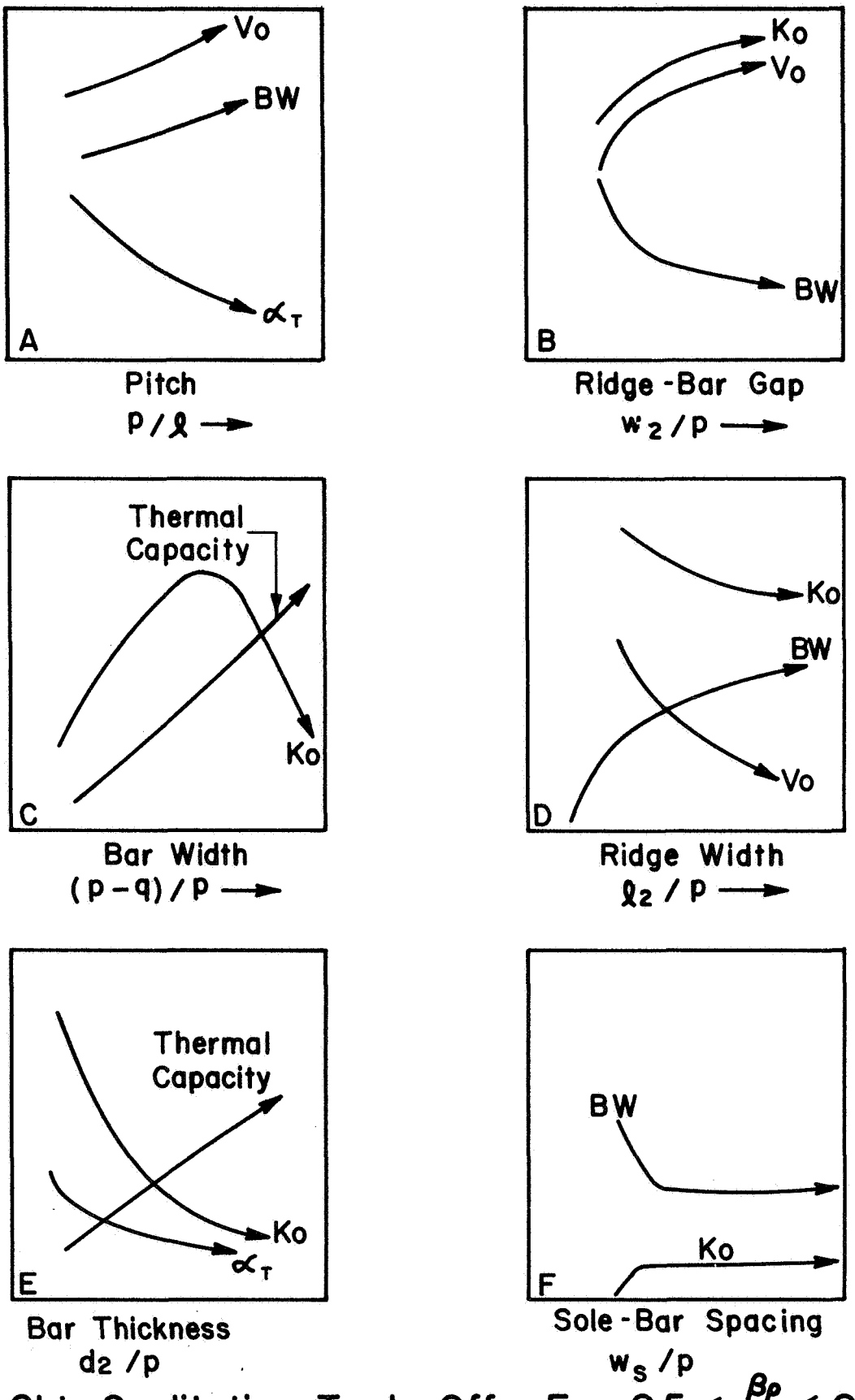

Karp Ckt Qualitative Trade Offs For $0.5 \leqslant \frac{\beta p}{\pi} \leqslant 0.8$

Fig. 13

normalized to the circuit pitch, and for $0.5 \leq \beta p/\pi$ 0.8:

A. Beam velocity voltage and bandwidth increase with pitch while the total circuit attenuation decreases.

B. Interaction impedance and beam velocity increase as the ridge loading is decreased. Maximum bandwidth and lowest impedance result from heavy loading.

C. Bars which are wide in the direction of propagation result in high thermal capacity. Maximum impedance is obtained for bar and gap widths approximately equal.

D. Width of the loading ridge controls the stored energy per unit length. Heavy loading corresponds to low beam velocity and low impedance with increased bandwidth.

E. A thick bar has high thermal capacity. Impedance and total circuit attenuation decrease with increasing bar thickness.

F. A sole electrode does not affect impedance or bandwidth except when the sole-circuit gap is considerably less than the circuit pitch.

The significant of circuit attenuation is discussed in conjunction with large signal efficiency optimization. Attenuation of many slow-wave circuits - including the Karp circuit - is a quantity which is difficult to determine analytically. Cold test measurements were performed with two circuits and various loading geometries to determine the tradeoffs between attenuation, bandwidth and impedance. Circuits with 24 and 30 cells were used for these tests in order to improve measurement accuracy.

Figure 14 shows the dispersion and attenuation characteristics for circuit K-5-24 with the loading dimensions noted. Attenuation per cell is approximately 0.03 db except for the region near the slot resonant frequency where loss increases. Experiments were conducted to determine if the attenuation of the copper circuits could be reduced. Photomicrographs were obtained for two circuits in the as-machined condition. Attenuation data and photomicrographs were obtained after each of several stages of electropolishing. No significant change in attenuation was observed during any of these experiments although the total material removed was nearly 2% of the original.

Another important circuit parameter which is not treated adequately in the literature is transverse variation of interaction impedance. A conventional bar line with minimal ridge loading exhibits a sin (x) electric field distribution where x varies from 0 to π. (Figure 15a) The resulting impedance

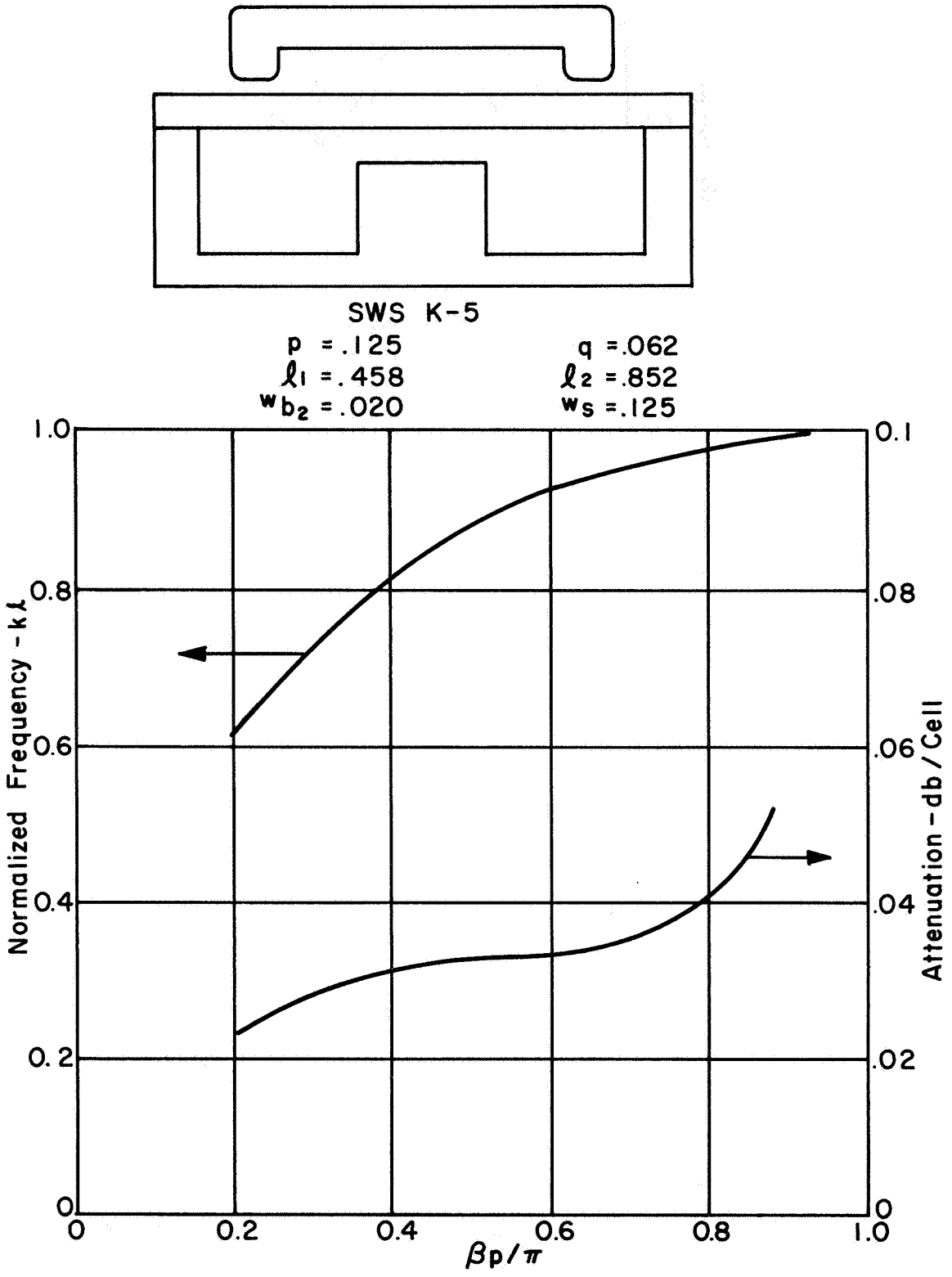

Dispersion And Attenuation Characteristics Of SWS K-5 With 24 Cells.

Fig. 14

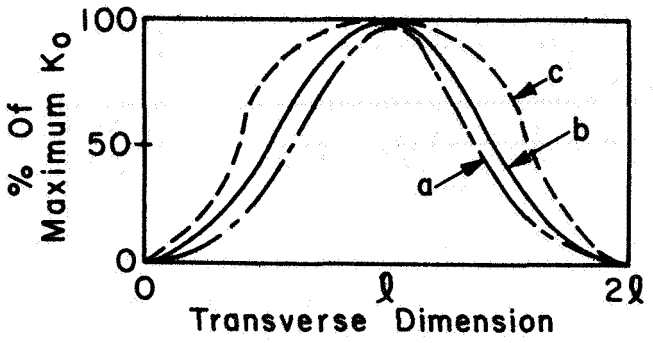

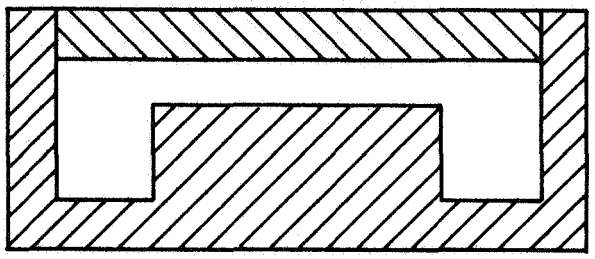

a. Conventional Bar And Ridge

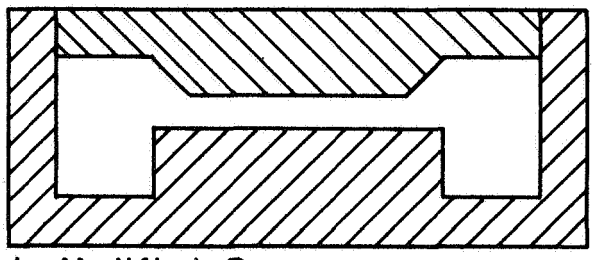

b. Modified Bar

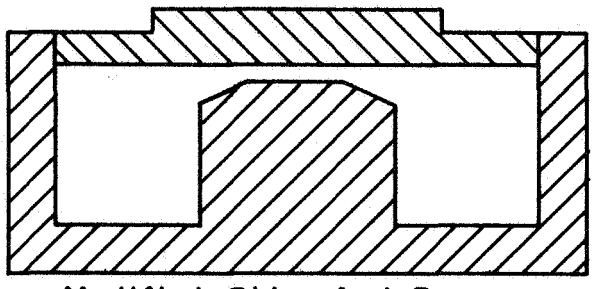

c. Modified Ridge And Bar

Karp Circuit Modifications To Reduce Transverse Impedance Variation

Fig. 15

varies as $\sin^2(x)$.

Experiments were performed with three Karp circuits to determine optimum bar and ridge geometries which minimize the transverse impedance variation. Analytic impedance values were generally 20-30% higher than measured values. Cold test impedance data were obtained by perturbing rf electric fields with dielectric slabs (Appendix B) as wide as the anticipated electron beam. These values represented the average interaction impedance whereas the analytic results considered impedance only at the center of the bars. Narrow strips and small diameter dielectric rods were used for measuring local impedance at various points across the circuits. From these data the transverse impedance variation for each circuit configuration was established.

The bar and ridge geometry shown in Figure 15c resulted in an impedance variation of less than 25% across a useful beam width of one inch. Several bar and ridge combinations were found to give similar results. In each case the loading was greatest at the center of the bars.

One practical variation of the planar Karp circuit is shown in Figure 16. Folding the low impedance portion of the bars into a ground plane provides a narrower magnet gap while retaining the full useful beam width.

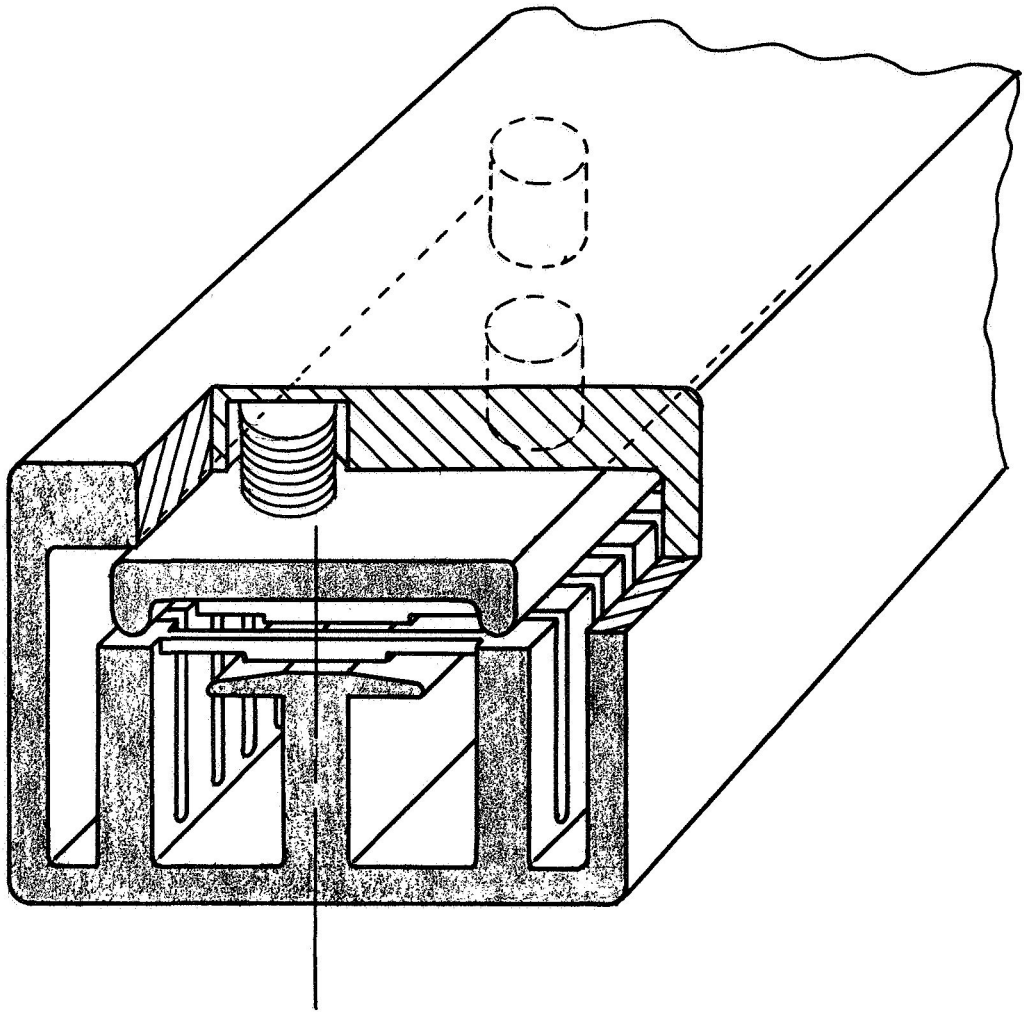

Modified "T" Bar Folded Karp Circuit

Fig. 16

Two variations of this structure were studied at cold test. Dispersion and impedance characteristics of the folded Karp circuits were similar to those obtained with planar structures except that the electrical bar length was reduced by approximately 10% in the folded geometry. The T shaped ridge reduces the degree of loading near the bar ends. With a greater ridge to bar separation the bar cross section can be more massive for a given impedance, hence the bar center can operate at a lower temperature for a given power dissipation.

3.4 RF-BEAM INTERACTION

The theoretical maximum efficiency of injected-beam crossed-field amplifiers is very high because of the nature of crossed-field interaction. Instead of converting potential energy of the power supply to kinetic energy and then in turn converting the kinetic energy of the beam into useful rf energy, the crossed-field amplifier beam is injected into the interaction space with a relatively low velocity (kinetic energy) but with relatively high potential energy. It is the potential rather than kinetic energy of the beam which is then converted directly into rf energy.

In crossed electric and magnetic fields, electrons have an average drift velocity given by

$$v = \frac{E}{B} , \qquad (3\text{-}3)$$

where E is the dc electric field and B is the transverse magnetic field.

Consequently, when an electron is collected on a slow-wave structure, kinetic energy is converted into heat. If all non-cycloiding electrons are collected on the slow-wave circuit, the total power dissipated by the beam in the circuit is

$$P_{diss} = V_o I_b \quad , \qquad (3\text{-}4)$$

where V_o is the beam kinetic energy potential and I_b is the beam current. Thus, the maximum electronic efficiency for a thin non-cycloiding beam of electrons is given by

$$\eta_e(max) = 1 - \frac{V_o}{V_k} \quad , \qquad (3\text{-}5)$$

where V_k is the cathode-to-circuit voltage. It is feasible to design a crossed-field amplifier with electronic efficiency greater than 90 percent at S-band. In any practical crossed-field amplifier there are several factors which limit overall efficiency to a value less than the theoretical electronic efficiency.

The most obvious factor which reduces crossed-field amplifier efficiency below the ideal is rf circuit loss. Another very important consideration is the difficulty in building a crossed-field amplifier which duplicates the ideal model assumed in the calculation of electronic efficiency. Finally and perhaps most important, is the very

nature of crossed-field interaction, which makes it impractical to operate an injected-beam CFA so that all electrons undergo complete interaction and are collected on the slow-wave circuit. In a conventional crossed-field amplifier it is advantageous to recover the kinetic and potential energy of the spent beam on a multi-element depressed collector.

The following section explains in detail the above observations.

The overall or total efficiency of a crossed-field amplifier may be written as

$$\eta_o = \eta_e \, \eta_c \quad , \qquad (3\text{-}6)$$

where η_e is the actual electronic efficiency and η_c is the circuit efficiency. The maximum electronic efficiency is only obtained if the crossed-field amplifier is operated so that all of the beam is collected on the slow-wave circuit. Due to the formation of a secondary electron bunch which undergoes unfavorable interaction and moves closer to the sole, it is impractical to operate an injected-beam crossed-field amplifier so that 100 percent of the electrons are collected on the circuit. For any practical case with finite circuit attenuation, the maximum efficiency occurs at a tube length at which less than the total beam has been collected on the structure. Another reason for not operating the tube at 100

percent circuit collection is the related problem of small-signal gain, which continues to increase at the same rate in the saturation region, while the saturated gain stays nearly constant.

Of course, increasing the tube length is not the only way to provide total beam collection on the slow-wave circuit. One can also increase the input power in order to force the tube to saturate at any give length. Again because of circuit loss and the formation of the secondary bunch, maximum efficiency occurs at a value of input power less than that needed to achieve total beam collection. Also, when the crossed-field amplifier is operated much beyond the knee of the curve of power gain as a function of input power, reduced power gain results. Thus, considering maximum power gain and maximum efficiency, for a given tube length, it has been found that the crossed-field amplifier should be operated where there is still a rather large fraction of the beam available for collection at depressed potentials at the end of the interaction region.

All of the above limitations on crossed-field efficiency were studied under this program. The main tools used for this study were large-signal computer analyses. These large-signal programs made it possible to study various efficiency improvement schemes quickly and (in comparison with experimental studies) inexpensively.

3.4.1 Small-Signal Parameters

In order to determine the relative importance of various design parameters on the efficiency of a conventional CFA one should examine small-signal parameters. Small-signal equations are particularly useful during the initial design phase since explicit parametric relationships can be established.

Consider the interaction circuit and sole cross section sketched in figure 17. The electronic efficiency given by Eq. (3-5) may be rewritten as

$$\eta_e = \frac{1}{1 + \frac{1}{2\beta(a-x_o)} \frac{\omega}{\omega_c}} \qquad (3\text{-}7)$$

The interaction impedance at the position of the beam is

$$Z_i = K_o \frac{\sinh 2\,\beta x_o}{2 \sinh^2 \beta a} \qquad (3\text{-}8)$$

where K_o is the impedance at the beam face of the circuit. The gain of a crossed-field amplifier is most influenced by D, the gain parameter, given by

$$D = \frac{\omega}{\omega_c} \left(\frac{I_b Z_1}{2 V_o} \right)^{1/2} \qquad (3\text{-}9)$$

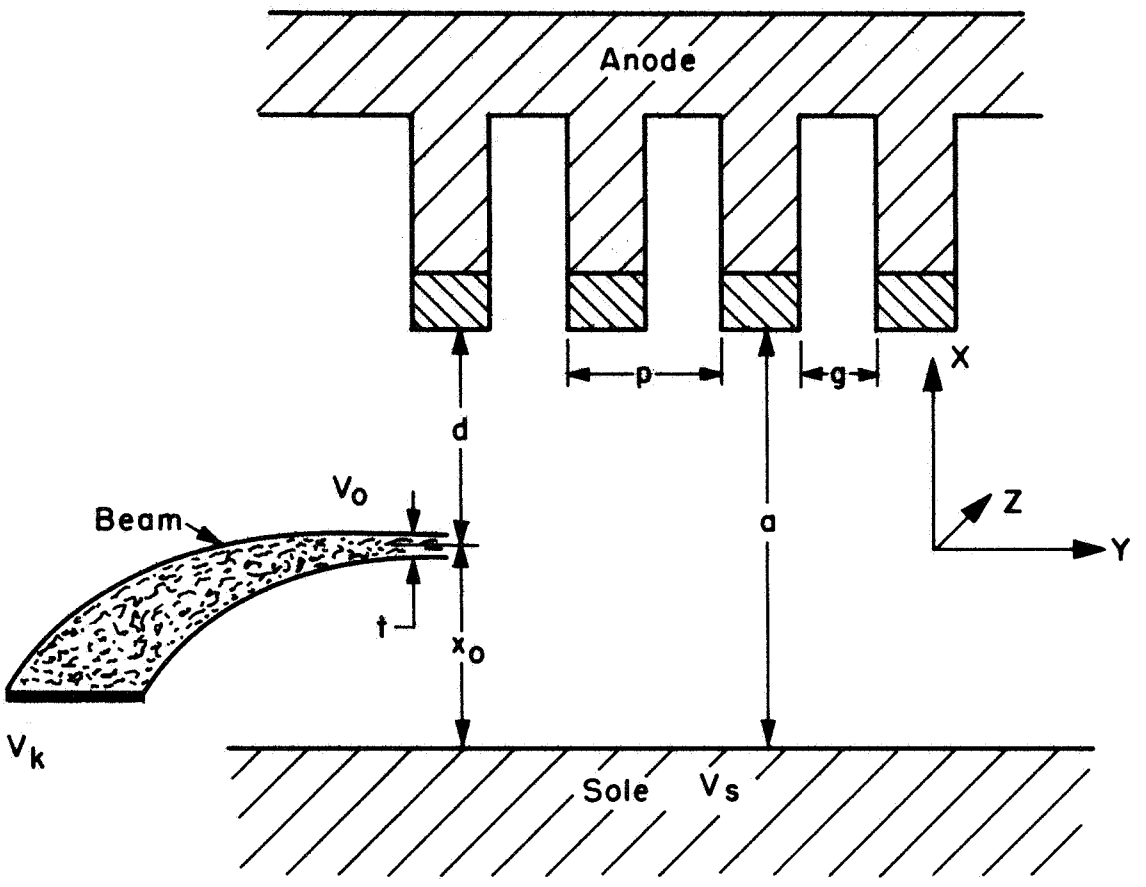

Schematic Drawing Of Crossed-Field Amplifier Defining Parameters Used In The Small-Signal Analysis Of Efficiency.

Fig. 17

or, using Eq. (3-8),

$$D = \frac{\omega}{\omega_c} \left(\frac{K_o}{Z_{dc}} \frac{\sinh 2\beta(a-d)}{4 \sinh^2 \beta a} \right)^{1/2} \qquad (3\text{-}10)$$

where $Z_{dc} = V_o/I_b$.

If we choose to optimize the product of gain parameter and interaction efficiency

$$M = D\eta_e \qquad (3\text{-}11)$$

which leads us to the relationship

$$\tanh 2\beta(a-d) = \beta d \left(1 + \frac{2\omega_c \beta d}{\omega} \right) \qquad (3\text{-}12)$$

We can now solve this equation for the optimum d/a for a given βd and ω/ω_c. The results are shown in figure 18 for ω/ω_c varying from 0.5 to 10 (the values of interest for most crossed-field amplifiers). The results give an optimum beam injection position rather close to the line.

Similar parametric relationships were obtained for other conditions of optimization. (product derivatives). The results, however, did not illustrate realistic tradeoffs as well as solutions to the actual small signal equations.

Another important parameter, relating noise growth in a crossed-field beam to desired signal growth, is defined as

$$S = \frac{I_b}{4\epsilon_o B_o D V_o h} \qquad (3\text{-}13)$$

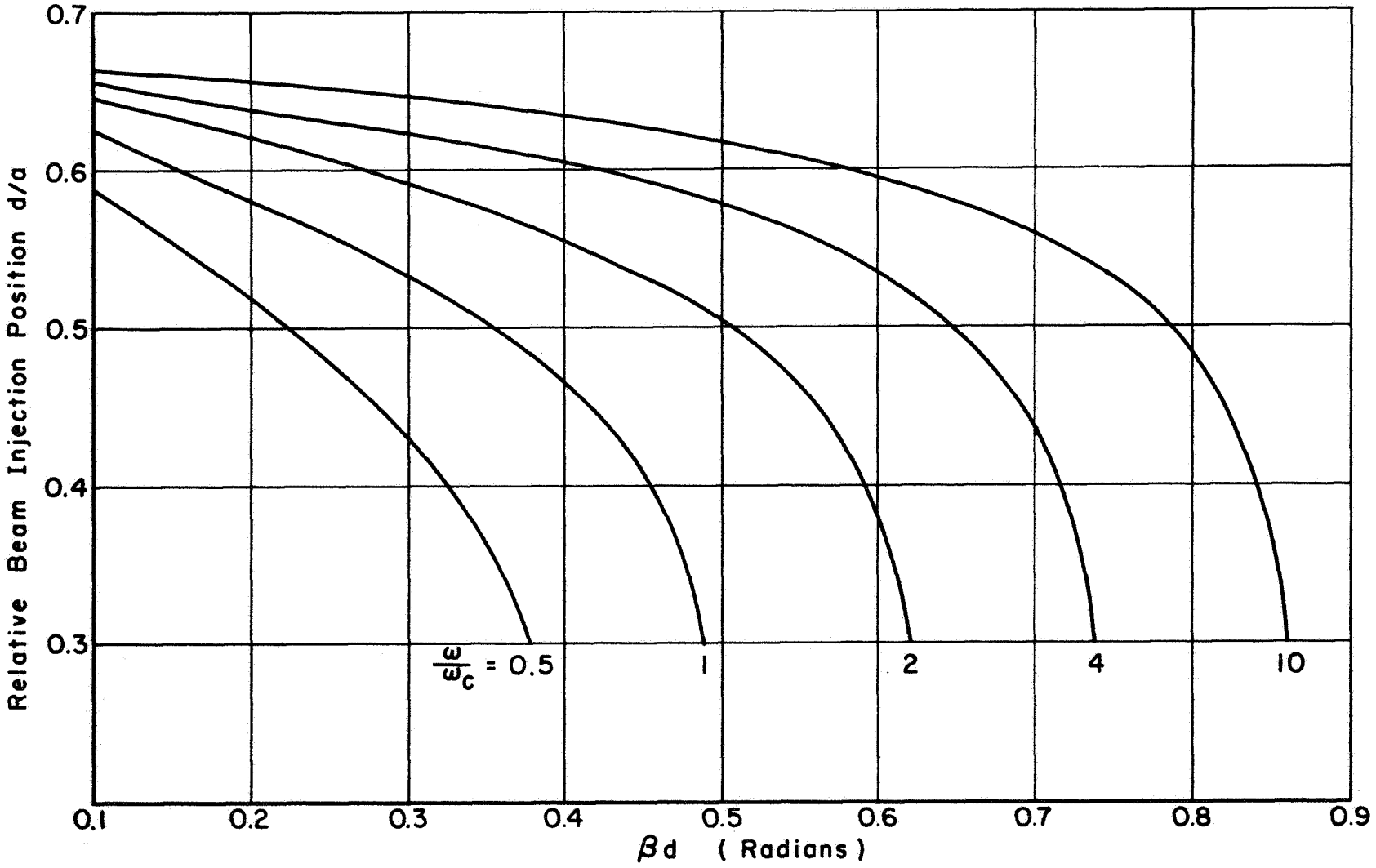

Optimum Beam Injection Position For Small Signal Calculations With Constant Sole-Circuit Dimension.

Fig. 18

where h is the beam width in the direction of magnetic field, ϵ_o is the permitivity of free space and other parameters are as previously defined. Values of S less than 2 are necessary for a stable, low-noise amplifier.

A computer program was written to evaluate the algebraic small-signal equations over a wide range of parameters. A list of this program is included in Appendix A. Several assumptions were made for each set of solutions in order to treat the following parameters as incremental variables.

Parameter	Region Examined	Increment
V_k (kV)	2 - 20	2
B_o (Gauss)	500 - 7000	500
V_k/V_o	5 - 25	5
x_o/a	0.3 - 0.7	0.05

V_k/V_o is the ratio of cathode voltage to synchronous voltage and x_o/a is the relative beam injection position between sole and slow-wave structure. Certain restrictions were imposed to limit solutions to those with practical significance, i.e., space charge parameter S less than 4, impedance at beam injection position Z_i greater than 1 ohm, dc voltage gradient in interaction region less than 500 volts/mil, and interaction length (corresponding to DN = 0.5) less than 20 inches. Additional restrictions were imposed in subsequent iterations to define thermal dissipation

and cathode current density limitations.

Fixed parameters for each set of solutions were:

1. Total dc beam power, $V_k I_b$
2. Interaction impedance at the circuit beam face, K_o
3. Circuit phase shift per period, βp
4. Frequency, f_o
5. Circuit attenuation per period, α_p
6. Normalized cathode length (Kino units), L_k

The following dependent variables were computed and tabulated by the program:

1. Sole to circuit spacing, a
2. Circuit pitch, p
3. Space charge parameter, S
4. Cathode current density, J
5. Small-signal gain parameter, D
6. Interaction impedance at x_o, Z_i
7. Sole to cathode potential, V_{sole}
8. DC electric field in interaction region, E_{dc}
9. Circuit attenuation per unit length α
10. Interaction length corresponding to DN=0.5, L where N is the number of space-harmonic wavelengths in the length L

Fixed circuit parameters were measured values obtained from cold test structures. A portion of the data from each computer run was plotted, analyzed and projected to the next logical choice of parameters.

Figure 19 is a typical family of curves for the case B_o = 3000 gauss, x_o/a = 0.5, K_o = 300 Ω, $\beta p = 0.8\pi$, αp = 0.3 db per pitch, P_{dc} = 6500 watts and f_o = 2000 MHz. Values of V_k/V_o for each curve are indicated on the right side of the figure. For the previously defined incremental variables, the dependent parameters vary in the following manner:

1. a varies from 0.050 to 0.300 in. with larger values corresponding to higher electronic efficiency ($\eta_e = 1 - V_o/V_k$)

2. L varies from less than 0.5 in. to the constraint value of 20 in. Decreasing V_k implies higher I_b, hence higher gain per unit length and a shorter length.

3. Attenuation is less than 0.02 db/in. for a high velocity circuit, and greater than 0.5 db/in. for an extremely short interaction length.

4. S is limited to 2 by the constraint, and is as low as 0.1 for a high velocity circuit.

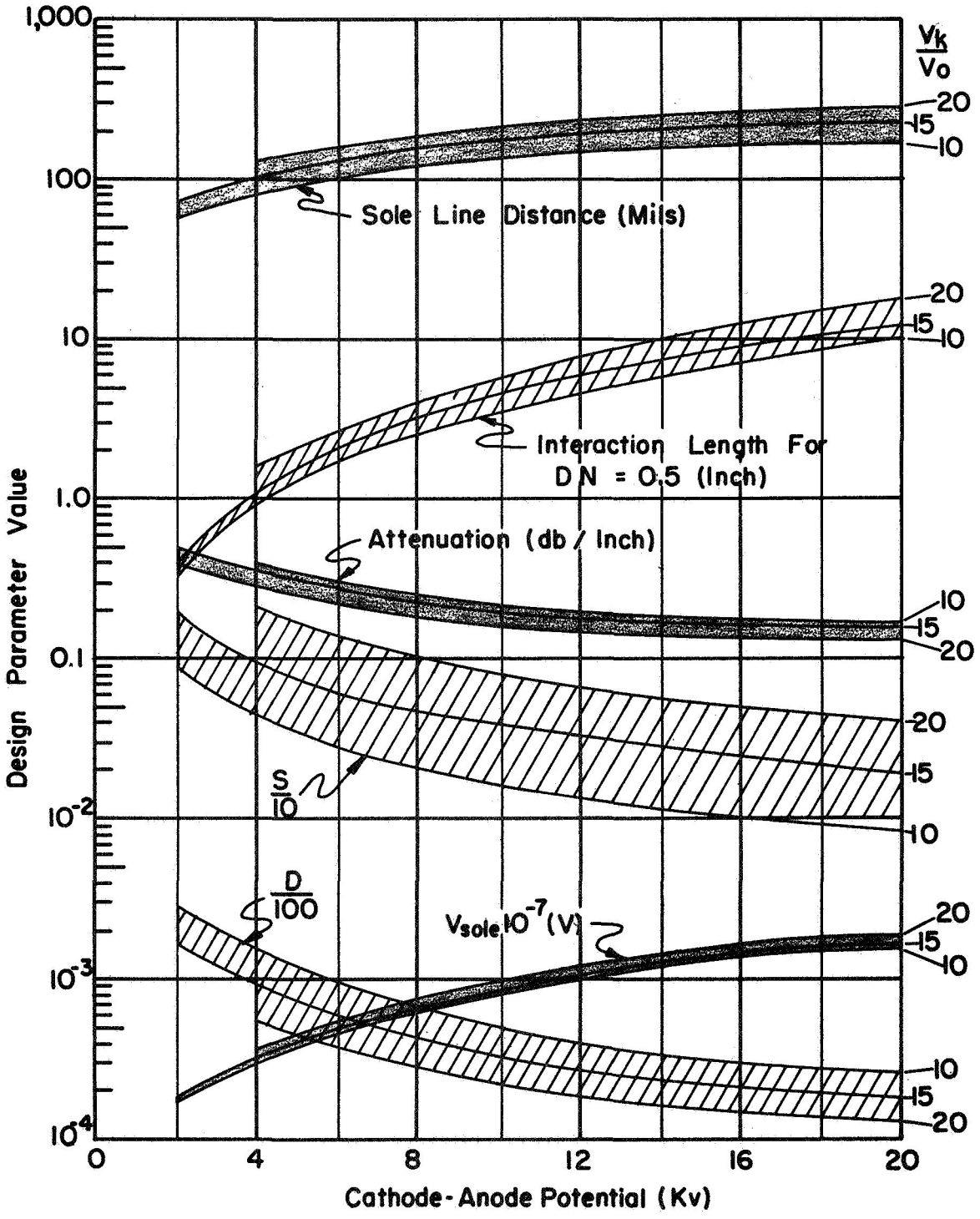

Design Parameters For High Efficiency CFA As A Function Of V_k And V_o. B_o= 3000 Gauss, f=2GHz, x_o/a = 0.5

Fig. 19

5. D varies from 0.3 to 0.002, reflecting higher gain per unit length for more beam current and lower cathode potential.

6. V_{sole} varies with V_k in an almost linear fashion in order to maintain a constant beam injection position:

$$x_o/a = (V_{sole} + V_o)/(V_{sole} + V_k)$$

Another family of curves in figure 20 was plotted from the same data tabulation. However magnetic field, B_o, is now the independent variable and V_k is held constant at 8000 volts. Similar parametric relationships exist with higher gain and beam impedance corresponding to lower values of S andL as magnetic field is increased.

These particular figures are shown since they bracket the design region of greatest interest. Certain desirable parametric combinations were analyzed in greater detail with large signal interaction programs. These designs are evaluated in the following section.

3.4.2 Large-Signal Analysis

The mathematical models used to analyze beam-wave interaction in crossed electric and magnetic fields are similar for each of the Litton large signal computer programs. Differences between the programs are primarily in the degree of complexity (space-charge or no space-charge, etc.), the type of computer used, and in the print and

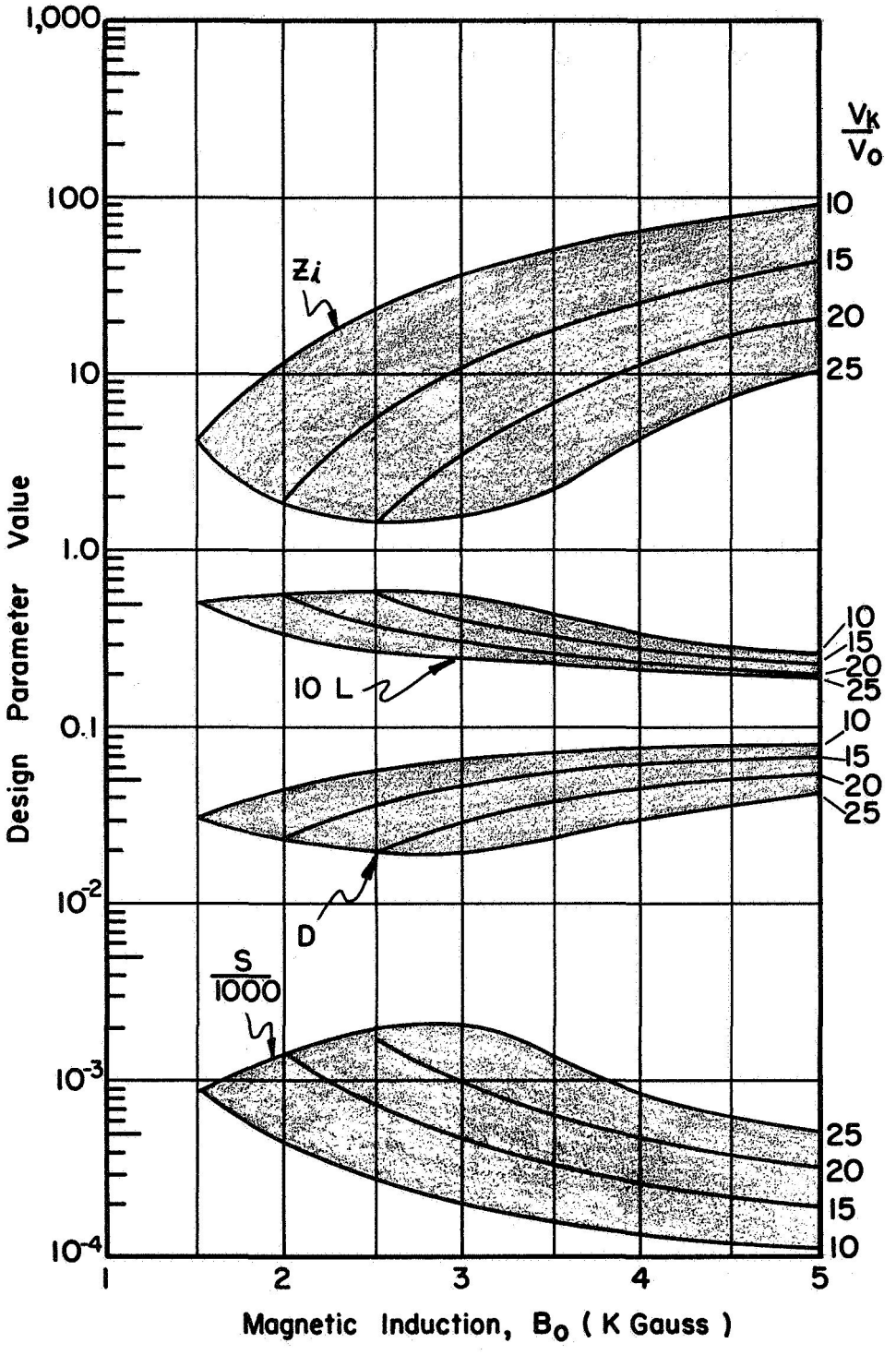

Design Parameters For High Efficiency CFA As A Function Of B_o And V_k To V_o Ratio

V_k = 8 Kv, f = 2 GHz, x_o/a = 0.5

Fig. 20

plot output capability of each.

The programs designed for batch processing (LSCFA 002, LSCFA 022 and LSCFA 122) include space charge and acceleration terms, and provide for beam-wave asynchronism. Each model requires certain basic assumptions in order to reduce the complex problem of crossed-field interaction to a tractable procedure. These assumptions include the following:

1. An electron beam is periodic along the length of interaction, and when interacted upon by a traveling rf wave, the beam forms periodic bunches.

2. Only one wavelength of the electromagnetic wave and the portion of beam which corresponds to this wavelength are considered simultaneously.

3. An electron beam travels at less than one-fourth the velocity of light so that relativistic effects can be neglected.

4. A beam is considered as a finite number of rods of charge. Up to 200 rods are used to simulate one wavelength of a beam. Each rod is as long as the beam width in the direction of magnetic field.

5. RF-beam interaction occurs with a single space-harmonic of the composite circuit wave.

6. Boundaries at sole and circuit have infinite conductivity. Doubly periodic elliptic functions treat image charges reflected by conductive planes to compute space charge electric fields.

7. A modified Lagrangian formulation is used to calculate rod trajectories by a finite difference procedure.

8. Energy exchange between rods and rf wave is computed by summing velocity and work done on the rf fields of each rod.

9. No variations exist across the beam in the direction of magnetic field.

10. Circuit velocity and dc electric field may vary as the interaction progresses in any predetermined fashion.

11. Initial rod positions and velocities may describe Brillouin flow for any finite beam thickness, or may be defined individually in any reasonable manner which adequately describes a realistic electron beam.

The original large signal interaction program, CFA022, has been used for six years as the primary analytic design

tool for Litton injected-beam CFAs. Improvements incorporated into the original program, and more recent versions written for other computer facilities, have decreased computation time and added to program flexibility. However, the basic program function - the analysis of gain, power growth and efficiency for any specific set of parameters - has not changed.

The value of any mathematical formulation describing CFA interaction can be determined by its ability to predict the performance of experimental devices. A valid comparison of nonlinear theoretical analyses with experimental data can be complicated by the difficulty in determining accurately the actual beam thickness and position in an experimental device. By considering realistic beam approximations we have continually improved agreement between experimental and analytic results. Predicted and experimental values of saturated gain and efficiency generally agree within 5% for current CFA designs which have a beam width at least four times the width of the interaction gap. ($h/a \geq 4$). For the designs studied on this program h/a varies from 6 to 8.

When less detailed design information was desired in the early phase of the study we used several variations of the timeshare large signal program, PVL 6. The model is similar to that used in LSCFA 002 except that space-

charge and acceleration terms are neglected. Also the approximate model assumes synchronism between beam and wave.

Variations of PVL 6 were quite useful for establishing large signal parametric tradeoffs. Approximate solutions were obtained for a fraction of the cost of the more complex space-charge solutions. Following a series of iterative solutions where one or more design variables were incremented, the more favorable cases were repeated with a batch program including space-charge, acceleration terms and asynchronism.

Selected results from the large signal study are illustrated in figures 21 - 25. The ordinate axis for each graph represents rf power on the circuit, and each abscissa represents interaction length measured from the rf input port. Design parameters for each figure are slight perturbations about the optimum values tabulated in figure 25 as design J-3/93xx. Letters following J-3/93 are used to distinguish between the various perturbations, with voltages, beam current and circuit velocity fixed.

The effect of including space charge in a large signal analysis is illustrated in figure 21. Somewhat higher gain is evident near the input without space charge. A three-layer beam with a thickness equal to 10% of the interaction gap shows a 2-3% higher power at saturation when space-charge is included.

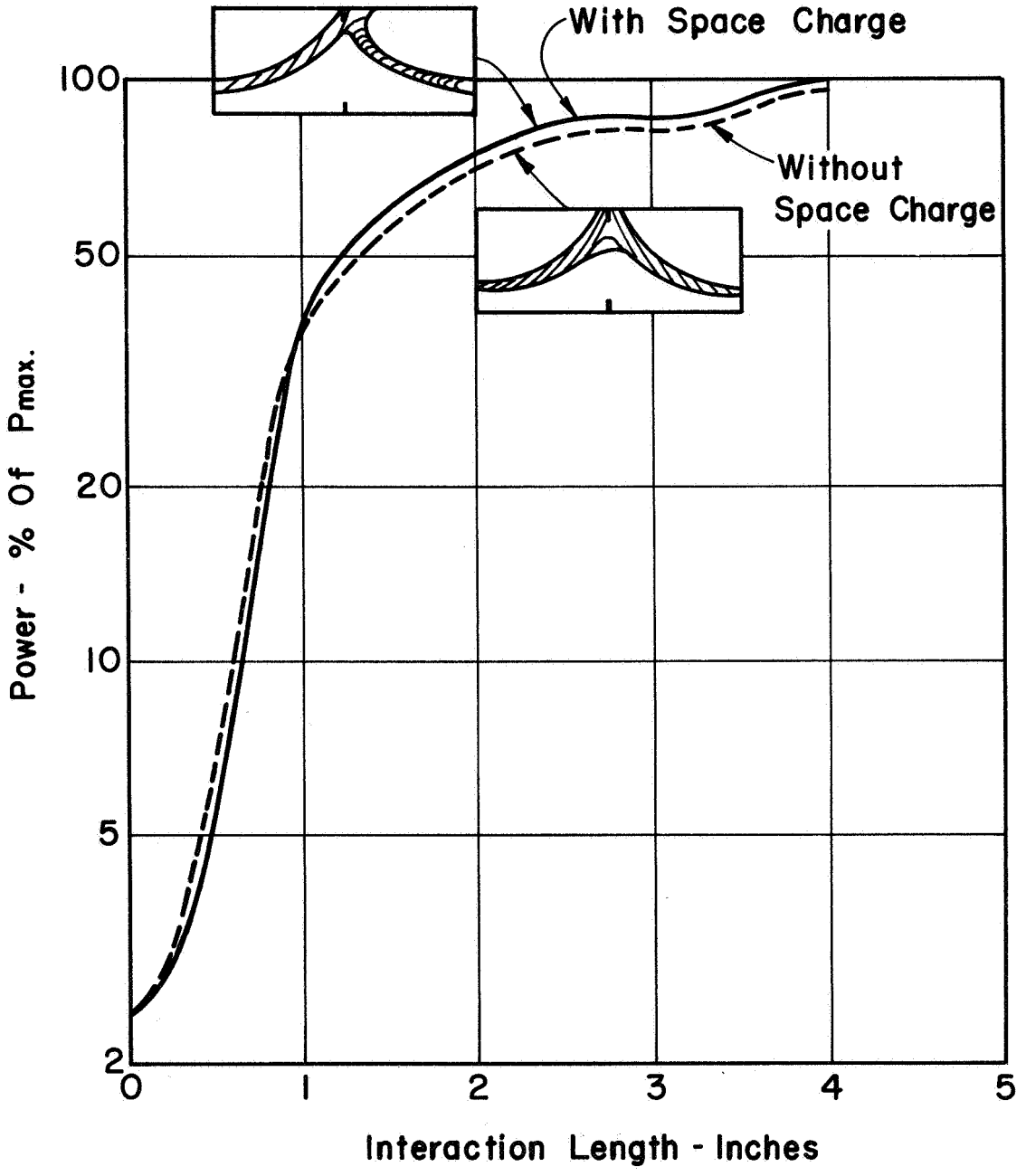

Comparative Results Illustrating The Effects Of Including Space Charge In Large Signal CFA Program

Fig. 21

Boxes shown in the figure represent profiles of rod positions within the moving frame at the lengths noted. Striations are obvious within each bunch. Space charge fields also tend to curl the profile of those rods which are in the most favorable initial phase.

For synchronous beam-wave interaction in preliminary designs it is not particularly enlightening to include space-charge in the calculations. Detailed analysis of interaction efficiency, bandwidth and collector efficiency require space-charge fields.

The necessity of detailed and accurate cold test attenuation measurements is obvious from figure 22. All parameters were held constant except circuit attenuation which was allowed to vary from zero to 0.6 db/in. Circuit length required to reach a power level of 5 KW is 25% greater for 0.6 db/in attenuation than for measured values of 0.3 db/in. If it were possible to reduce attenuation of present circuits by a factor of two one could expect an additional 3-5% increase in interaction efficiency.

Figure 23 illustrates the relationship between saturated output power, interaction efficiency and interaction impedance. The analytic and experimental circuit study verified the impedance-bandwidth trade off which exists for variations of the Karp circuit. Values of K_o in excess of 1000 ohms were measured at $\beta p = 0.7\pi$ for

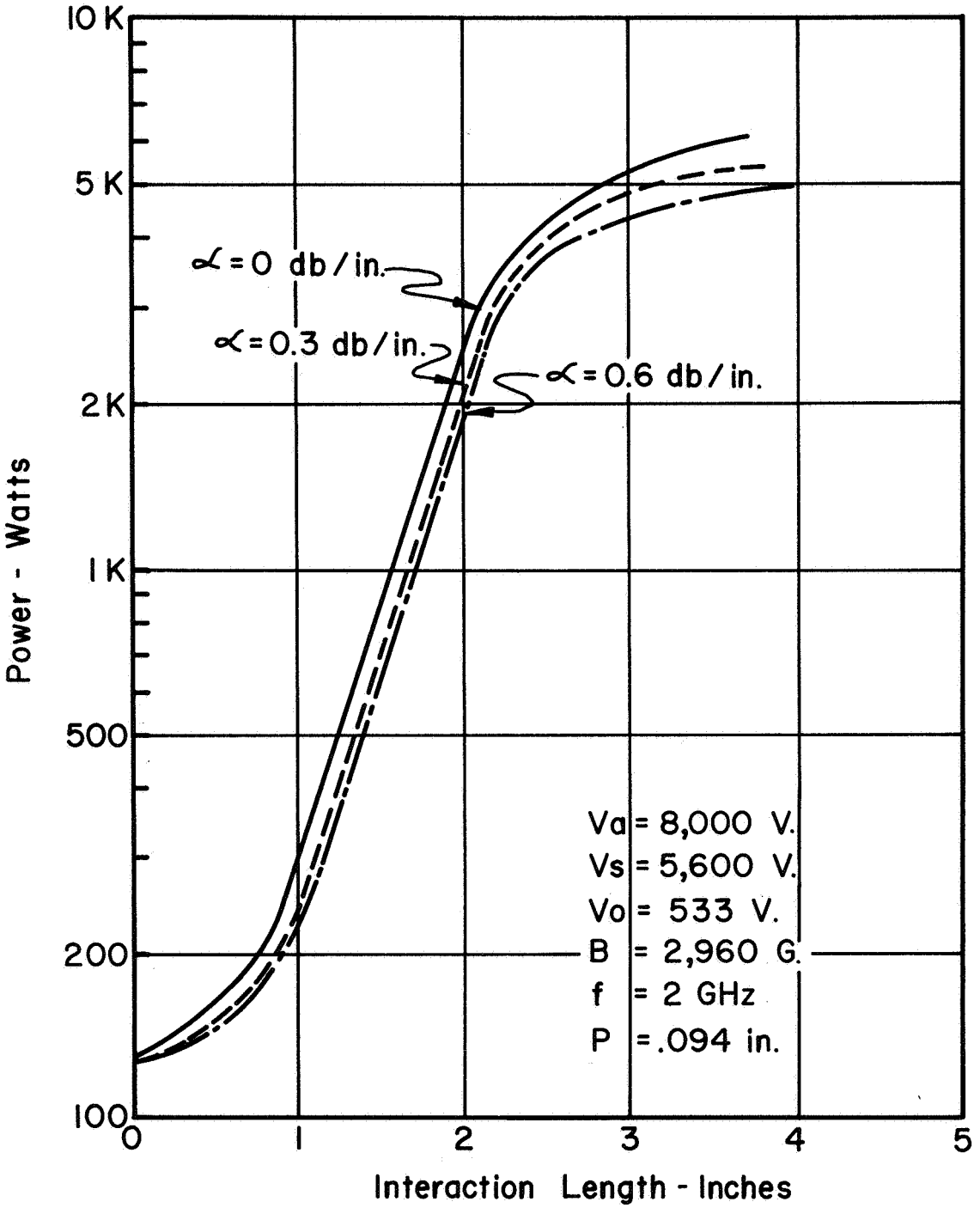

Saturated Power As A Function Of Inherent Circuit Attenuation.

Fig. 22

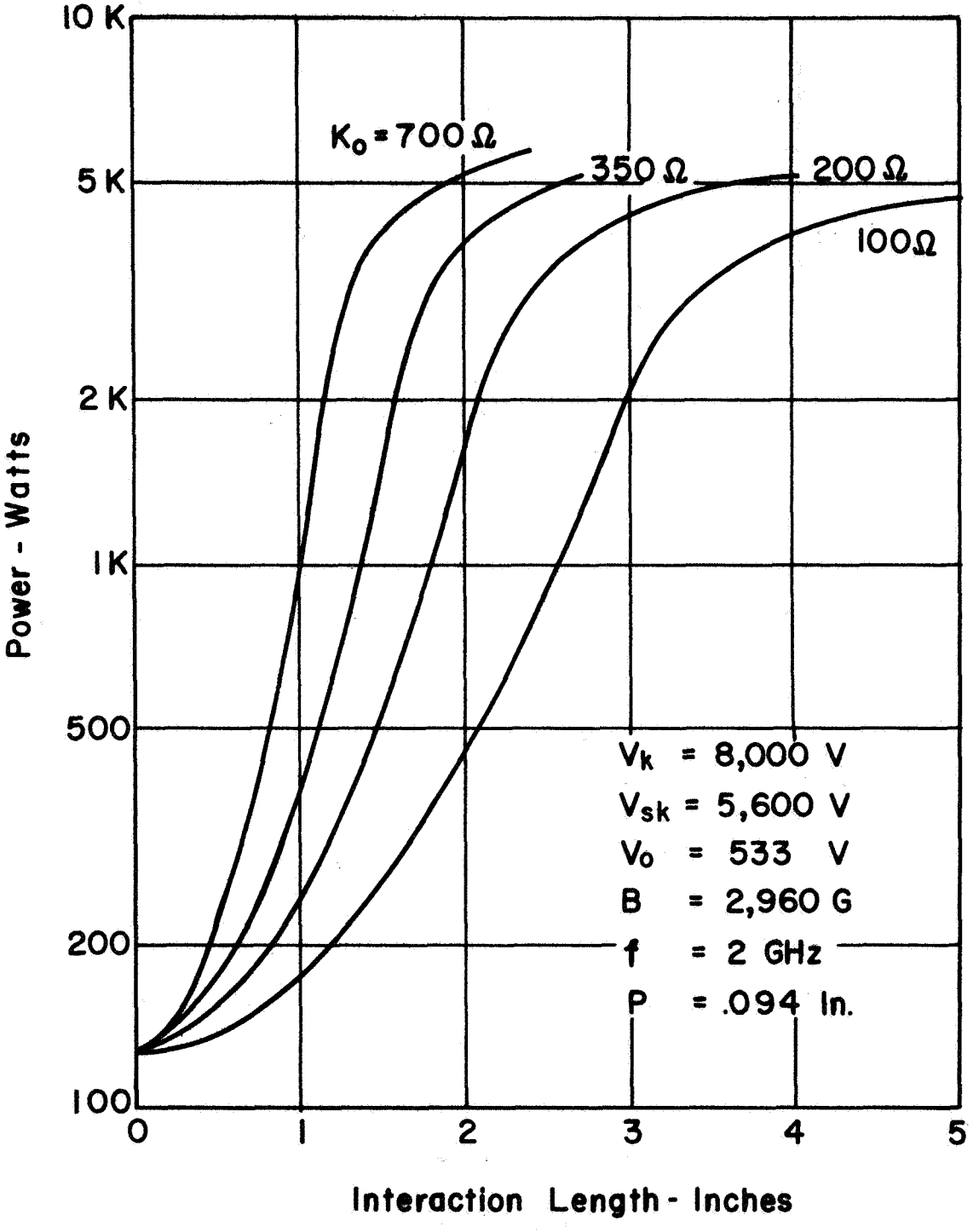

Saturated Power As A Function Of Interaction Impedance

Fig. 23

several circuits with high dispersion.

For the midband synchronous calculations plotted in figure 23 impedance was varied from 100-700 ohms. The case with K_o = 100 ohms requires nearly three times the interaction length to reach saturation as the case with K_o = 700 ohms. The difference in interaction efficiency amounts to nearly 10% for the two extreme cases.

Figure 24 illustrates the effect of input signal level on the rate of power growth and the interaction efficiency with all other parameters fixed. Lower drive power requires a longer interaction length to reach a particular power level. Decreased circuit losses and higher electronic efficiency result from a shorter interaction circuit.

Overall conversion efficiency is the ratio of rf output power to total input power, including rf drive power. Highest output stage overall efficiency for these J-3/93xx designs occurs with drive power between 75 and 150 watts. The required output stage gain for the final design, J-3/93E, was selected as 16 db.

This established the required CFA drive power at 125 watts. For 40 db gain in the amplifier chain 24 db gain is required in the driver stage. These requirements are readily met by number of existing microwave amplifiers.

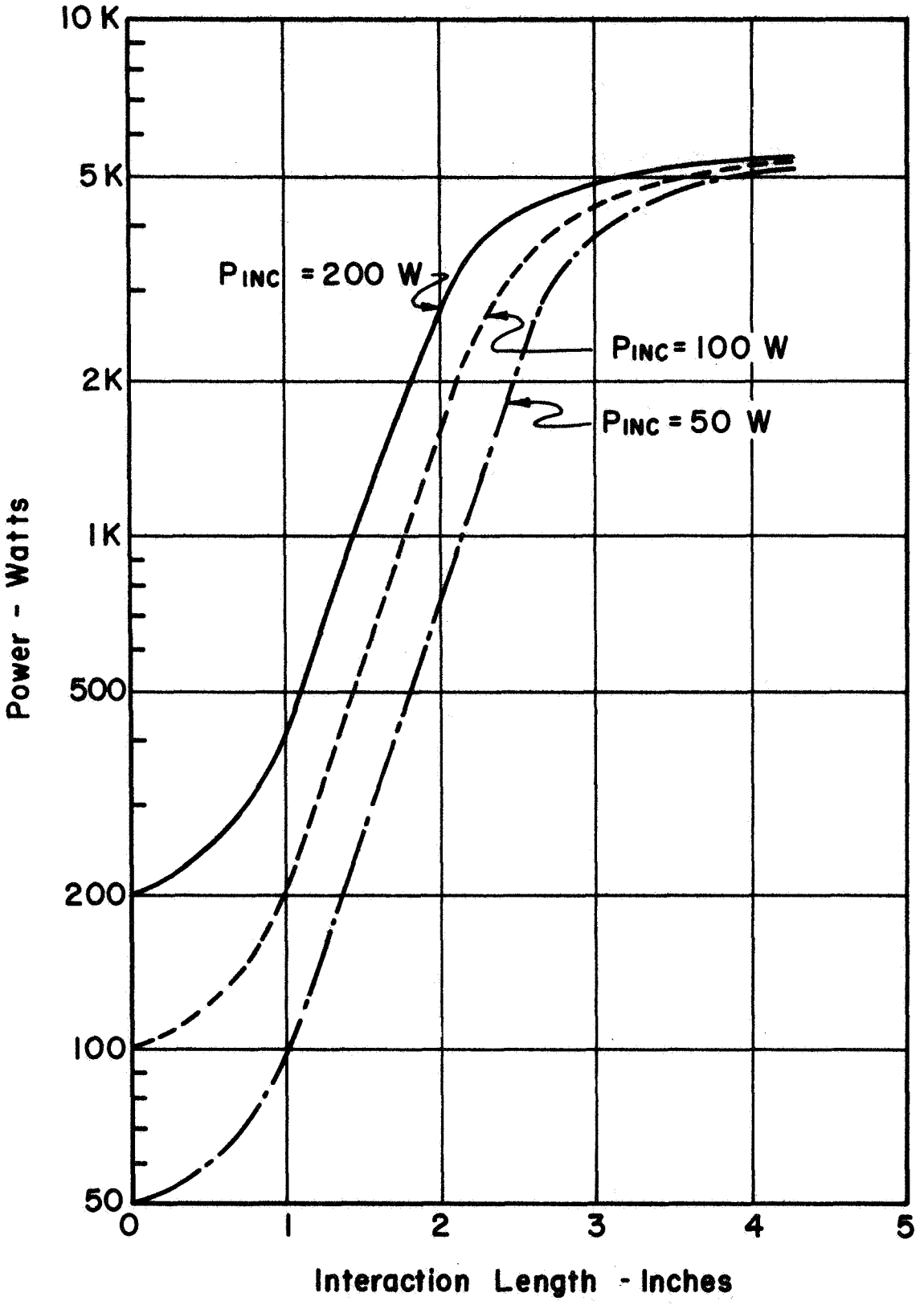

Power Saturation Characteristic Of Design J-3/93C

Fig. 24

Large signal analyses were used to establish a reasonable trade off between dispersion and interaction impedance. Each band-edge frequency (1985 MHz and 2015 MHz) and the center frequency (2000 MHz) were analyzed for fixed dc electric and magnetic fields. The highest dispersion which resulted in nearly uniform saturated output power across the 30 MHz band was approximately 6% corresponding to a K_o variation from 216-277 ohms. Figure 25 illustrates the large signal power response for values of b, the beam-wave velocity difference, equal to -5.4%, - 1.3% and + 0.4% at low, mid and high frequencies respectively. Other choices of synchronous velocity resulted in higher power at one or the other band edge and greater power variation across the frequency band.

Optimum device efficiency requires high interaction efficiency in conjunction with high collector efficiency. Throughout the large signal study we considered the distribution of kinetic and potential energy in the uncollected portion of each beam at any particular distance along the circuit. Interaction distances were normalized so that various designs could be compared. The common method of normalization refers to the fraction of total beam current which has been collected on the circuit (i.e., a 70% collection plane is that interaction length at which 70% of the total beam current has reached the circuit).

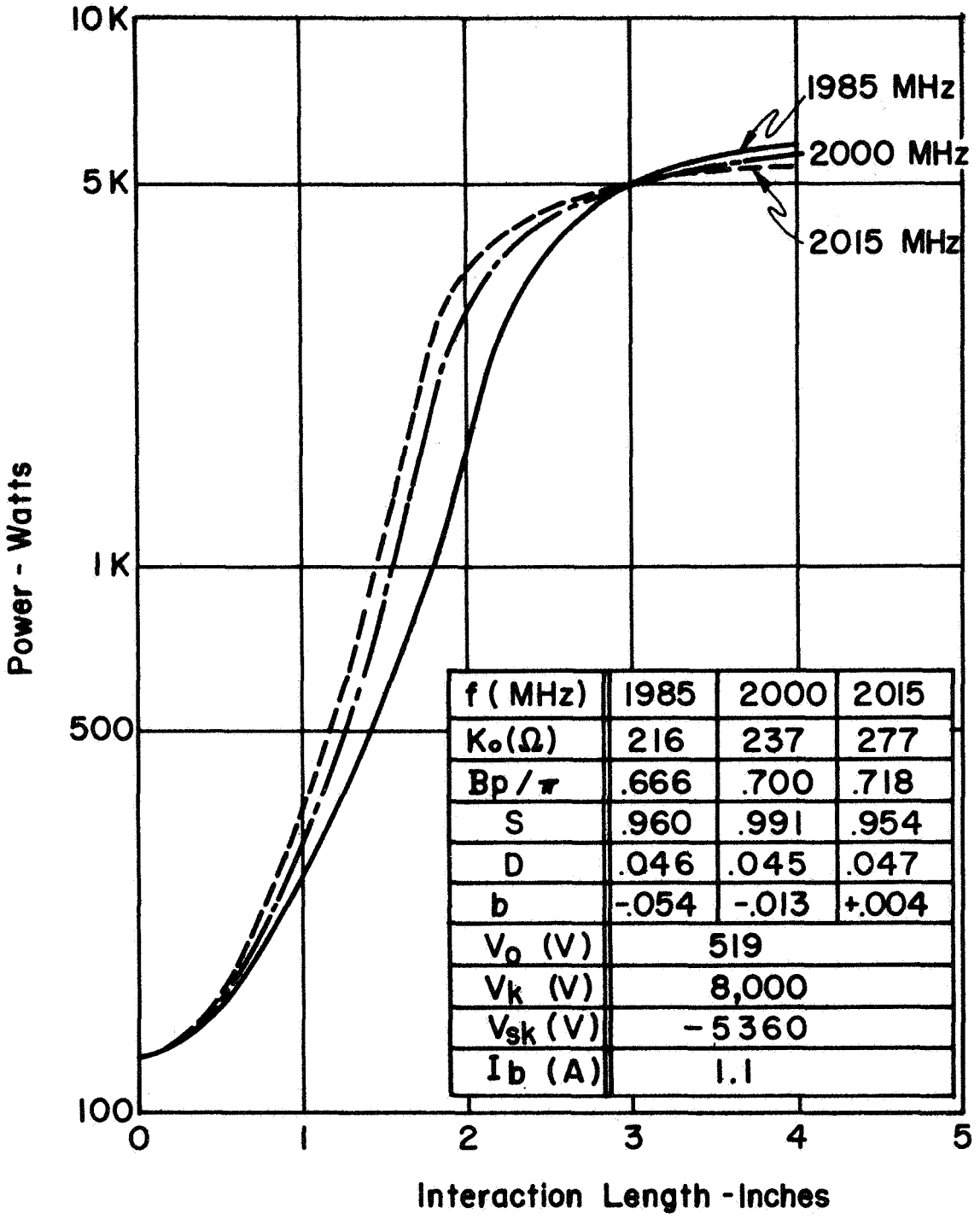

Power As A Function Of Length At Low, Mid , & High Frequencies With Experimental Dispersion And Impedance Values.

Fig. 25

Figure 26 illustrates the distribution of potential energy at collection planes of 1%, 62% and 81%. Axes of the figure represent relative electron density, interaction length and potential energy referenced to circuit potential. Potential energy is zero for an electron grazing that portion of a slow-wave structure which is adjacent to the electron beam, and is maximum for an electron grazing the sole electrode.

The formation of two distinct electron bunches is evident at the 2050 watt power level where the first favorably phased electrons are intercepted by the circuit. Those electrons which began in an unfavorable phase are shown bunched about a potential level slightly below the energy level, V_o, about which they were injected.

Further along the interaction length, where the circuit power has reached 5045 watts, most of the favorably phased electrons have been collected. Those electrons which have not been collected are spread out between sole and circuit. A substantial portion of the beam is bunched about an energy level nearly 3KV below cathode potential. This energy is recoverable, as discussed in section 3.5.

The third energy profile is beyond the region of useful interaction for this particular choice of interaction parameters since circuit loss increases at nearly the same rate as the amplified wave.

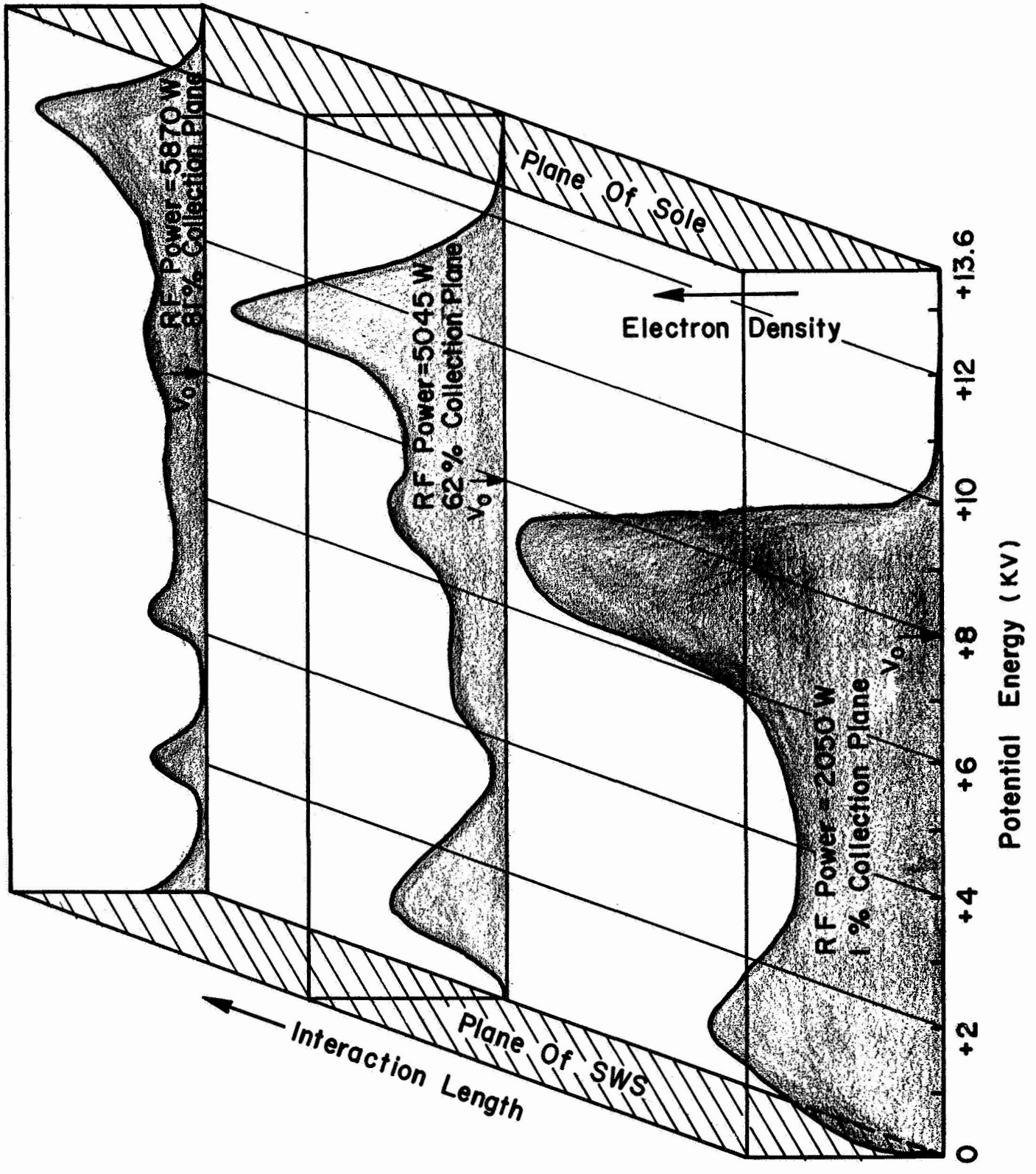

Potential Energy Distribution Along Interaction Length For J-3/93-A Design Parameters

Fig. 26

Parameters which represent an optimum combination of high interaction efficiency and high collector efficiency are defined as design J-3/93E. These parameters are listed in Table I.

3.5 COLLECTOR ANALYSIS

The large-signal interaction study showed that in all conventional CFA designs a substantial fraction of the total beam energy was recoverable. In order to compare preliminary designs we assumed a hypothetical four element collector. Potentials were chosen which resulted in recovery of each electron with potential energy greater than the potential of the electrode with the largest depression less than the electron potential energy. Detailed collector analyses were conducted only for certain practical electrical designs which exhibited extremely high efficiency.

The large-signal space-charge programs provide a printout of velocity, energy and charge distribution information as a function of interaction length. At any particular rf power level or interaction distance the computer program can direct data cards containing this information to be punched in a format suitable for any one of the trajectory analysis programs.

Early in the collector study a question was raised regarding the practicality of recovering electrons at

TABLE I

J-3/93E DESIGN SUMMARY

Frequency Dependent Parameters

Frequency	f	(MHz)	1985	2000	2015
Phase Constant	β	(rad/m)	873	917	941
Interaction Impedance	K_o	(Ω)	216	237	277
Gain Parameter	D	--	0.046	0.045	0.047
Space Charge Parameter	S	--	0.960	0.991	0.954
Circuit Attenuation	α	(db/in)	0.36	0.37	0.39
Computed Gain	G_{sat}	(db)	16.06	16.06	16.18
Output Power	P_{out}	(watts)	5045	5042	5187
Collector Current	ΣI_{cn}	(mA)	407	319	308
Asynchronous Parameter	b	($^o/_o$)	-5.4	-1.3	+0.4

Frequency Independent Electrical and Geometric Parameters

Circuit Pitch	p	(in)	0.0944
Beam Width	h	(in)	1.000
Sole-circuit gap	a	(in)	0.132
Interaction Length	L	(in)	3.022
Circuit-Cathode Potential	V_k	(V)	8000
Sole-Cathode Potential	V_{sole}	(V)	-5360
Total Beam Current	I_b	(A)	1.100
Transverse Magnetic Field	B_o	(Gauss)	3000
RF Input Power	P_{in}	(W)	125

a potential below that of the cathode. M-type interaction is primarily the conversion of beam potential energy into rf energy, while kinetic energy remains relatively constant throughout the interaction. A favorably phased electron moves from its injection position, x_o, toward the circuit. The total energy given to the rf wave by a single non-cycloiding electron that is collected on the slow-wave structure is $e\ (V_k - V_o)$ where V_o is the kinetic energy voltage of the electron and V_k is the cathode to anode potential.

Electrons which enter the interaction region in an unfavorable phase will initially gain energy from the rf wave and move toward the sole. Since rf fields decay exponentially from the circuit the unfavorably phased electrons will not acquire sufficient energy to reach the sole, but will eventually move into a favorable phase and transfer energy to the rf wave as they are driven toward the circuit. For the reasons discussed in Section 3.4 the optimum interaction length is less than that required for total beam collection on the circuit. Hence a certain fraction of the beam will have potential energy greater than cathode potential at the end of a high efficiency interaction region.

Recovery of a portion of the spent electron beam on a collector element biased more negative than cathode

potential has been shown to be quite realizable in experimental CFA's and in analytic collector studies. However, the power supply required for each collection element biased more negative than cathode potential must transform electrical energy to a different voltage. Such a supply is not considered practical for present airborne or ground-based applications where the additional supply complexity outweighs the advantage of increased system efficiency. For spaceborne applications the premium on system efficiency outweighs the complication of converting a high energy stream of electrons into usable power at another potential level. Thus all conventional electrical designs were analyzed during this study with the assumption that electron collection at the highest possible energy level was desirable.

In addition to potential energy the spent electron beam has kinetic energy equal to $mv^2/2$ per electron. This represents only a small fraction of the total beam power in a high efficiency design yet the recovery of at least 60% of thekinetic power is both possible and desirable.

One practical method involves conversion of kinetic energy into potential energy in a slowly decreasing electric field. Average electron velocity is given by E_o/B_o and the dc electric field is $E_o = V_s/a$. Hence an increase in the sole-anode spacing and/or a decrease in potential provides

the required variation in dc electric field.

Figure 27 is the fourth space-charge iteration of a collector design which includes a tapered drift space. Average kinetic energy of electrons as they leave the interaction region is 563 eV. At the widest portion of this collector the average kinetic energy is only 227 eV. The total power involved in the conversion from kinetic to potential energy amounts to (563-227) eV * 11 mA=370 watts. (Each charge group for this collector design represents a current of 11mA).

Twenty seven individual elements were set up for this collector geometry. For the 1985 MHz case (illustrated) electrons were collected on only 16 elements in addition to the anode. This is in part due to the partitioning of the electron beam into a finite number of rods or charge groups. To obtain rod initial conditions for most collector studies of J-3/93xx designs the beam was represented by 100 rods. Following the interaction region 33-40% of the initial beam current was available for collection at depressed potentials.

Computation time for the large-signal space-charge interaction programs increases approximately as the square of the number of rods used in the calculations. While 25 rods was an adequate number of analyzing gain of these designs, the larger number was chosen for collector analyses as a compromise between accuracy and cost.

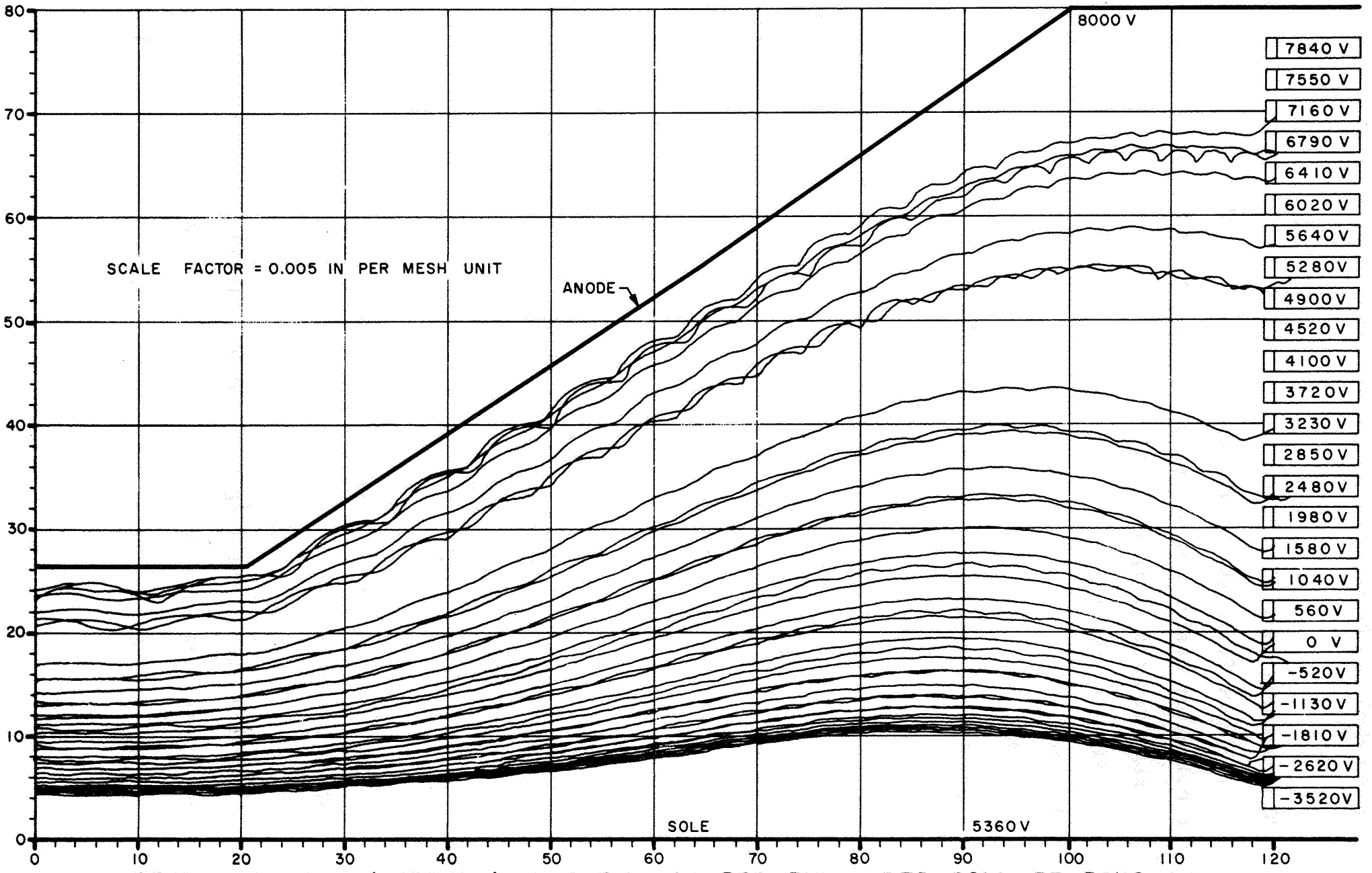

CDM J-3/93A (5/20/68) 1.985 GHz 100 ROD RUN --- DEP COLL-37 RAYS IN

Fig. 27

Up to 200 rods can be used for any computation when additional trajectory details are desired.

The potential distribution for the collector shown in Figure 27 was chosen so that equipotential lines curved downward into each element. The geometry and crossed electric and magnetic fields are arranged so that secondary electrons have a low probability of reaching a more positive electrode. Also the possibility of secondary electron avalanche is minimal because of the strong component of transverse magnetic field.

The depressed collector elements and the sole electrodes in most Litton CFA's are fabricated with slotted surfaces exposed to the beam to minimize secondary electron emission. In the complete collectors studied in conjunction with this design there was insufficient resolution to include the effect of slotted collector faces. It is quite feasible, however, to expand any portion of the collector geometry for a more detailed analysis with the space-charge trajectory program used in this study (TRAJ360).

Grooved or slotted surfaces have little effect on primary electron trajectories; however, any secondary electrons which are generated in a slot are shielded from electric fields and generally remain in the slot. This is equivalent to reducing the secondary yield of the collection surface by the ratio of the grooved area to the

ungrooved area of the sole face.

Attempts to convert more than 60-70% of the electron kinetic energy into potential energy in the simple collector geometry if figure 27 resulted in excessive cycloiding due to high space-charge forces in the region near the sole electrode. If the collector were allowed to expand in the direction of magnetic field, a flared geometry might permit additional kinetic-energy recovery.

We analyzed another collector geometry which resembled a common two stage collector used in certain CFA's. The sole electrode was transformed into several potential steps, each at a more negative potential than the previous element. Each step was designed to provide an abrupt decrease in electric field. Electrons entering a decreased field should cycloid. If collection occurs at the lowest point of a cycloidal trajectory all kinetic energy will be converted into potential energy since each electron is at rest at the instant of collection.

A ten step collector with this geometry did not yield useful results during the short time it was studied. Unfortunately an abrupt change in electric field does not result from a simple step in electrode potential or electrode spacing. More complex electrodes could be designed to create potential wells into which electrons could be trapped. In a similar manner it should be possible to inhibit the acceleration of secondary electrons emitted from within a

well by proper geometries and/or materials with low secondary yield.

The collector geometry of figure 27 can be fabricated and experimentally optimized without difficulty. Each element can be supported on shielded strips of high thermal conductivity dielectric blocks such as beryllium oxide ceramic.

A concentration of current on the -2620 V electrode indicates the need for additional potentials between -2KV and -3KV. Similarly, fewer potentials are required between 2KV and 6KV.

Table II is a summary of efficiency calculations for this particular collector following the interaction region described by design J-3/93E. Overall computed conversion efficiency is 81.4%.

3.6 COMPOSITE DESIGN ANALYSIS

The electrical parameters defined as design J-3/93E describe a conventional injected beam CFA which is fully compatible with the objective specifications. Throughout the electrical design phase we performed the necessary thermal and mechanical design calculations to assure that reasonable tradeoffs were being evaluated.

TABLE II SUMMARY OF EFFICIENCY CALCULATIONS

Element	Potential* (Volts)	Current (mA)	Power (Watts)
N	V_{cn}	I_{cn}	P_{cn}
7	7160	11	78.8
8	6790	22	149.4
9	6410	11	70.5
11	5640	11	62.0
12	5280	11	58.1
13	4900	11	53.9
17	3230	11	35.5
19	2480	22	54.6
21	1580	11	17.4
22	1040	22	22.9
23	560	11	6.2
24	0	22	0.0
25	-520	33	-17.2
26	-1130	33	-37.3
27	-1810	55	-99.6
28	-2620	110	-288.2
Total Collector . . .		370	167.0
SWS	8000	730	5840.0
Sole	-5600	0	0.0
Accel.	4000	0	0.0
BFE	0	0	0.0
Total Beam		1100	6007.0
Filament	6.3	6000	37.8
Magnet	0	0	0.0
RF P_{in}	-	-	125.0
Total Input Power			6169.8
RF Output Power			5022.7
Conversion Efficiency			81.4%

* Potentials are referenced to cathode

3.6.1 Electron Gun

Modified Kino guns operate successfully in many MBWO and injected-beam CFA tubes. Figure 28 illustrates this type of gun. Cathode supports form an integral part of the cathode body and provide a rigid assembly with good thermal isolation. A heater is supported inside the cathode body by ceramic potting for optimum vibrational characteristics and uniform cathode temperature. The complete assembly is supported on a rigid one piece ceramic insulator.

The emitting surface is a Phillips B impregnated cathode. The relationship between cathode temperature, available current density and cathode life is shown in figure 29. The design range indicated in the figure provides an adequate safety margin for a minimum amplifier life of 20,000 hours. (65,000 hours predicted life at 970° C with a maximum current density of 1 Amp/cm^2).

Total beam current of 1.1A requires 1.1 cm^2 emitting area for a current density of 1 A/cm^2. Dimensions of the emitting surface are 1.000 x 0.170 in. for these conditions.

We have recently studied a new type of electron gun which should allow operation with cathode current density less than 200 mA/cm^2 for this design.* This type of gun

* Dr. T. Van Duzer, Consultant to Crossed-Field Dept., Litton Industries

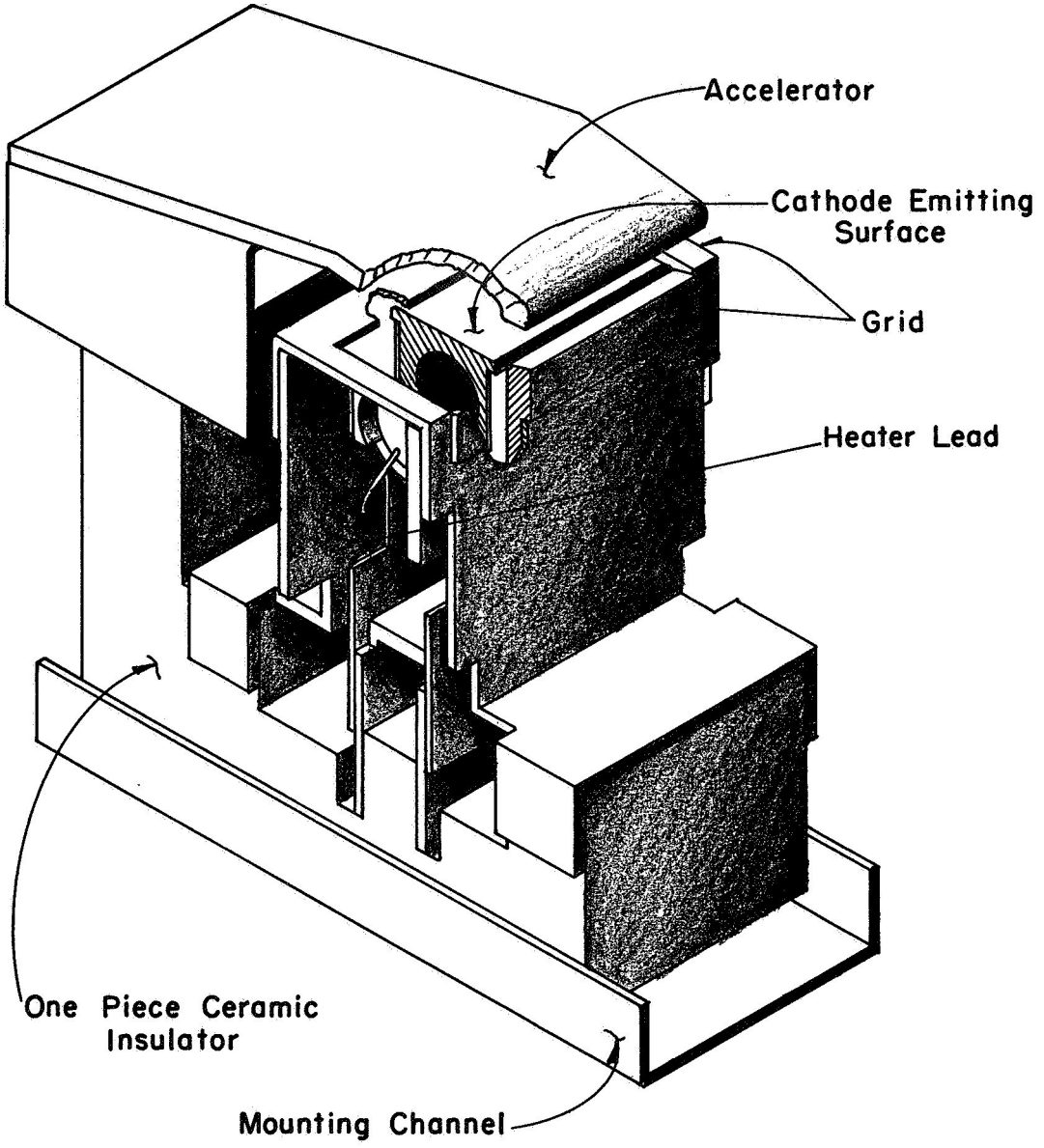

Note - Drawing is Simplified for Clarity. Cathode End Shield and Heater Connections are Not Shown. Part Radii and Some Ceramic Grooves are Also Eliminated.

Electron Gun Mechanical Assembly
Fig. 28

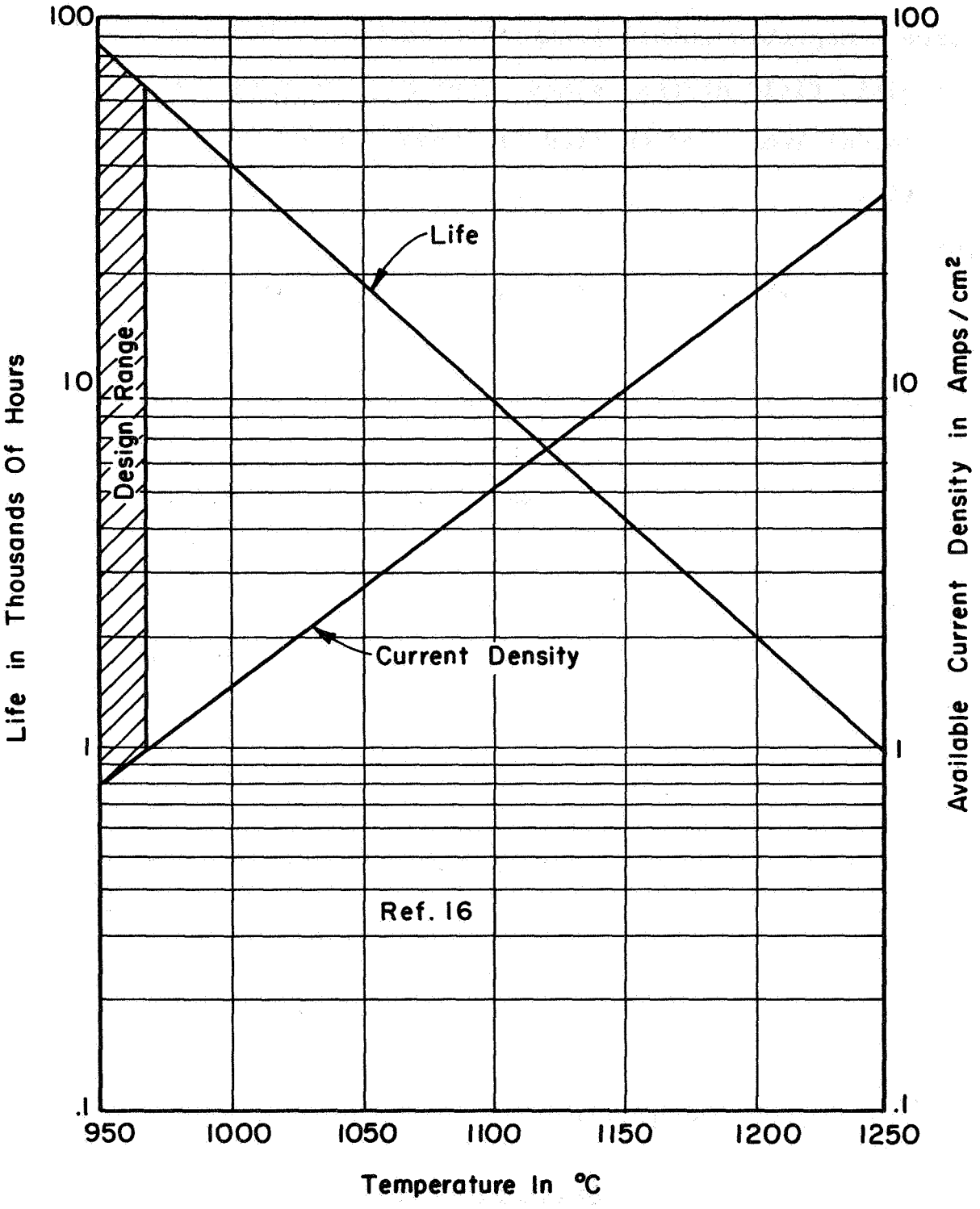

Cathode Life And Available Current Density As A Function Of Cathode Temperature

Fig. 29

uses a magnetic shield around the cathode. Reduced magnetic field at the cathode surface increases the cycloidal length of emitted electrons, hence the physical cathode length can be increased without degrading beam optics.

Three shield variations were analyzed for an electron gun designed to produce a 2.5 amp beam in a magnetic field of 2800 gauss. Electron trajectories in varying B fields have been synthesized by solving the paraxial ray equations for specified values of convergence and curvature. Field plots (figures which were obtained from these data) were converted into computer input data so that the transverse component of magnetic field could be computed at all points which were on the resultant trajectories.

Higher efficiencies are expected from amplifiers with shielded guns. Preliminary analytic results indicate that low-noise thin beams with minimum cycloiding and crossovers can be obtained from cathodes situated in a magnetic shield. Experimental verification of analytic designs must precede the actual use of shielded guns in crossed-field tubes.

3.6.2 Thermal-Mechanical Design

Figure 30 illustrates one practical tube mounting configuration. In order to maintain maximum internal

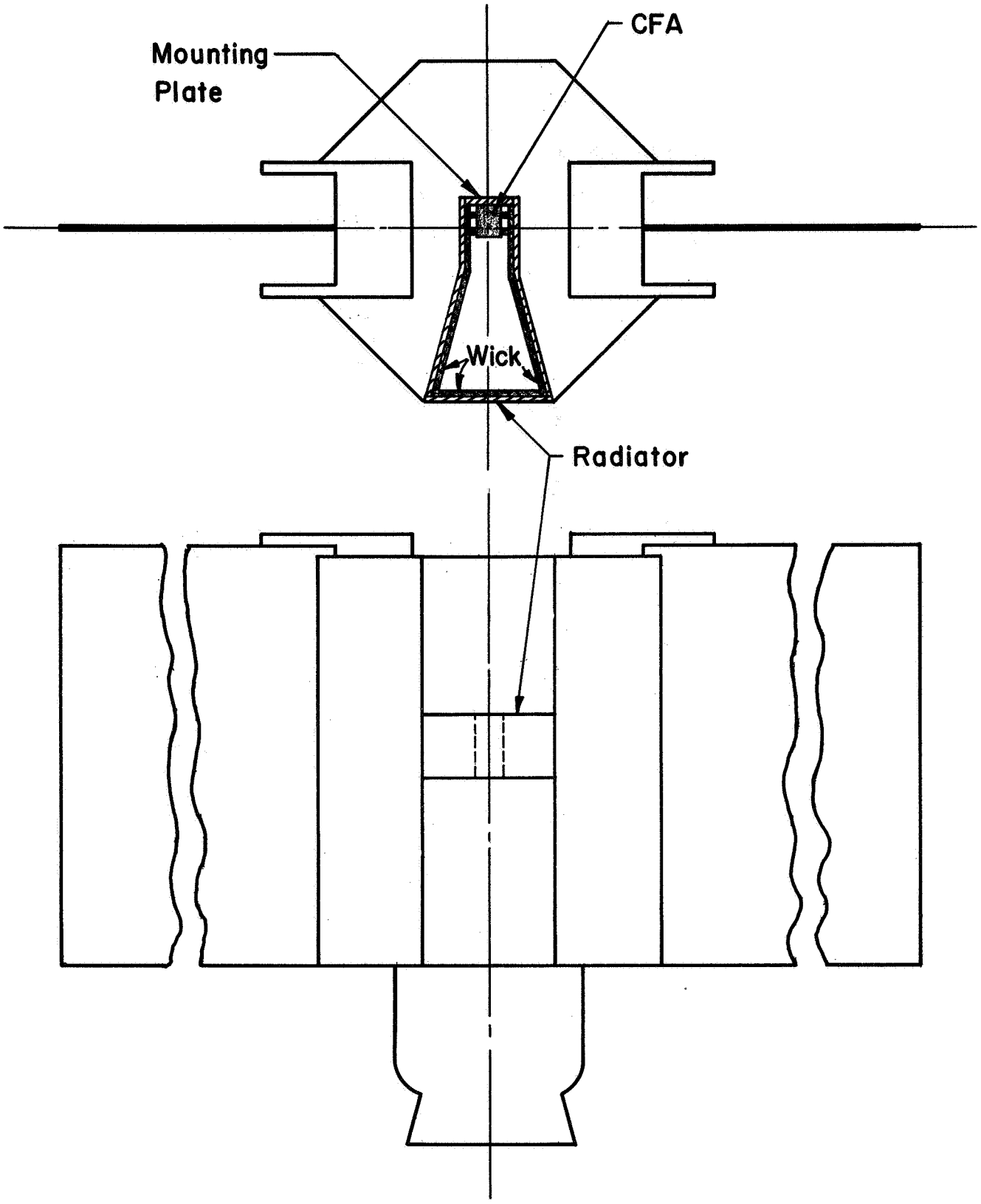

Tube Mounting Configuration For Dual Panel RF Joint Concept
Fig. 30

tube temperatures below 500°C, mounting plate temperature should not exceed 250°C. Heat from the tube mounting plate transfers to a suitable radiator through peripheral heat pipes.

Figure 31 shows the radiator area requirements as a function of radiator temperature for 1250 watts dissiptation for an assumed thermal emissivity of 0.8. The curve shows that a 550 in^2 radiator will maintain a plate temperature of 250°C for the worst possible combination of parameters. If drive power were removed with all collector elements previously optimized for the case with saturated drive power, total CFA dissipation should not exceed 750 watts.

Overall CFA dimensions are 1.25 in. wide by 2 in. high by 9 in. long with a total volume of 22.5 $in.^3$ and weight of approximately 4 pounds.

Magnetic focusing can be obtained from a shielded permanent magnet assembly. Using Alnico 9 in the configuration shown in figure 32 one may estimate the size and weight of the overall package.

Area and length of magnetic material are related by:

$$A_m = F\ B_g\ A_g\ /\ B_m \text{ and } l_m = f\ B_g\ l_g /\ H_m,$$

where the subscripts g and m refer to gap and magnet respectively.

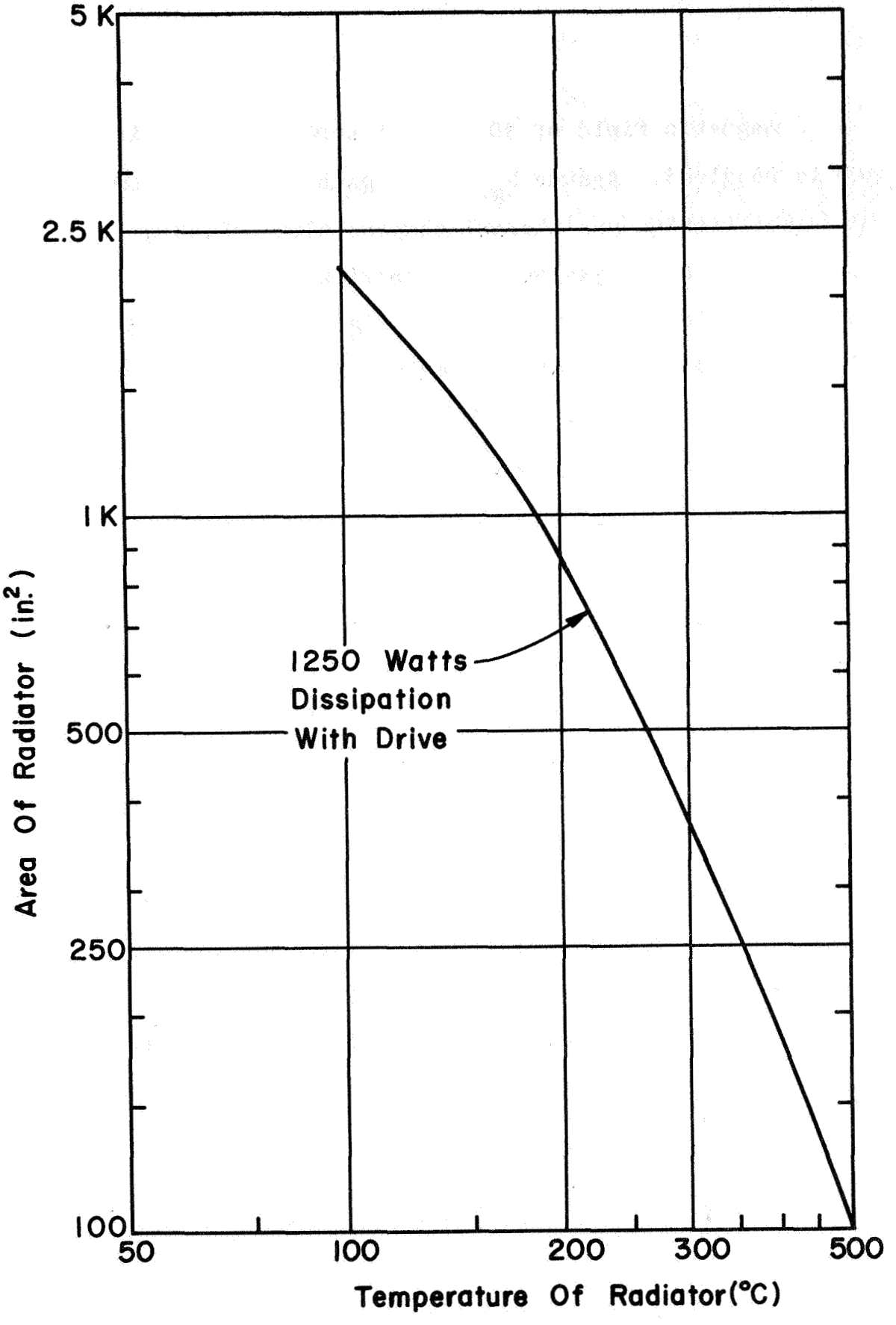

CFA Radiator Area Vs. Radiator Temperature

Fig. 31

A magnetic field of 3000 gauss across a 1.250 in gap is required. Assume B_g = 3300 gauss to allow for 10% stabilization and thermal compensation. Leakage factors for this geometry are approximately f = 1.2 and F = 5.0 for pole tips 0.8 in. high. B_m = 7700 gauss and H_m = 1300 oersted at the region of highest energy product for a normal Alnico 9 design.

Magnet cross sectional area is A_m = (5) (3300) (018)/7700 = 1.71 $in.^2$, or 1.71 in. height per inch of magnet length along the tube.

Total magnet length in the direction of magnetization is

$$l_m = (1.2)\ (3300)\ (1.25)/1300 = 3.8 \text{ in.}$$

With 1.9 in. of Alnico 9 and a pole tip 0.2 in. thick on each side of the CFA, the inside dimensions of the return path are approximately 5.5 in. x 3.8 in.

Armco iron 0.200 thick is adequate to prevent saturation in the shielded return path. The mean peripheral length around the return path is 2(5.7 + 4.0) = 19.4 in.

These requirements may be summarized as follows:

Component	Dimensions in.	Volume $in.^3$	Density $lb./in.^3$	Weight lb.
CFA	2x1.250x9	22.5	0.180	4.1
Magnet	1.71x3.8x9	58.4	0.263	15.3
Pole Tips	0.8x0.4x9	2.9	0.280	8.0
Return Path	0.2x19.4x9	34.8	0.280	9.8
				37.2
Fittings, waveguide, heat sink, etc.				9.0
Total weight, CFA and shielded package				46.2

Figure 32 also shows the type of adjustable magnet which has proven to be of great value in optimizing CFA efficiency during test. The magnet is held stationary with respect to the tube on one side, while the opposite magnet is segmented to allow for minor individual gap adjustment. Following optimization the adjustable segments are locked in place, the adjusting mechanism is removed, and a lightweight protective cover is installed.

3.7 NEW EFFICIENCY ENHANCEMENT CONCEPTS

Design J-3/93E discussed in the preceding sections is the result of optimizing a conventional CFA interaction region for highest efficiency consistent with other objective specifications. It should be emphasized that, with the exception of the multi-element collector and the new magnetic shielded guns, all design concepts have been verified in conventional crossed-field amplifiers.

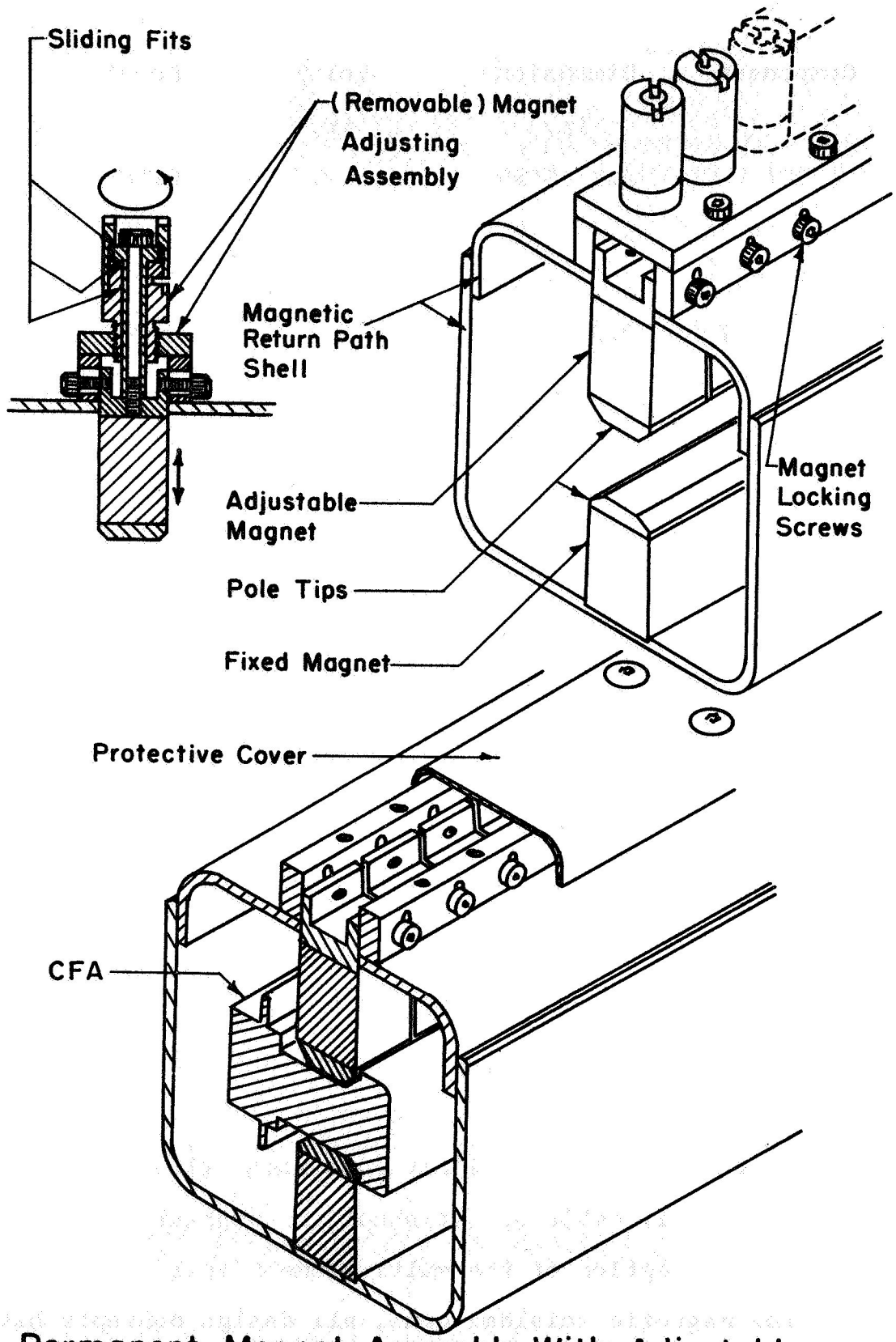

Permanent Magnet Assembly With Adjustable Pole Pieces.

Fig. 32

Design J-3/93E differs from that of most CFA's in that a new high impedance interaction circuit has been optimized for the narrow-bandwidth requirements of a spaceborne FM television transmitter.

This section outlines a number of new techniques; concepts which have not been verified in experimental devices. We studied several new methods which could result in a significant increase in the normally high efficiency of crossed-field interaction.

3.7.1 Phase Focusing

One factor which limits the efficiency of a conventional injected-beam crossed-field amplifier is the interaction of an out-of-phase group of electrons with the RF circuit wave. This interaction extracts energy from the slow-wave circuit and causes the unfavorably phased electrons to move toward the sole. This group of unfavorable electrons is generally referred to as the secondary bunch. If a crossed-field amplifier is made long enough the secondary bunch will move into a favorable phase and be collected on the slow-wave structure, thus converting potential energy into rf power. It would be most desirable to avoid the secondary bunch entirely.

We have investigated the technique of increasing efficiency by magnetic and/or electro-static focusing of the out-of-phase electrons. One method for preventing

the formation of the secondary bunch uses a varying dc magnetic and/or electric field in the sole-to-line region. Consider the higher order variation of magnetic field shown in figure 33. If we inject the beam into a uniform magnetic field, the interaction of the favorably phased electrons will not be affected since they move toward the slow-wave circuit through a uniform magnetic field. However, when the electrons of the secondary bunch begin to move toward the sole, they see an increasing magnetic field. Their average velocity along the tube will decrease, since

$$v_z \text{ (ave)} = \frac{E_x}{B_y} \qquad (3\text{-}14)$$

These unfavorably phased electrons will continue to be slowed with respect to the moving frame until they reach the favorable phase.

In order to check the qualitative arguments given above, the large-signal computer program was rewritten to allow the dc magnetic field variation shown in figure 33. The very encouraging results of using magnetic focusing for a typical crossed-field amplifier computer calculation are shown in figure 34 where a conventional broadband CFA design is compared, on the basis of power output vs. length, with the same design modified by various amounts of magnetic focusing. For a 10% increase in dc magnetic field from the

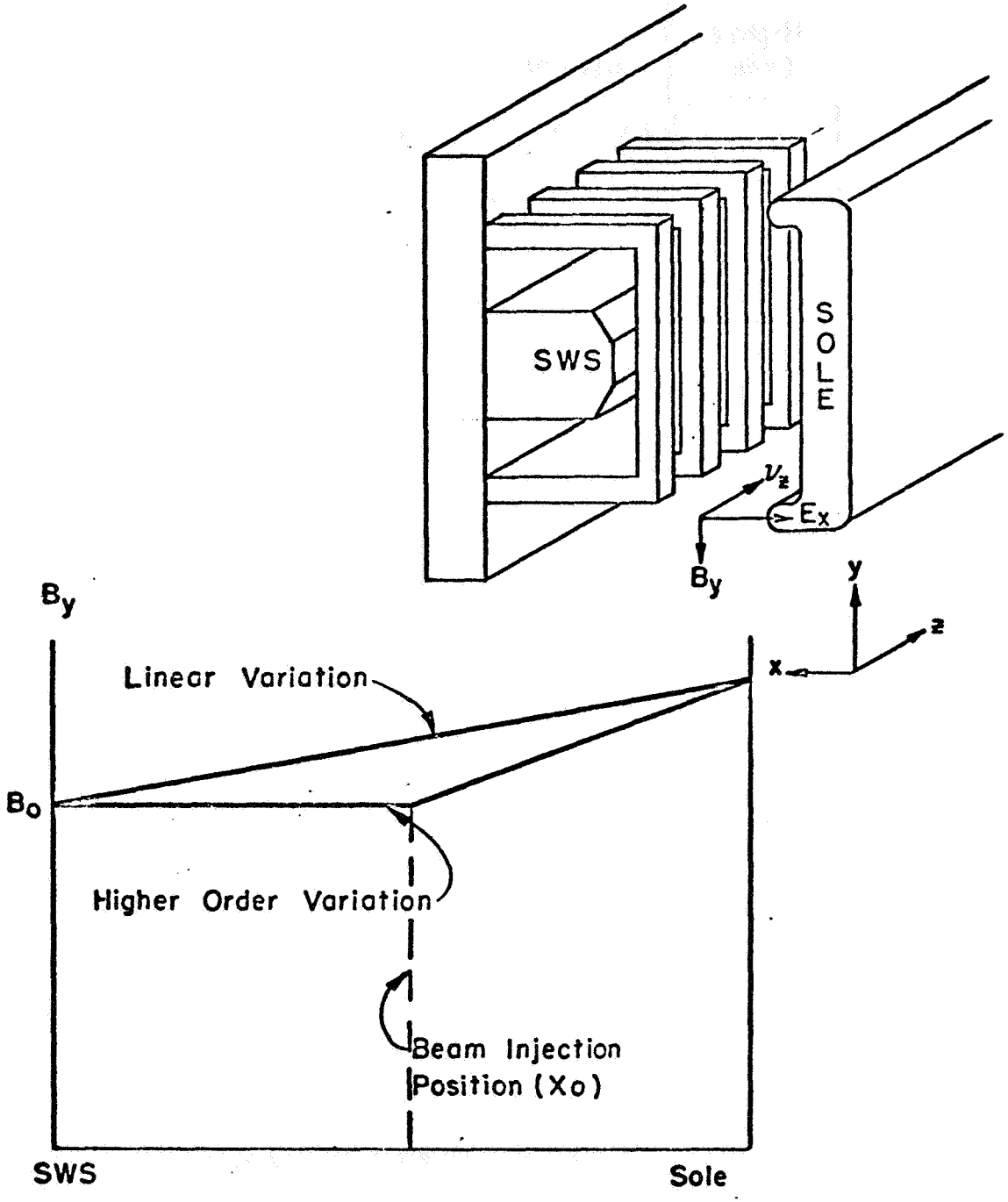

Magnetic Field In The Sole-Anode Region For Magnetic Focusing

Fig. 33

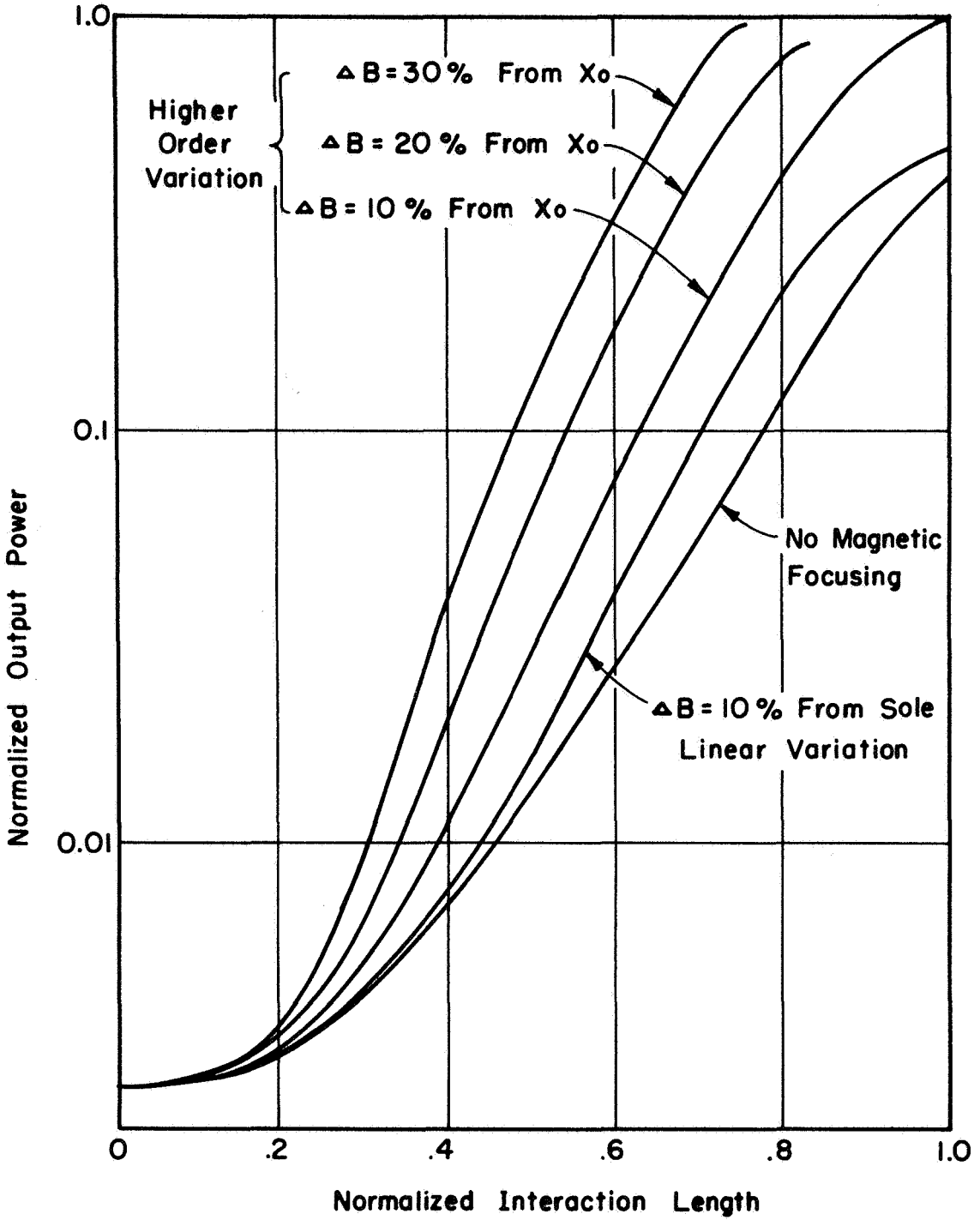

Comparison Of Output Power For Magnetic Focused And Conventional Crossed Field Amplifiers.

Fig.34

point of beam injection to the sole, the power output is 48% greater than for a conventional crossed-field amplifier of the same length. Even more impressive is the fact that without magnetic focusing, the conventional crossed-field amplifier saturates at a much lower value of output power even at a normalized length of 1.4.

Figure 35 shows a comparison of the bunching for conventional and magnetically-focused crossed-field amplifiers at various lengths along the slow-wave circuit. Each dot represents a rod of charge positioned in the moving frame ($v_z = E_x/B_y$). In the magnetically-focused case nearly all of the beam is collected at a normalized length of .875 and there is no secondary bunch, while in the conventional case there is still 29% of the beam in a secondary bunch at a normalized length of 1.4.

Conventional magnet geometries provide B_y (x) variations which are nearly linear when the interaction region is offset in the x direction with respect to the center of the pole pieces. Using B_y values which decreased linearly 10% from sole to SWS the total increase in interaction efficiency for design J-3/93E was only 10% and 1% at collection planes of 83% and 92% respectively.

The difficulty associated with obtaining higher order $B_y(x)$ variations, and the limitations of the present analyses become clear when the three-dimensional nature

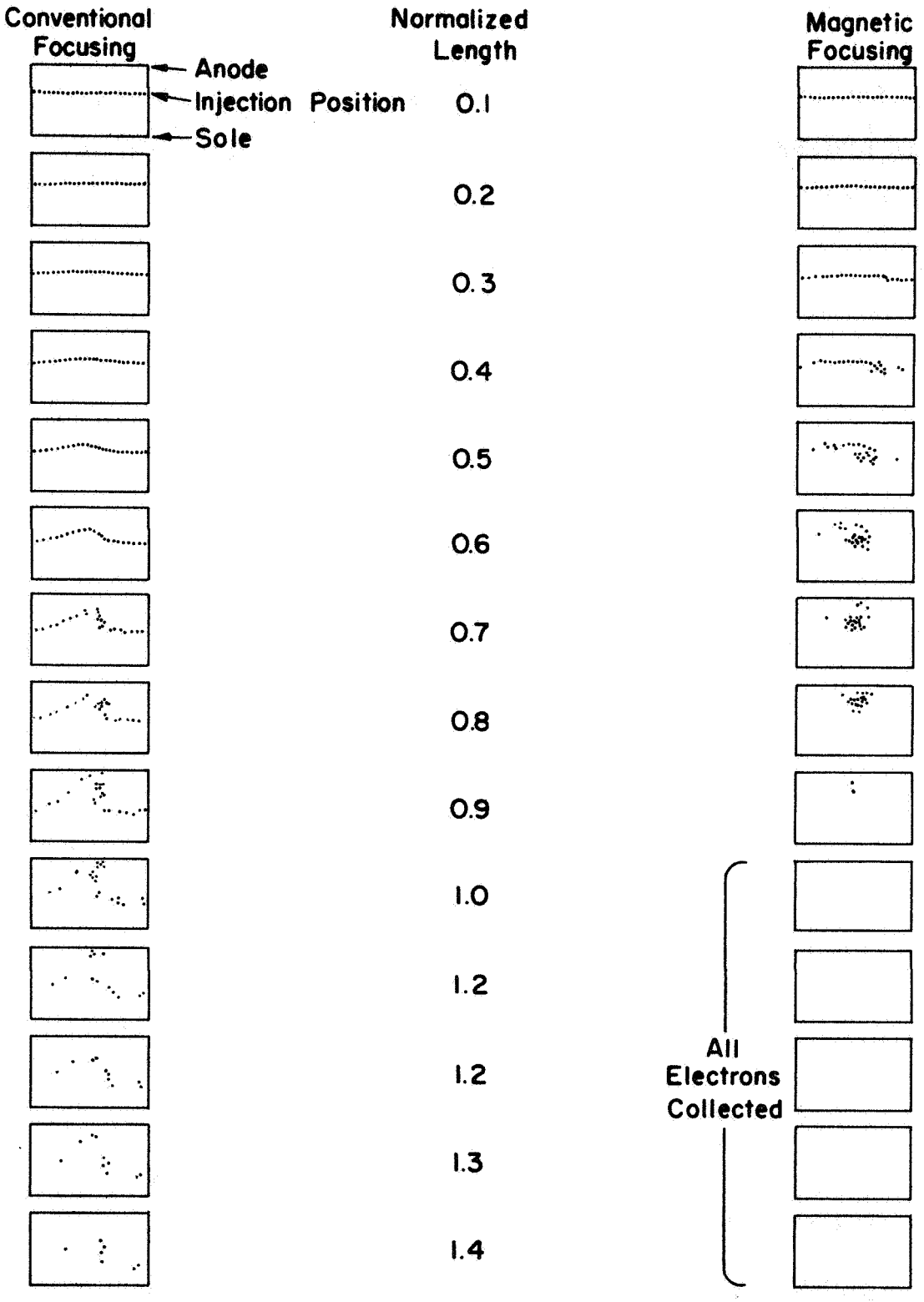

Comparison Of Conventional And Magnetic Focusing In A Crossed - Field Amplifier

Fig. 35

of the problem is considered. Although the concept of phase focusing is basically sound, the computer program neglects transverse variation of the magnetic field in the near sole region. Numbers which it predicted for efficiency are reasonable only for an electron beam which is narrow in the direction of magnetic field. It is impossible to obtain the correct magnetic profile for magnetic focusing without introducing some transverse variations in magnetic field. In order to get a variation in magnetic field in the sole-anode region greater than linear, the variation in the transverse direction has to be such that the magnetic force used to confine the beam in the transverse direction becomes negative, so that the beam tends to be forced out past the end hats. Electric confinement then could be used to confine the beam.

Experimental verification of a technique to obtain a magnetic focusing scheme without a transverse velocity gradient has not been established. The following analysis is given to indicate the problem involved.

The average velocity of the beam is given by:

$$\bar{v} = \frac{\bar{E} \times \bar{B}}{\bar{B} \cdot \bar{B}} \qquad (3\text{-}15)$$

In two dimensions (assuming no variation of E or B in the longitudinal direction), this equation is

$$v_z(x,y) = \frac{E_x B_y - E_y B_x}{B^2} \qquad (3\text{-}16)$$

Since the problem is a static one, E and B can be written as gradients of scalers

$$E = -\nabla\varphi \qquad (3\text{-}17)$$

$$B = -\nabla\Theta \qquad (3\text{-}18)$$

Thus,

$$v_z = \frac{\frac{\partial\varphi}{\partial x}\frac{\partial\Theta}{\partial y} - \frac{\partial\varphi}{\partial y}\frac{\partial\Theta}{\partial x}}{\left(\frac{\partial\Theta}{\partial x}\right)^2 + \left(\frac{\partial\Theta}{\partial y}\right)^2} \qquad (3\text{-}19)$$

Now also

$$\nabla^2 \varphi = 0 \qquad (3\text{-}20)$$

and

$$\nabla^2 \Theta = 0 \qquad (3\text{-}21)$$

Thus the problem is to solve Eqs. (3-20) and (3-21) with the boundary conditions that

$$S(x) = \frac{\frac{\partial\varphi}{\partial x}\frac{\partial\Theta}{\partial y} - \frac{\partial\varphi}{\partial y}\frac{\partial\Theta}{\partial x}}{\left(\frac{\partial\Theta}{\partial x}\right)^2 + \left(\frac{\partial\Theta}{\partial y}\right)^2} \qquad (3\text{-}22)$$

is a special function only of x (no transverse variation)

For many additionally imposed boundary conditions a solution to this does not exist. The overall solution and understanding of this velocity variation problem is the most important problem in crossed-field amplifier production today. In it are the roots of the instability problem; i.e., multi-velocity beams providing a path for feedback and thus decreasing the efficiency of the device.

The mathematical problem is as follows: given the above equations, find the shape of the equipotentials to give the desired variation. It is felt that even if this most ideal condition cannot be obtained, nevertheless the efficiency of the crossed-field traveling-wave tube should be significantly increased by the magnetic focusing scheme even if multivelocity components of the beam exist in the near sole region.

As previously discussed, the efficiency of the crossed-field amplifier should be improved if the magnetic field increases as the beam moves toward the sole. This not only slows the electrons down and moves them out of unfavorable phase, but also exerts a magnetic pressure which tends to push the electrons toward the anode. Computer calculations have indicated that a linear variation of magnetic field across the whole interaction space does little to enhance efficiency. An x^2 or more rapid vari-

ation, however, does markedly increase the calculated efficiency.

Ideally one would desire a constant value of transverse magnetic field between the circuit and the point of beam injection, x_o, and a rapidly increasing magnetic field between x_o and the sole. An additional requirement is zero variation in magnetic field in the direction of beam velocity. With these constraints a solution to Maxwell's equations requires a variation in magnetic field across the beam width. If this variation is too large a part of the beam will not be synchronous and will not interact efficiently with the circuit wave.

The problem may be approached analytically to determine the complexity required to obtain a second order variation in the transverse component of magnetic field.

Assume the desired variation at the center of the beam is

$$B_y = 1 + ax^2 = B_y\ (x,o) \qquad (3\text{-}23)$$

and

$$B_x = 0 = B_x\ (x,o) \qquad (3\text{-}24)$$

Then, using

$$\nabla \cdot \bar{B} = 0 \qquad (3\text{-}25)$$

and

$$\nabla \times \bar{B} = 0 \qquad (3\text{-}26)$$

we obtain in the x-y plane

$$\frac{\partial B_x}{\partial x} + \frac{\partial B_y}{\partial y} = 0 \qquad (3\text{-}27)$$

and

$$\frac{\partial B_y}{\partial x} - \frac{\partial B_x}{\partial y} = 0 \qquad (3\text{-}28)$$

Differentiating the desired variation given by equation (3-23), and using equation (3-25), we obtain

$$\frac{\partial B_y}{\partial x} = \frac{\partial B_x}{\partial y} = 2ax \qquad (3\text{-}29)$$

Integrating the second quality in the above equation and equation (3-27), we obtain

$$B_x = 2axy + f(x) \text{ and } B_y = -ay^2 + g(x) \qquad (3\text{-}30)$$

However we desire the variation

$$B_y = 1 + ax^2 = B_y\ (x,o) \qquad (3\text{-}31)$$

at y=0, and therefore

$$g(x) = 1 + ax^2 \qquad (3\text{-}32)$$

Thus,

$$B_y = 1 + ax^2 - ay^2 \qquad (3\text{-}33)$$

Since

$$B_x(x,o) = 0 \text{ from } (3\text{-}24)$$

then

$$B_x(x,o) = 2ax(o) + f(x) = 0, \quad f(x) = 0$$

and

$$B_x = 2axy \tag{3-34}$$

If we let Φ be the magnetic scalar potential, then

$$B_x = \frac{\partial \Phi}{\partial x} \tag{3-35}$$

and

$$B_y = \frac{\partial \Phi}{\partial y} \tag{3-36}$$

Integrating again, we obtain

$$\Phi = y \quad 1 + ax^2 - \frac{ay^2}{3} \tag{3-37}$$

By examining the above equation, we can find the shape of the pole pieces required to give the desired variation of magnetic field, since the edges of such pole pieces must be along equipotential surfaces.

It is observed that y=0 is an equipotential line, but this is the plane of symmetry. Also,

$$1 + ax^2 - \frac{ay^2}{3} = 0 \tag{3-38}$$

describes equipotential lines. The hyperbolas defined by this question are sketched in figure 36.

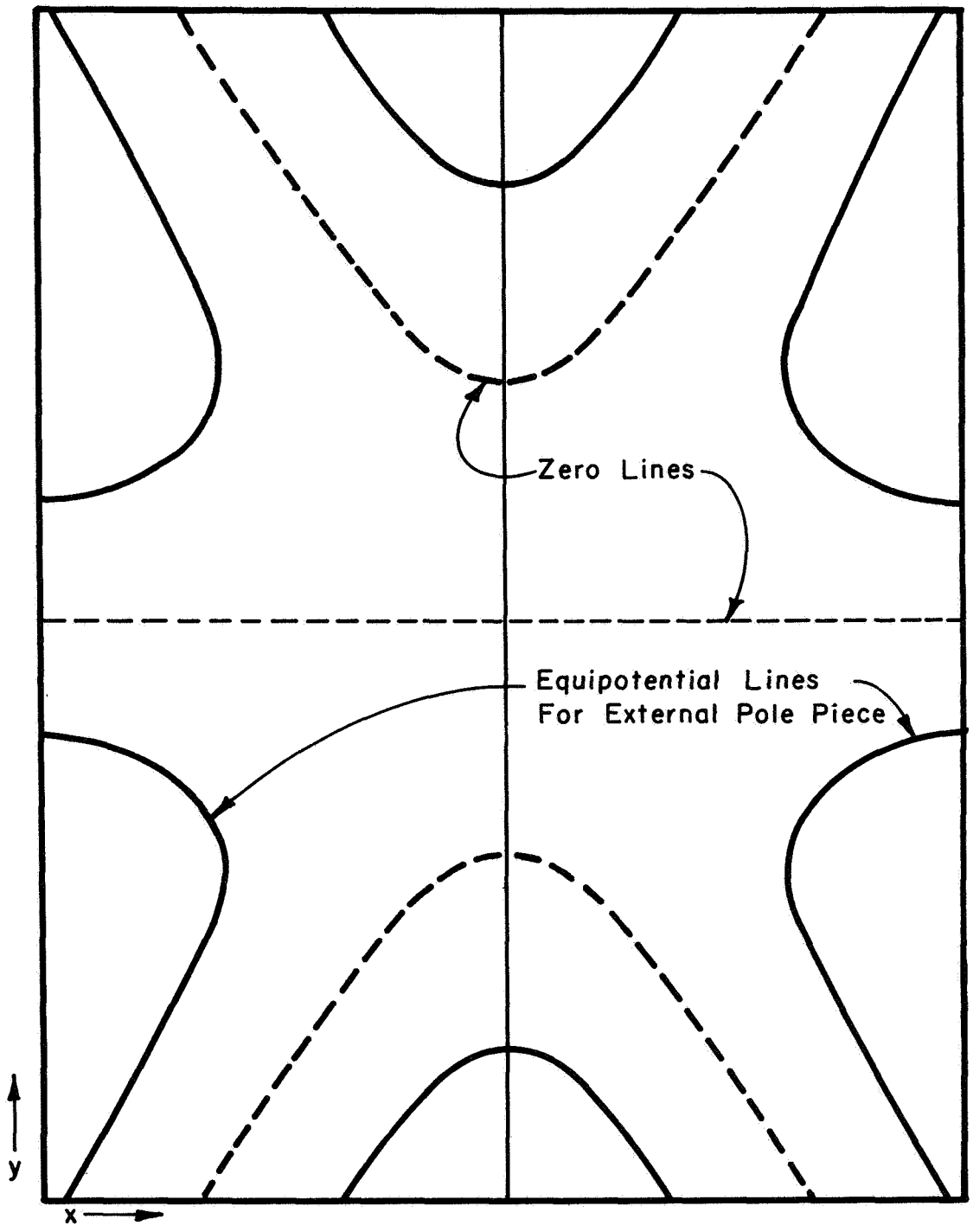

Zeros And Equipotentials For The Equation

$$\phi = y\left[1 + ax^2 - \left(\frac{y^2}{3}\right)\right]$$

Fig. 36

This analysis indicates that certain complex pole piece geometrics can provide higher order $B_y(x)$ variations. Similar variations can be obtained if magnetic pole pieces are placed inside the vacuum envelope directly under the sole electrode.

Additional three dimensional analyses are necessary to establish electric field variations which confine the electron beam with minimum velocity variation.

3.7.2 Line-on-Sole Structure

One factor which limits the electronic efficiency and the total efficiency of a crossed-field amplifier is the rapid fall-off of gain-per-unit-length as the beam is injected nearer to the sole. This is true because as one designs for a high electronic efficiency (small V_o/V_k, beam injected close to the sole), the longitudinal electric field approaches zero. One possible solution to this problem is a crossed-field amplifier with an electrically insulated rf circuit in the plane of the sole electrode. DC potential of the line-on-sole portion of the circuit could be approximately that of the sole electrode.

For this structure, the longitudinal electric field increases as the beam is injected closer to the sole. Such a crossed-field amplifier is shown schematically in figure 37. In order to determine the usefulness of the line-on sole structure, the adiabatic large-signal computer analysis was modified to include this case. Since the only difference

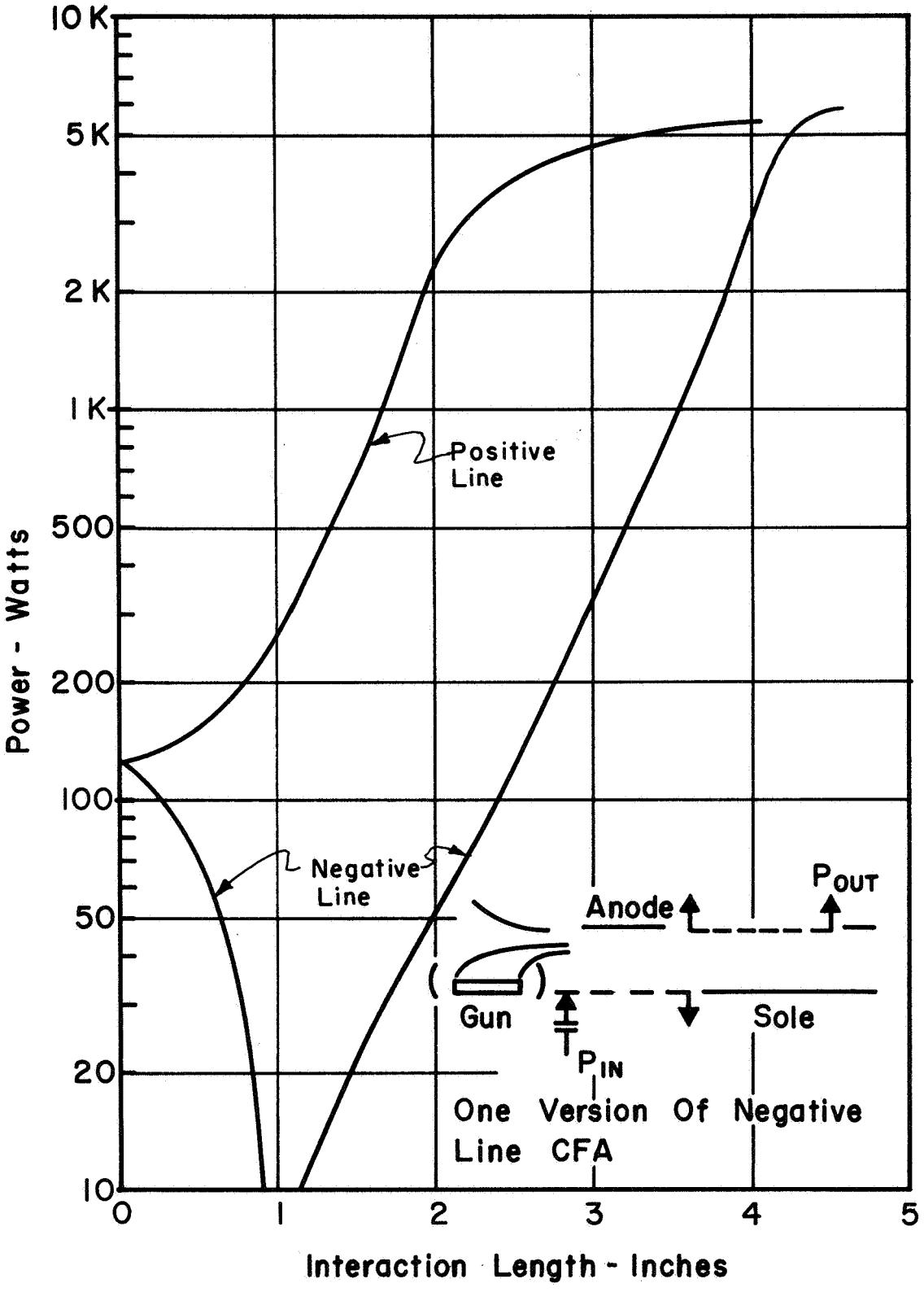

Comparison Of Negative Line And Conventional Positive Line Crossed Field Amplifiers.

Fig. 37

between the line-on-sole and conventional structure is in the nature of the rf electric fields, the program modification was relatively minor.

Whereas in the conventional interaction there is a bunching of electrons about the favorable phase (that phase about which the electrons give energy to the circuit) and a de-bunching about the unfavorable phase, in the line-on-sole structure the bunching is exactly opposite. This can best be understood by considering the fields of the line-on-sole structure shown schematically in figure 38. Consider an electron at z=0. Neglecting acceleration, the velocity of an electron (in a frame moving at E_{dc}/B_y) will be given approximately by

$$v_z = - \frac{E_x}{B_y} \qquad (3\text{-}39)$$

and

$$v_x = + \frac{E_z}{B_y} \qquad (3\text{-}40)$$

At z=0, as can be seen in figure 38, $E_x = 0$ and $E_z > 0$. Therefore, v_x is positive, as shown by the heavy arrow. Using this same procedure, one finds that the electrons tend to move in a manner perpendicular to the rf electric field and in the directions shown by the heavy arrows. Thus, one can see that the electrons will tend to bunch about the $\lambda/2$ and $-\lambda/2$, or unfavorable, po-

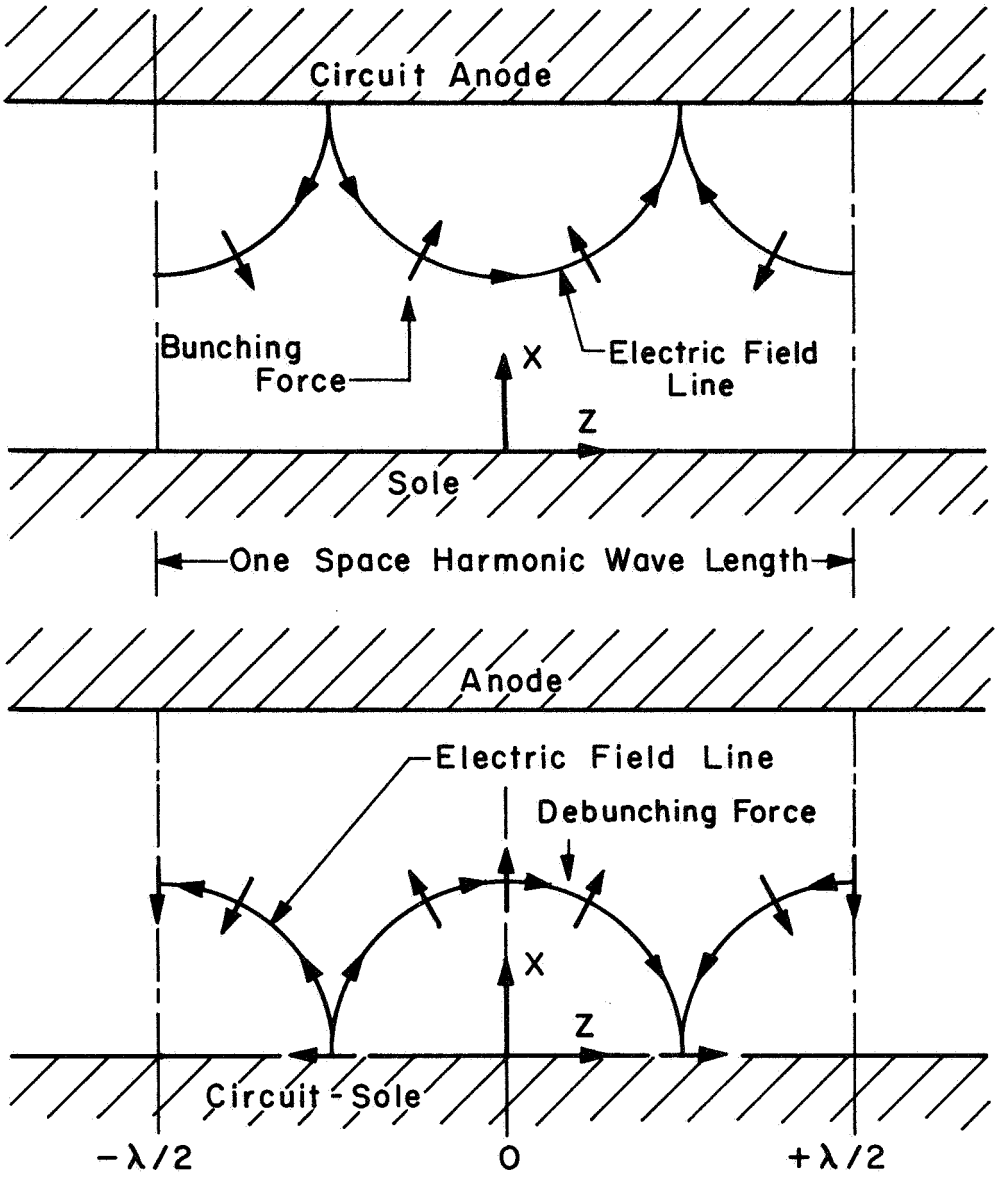

Schematic Drawing Comparing RF Fields And Bunching Forces Of The Line-On-Sole Structure And Conventional Structure.

Fig.38

sition and they will be debunched about the z=0, or unfavorable, position. This means that there will be a net loss of energy from the slow-wave circuit to the beam and a consequent decrease in power on the circuit as the beam moves further down the circuit. Therefore the line-on-sole structure cannot give gain; however, it does bunch the beam.

We have compared the interaction efficiency of a conventional circuit with that of a negative line (line-on-sole) structure using the adiabatic large signal interaction program PVL 6. Figure 37 shows that a slight increase in power can be obtained by coupling together two identical circuits. The negative line region for this case extends to a distance at which circuit power is equal to 1 watt.

Total circuit loss is lower for the negative line design since the gain per unit length is higher in the output section and the length of power saturation is less. The particular choice of input circuit, however, is not optimum. Since no beam interception occurs in this region the input circuit could have much higher impedance with a corresponding decrease in thermal capacity.

Another feature which could increase the gain rate in the output section is a change in potential between the negative line and the output sole electrode. If the

output sole were more negative than the input circuit, and the sole to output circuit gap larger to maintain a uniform dc electric field, the bunched beam could enter relatively close to the output circuit. Although the physical distance from beam to circuit does not change, the relative distance is less when the sole to circuit gap is larger. This results in higher interaction impedance.

Additional analytic and experimental effort should be directed toward optimizing CFA interaction using techniques outlined in this section.

4.0
CONCLUSIONS

The results of this analytical study program have shown that the performance of injected-beam crossed-field amplifiers can be significantly improved when new design features are included.

A high impedance type of interaction structure (a variation of the Karp circuit) was selected for a detailed analysis of the potential efficiency - bandwidth tradeoff. Experimental and analytic methods were employed to obtain a circuit with highest interaction impedance consistent with a 30 MHz instantaneous bandwidth, minimum transverse impedance variation and adequate thermal capability.

Multi-element depressed collectors were analyzed in conjunction with large-signal interaction computer studies. Recovery of nearly 80% of the beam energy existing at the end of a high efficiency interaction region was shown to be feasible. The optimum collector geometry is one which transforms kinetic-energy into potential energy, then recovers each electron at or near its potential level without emitting secondary electrons from the collection surfaces. The collector described in section 3.5 approached the ideal characteristics by geometric field shaping, adiabatic conversion of electron kinetic energy to potential energy

and potential sorting at the collector elements.

Computed efficiencies of greater than 80% were obtained for a thirty element collector coupled to a high efficiency interaction region.

Other less conventional techniques for optimizing interaction efficiency were studied. Negative line interaction and phase focusing by electrostatic and/or magnetic field shaping were shown to result in improved efficiency, and in certain cases, simpler collector design. These concepts require experimental verification before they can be incorporated into an orbital transmitter.

The conventional optimized design (J-3/93E, summarized in Table I) is compatible with other electrical and mechanical specifications for the proposed application. The design requires that the CFA baseplate temperature remain below 250°C. This can be accomplished with peripheral heat pipes connecting the base plate to suitable radiator panels on the external surface of the craft.

The objective operating life of greater than 20,000 hours is well within the predicted capability of the tungsten matrix cathode which is proposed for this device. Cathode temperature of 970° C is adequate for the required cathode loading of 1 ampere/cm^2, and the cathode life should exceed 60,000 hours.

5.0 RECOMMENDATIONS FOR VERIFYING EXPERIMENTS AND LONG TERM DEVELOPMENT

The design of a high efficiency injected beam crossed-field amplifier is discussed in detail in Section 3 of this report. Most of the design is conventional and within the present state of the art. Certain new design concepts, however, will require a thorough evaluation to verify feasibility before a prototype tube can be designed and developed. Design refinement and qualification should follow the prototype development phase.

5.1 VERIFICATION OF NEW DESIGN CONCEPTS

A twelve month series of vacuum experiments will be required to verify feasibility of several new design concepts. These experiments should include:

1. A study of collector efficiency, including suppression of secondary electron emission.
2. A study of beam generation and focusing with emphasis on uniform, low cathode loading and extended cathode life.
3. An extension of those novel concepts designed to enhance interaction efficiency (as discussed in Section 3.7).

5.1.1 Collector Efficiency

Vacuum experiments must be performed to evaluate any complicated collector geometry. In the preliminary design phase one must assume a value of secondary emission coefficient. Computed electron trajectories depend upon this assumed value to determine space charge and subsequent trajectories. In a vacuum environment it is highly unlikely that a uniform value of secondary electron yield will exist throughout a multi-element geometry. Hence the actual trajectories and the true collector efficiency may differ from calculated values.

The distribution of electron kinetic and potential energies at the end of an interaction region has been shown to be a complex function of many interaction parameters. Large signal computer studies were used to approximate the positions, velocities and energies of the recoverable portion of the electron beam throughout this study. However, certain limitations exist in any mathematical model. These approximations are discussed in Section 3.4 as they apply to rf beam interaction in the Litton large-signal interaction computer programs.

Experimental verification of collector efficiency should include a realistic electron beam which has experienced rf interaction over a prescribed length of slow-wave circuit. These experiments can be conducted

either in an existing CFA, modified for each test, or in a demountable vacuum test vehicle.

The demountable approach is generally considered superior to modification of an existing device when more than two or three iterations are anticipated. Furthermore, extensive monitoring of critical test parameters (pressure, temperature, potential, current, etc.) is feasible in a large vacuum enclosure although difficult in a compact amplifier.

5.1.2 Beam Generation and Focusing

Recent developments at Litton in 3-dimensional crossed-field electron guns indicate that significant design improvements are possible. Longer life can be expected from reliable Phillips cathodes if current density and cathode temperatures are reduced.

Injection guns presently used in military and commercial crossed-field devices are of the two dimensional variety. Magnetic-field is parallel to an emitting surface, and electron motion is perpendicular to the direction of magnetic field.

By allowing both electric and magnetic field variation along a beam it is possible to inject a low-noise, thin beam into a high efficiency interaction region. Computer studies have shown that cathode current density is quite uniform for certain three dimensional guns, while total cathode loading

can be reduced by a factor of five. The relationship between beam noise and device efficiency is not fully understood. Experimental verification of optimum gun design is considered necessary for maximum device efficiency.

As in the case of collector optimization, one must perform vacuum experiments to verify any computer design. Factors which are not included in a practical computer analysis include

1. lateral focusing
2. noise growth
3. thermal velocities
4. local temperature variations at cathode surface

A demountable vacuum system should also be used for electron gun optimization before committing any new type of gun to a particular design. Long term tests are advisable in separate vacuum enclosures (sealed-in bottles with internal or external magnets) since this avoids constant usage of extensive vacuum equipment. Cathode life tests should include conditions duplicating those which exist in an operating device rather than conventional diode experiments without magnetic field.

Electron gun characteristics should be evaluated by measuring and analyzing beam transmission, thickness and noise characteristics of each new iteration. Experimental

results should be compared with those obtained from analytic computer studies.

5.1.3 Enhancement of Interaction Efficiency

Several novel concepts of efficiency enhancement were studied during this program. Section 3.7 contains a complete discussion of those technique which should significantly improve device efficiency.

Phase focusing by electrostatic and/or magnetic field shaping has been shown to yield nearly twice the gain per unit length of an equivalent design without field shaping. This three-dimensional effect is not adequately described by existing mathematical models. However, the composite gun-collector model requires a demountable interaction circuit for complete analysis. It is logical to extend this vacuum model to include verifying experiments with phase focusing along the length of interaction.

Similarly, it is practical to experimentally verify efficiency enhancement due to prebunching. This requires only slight modification of the demountable circuit and sole electrode.

The tests and experiments outlines will provide verification of those design concepts which have not yet been evaluated in operating crossed-field devices. Use of demountable components in a bakeable vacuum system should result in rapid evaluation with great flexibility for subsequent iterations.

5.2 PROTOTYPE DEVELOPMENT PHASE

The preceding experiments are considered necessary to verify high efficiency concepts for an advanced design injected-beam crossed-field amplifier. The logical extension to these experiments is the development of a prototype amplifier with optimum parameters. These parameters should be determined by analyzing specific broadcast mission requirements as they relate to the design tradeoffs defined in the experimental phase.

The prototype development phase should include the design and demonstration of a suitable heat pipe configuration. These experiments could be performed independent of the transmitter development. However, the simulations would utilize dimensions and parameters determined by requirements of the CFA and other spacecraft components.

Operation of long-life cathodes should continue throughout this period. An accumulation of at least 30,000 hours of operation for each of six or more gun assemblies would be desirable.

The estimated time interval for prototype development is 24 months. During this period a total of approximately twelve tubes should be processed and evaluated.

5.3 DESIGN REFINEMENT AND QUALIFICATION PHASE

Approximately six tubes from the prototype devel-

opment phase should be available for modification and rework during this phase. Shock and vibration tests should be performed as part of the total environmental qualifications program.

Any design limitations evident during environmental testing should be eliminated, and a quantity of new tubes with optimum design features should be fabricated. From these tubes at least two space qualified crossed-field amplifiers should be available for specific mission requirements.

The design refinement and qualification phase should extend approximately 24 months. Life tests begun during the prototype development phase would be supplemented by final design tubes for qualification tests.

The total estimated time for these three phases is five years from initiation of the design concept verification phase.

6.0 SYMBOLS

A	cross sectional area of dielectric perturbation
A_m, A_g	cross sectional area of magnet and magnet gap
a	sole to circuit dimension (see figure 11)
B, B_o	transverse component of magnetic induction
B_m, B_g	magnetic induction in magnet and magnet gap
B_x, B_y	components of magnetic induction (see figure 31)
b	asynchronous parameter $(-1 + v_e/v_p)$
c	velocity of light in vacuum
C_B	capacitance per unit length between adjacent bars
C_H	capacitance per unit length between adjacent helix turns
d	distance from circuit to center of electron beam
d	dispersion
d_1, d_2	circuit dimensions (see figure 11)
D	gain parameter
e	electron charge
e/m	charge to mass ratio of electron
E	peak rf electric field
E_o, E_{dc}	static electric field in interaction region
F	helix dielectric loading factor
F, f	magnet leakage factors
f, f_o	operating frequency or resonant frequency
g	gap dimension between adjacent circuit conductors
h	width of electron beam in direction of transverse magnetic field
h	circuit dimension (see figure 6)

I_{acc}	accelerator current
I, I_b, I_B	total beam current
I_c	collector current
I_{cN}	current to Nth collector element
I_f	filament current
I_s	sole current
J	cathode current density
K_o, K	interaction impedance at plane of circuit
k	normalized radian frequency (ω/c)
k	general constant
L	interaction length
L_k	cathode length in direction of beam velocity (Kino units)
l	circuit dimension: helix peripheral length, bar half-length
l_1, l_2	circuit dimensions (see figure 11)
l_m, l_g	length of magnet and magnet gap
M	general product term
m,n	integer constants
p	circuit periodic length
P	rf power
P_{IN}	rf input power
P_{OUT}, P_o	rf output power
P_{diss}	circuit dissipation due to beam interception
q	gap between adjacent circuit conductors
S	space charge parameter
t	time

V_k	cathode to circuit potential
V_s	sole to circuit potential
V_{SK}, V_{SOLE}	sole to cathode potential
V_G	grid to cathode potential
V_{acc}	accelerator to cathode potential
V_o	kinetic energy voltage $(v^2/2\eta)$
v, v_e	average electron velocity
v_g	group velocity of rf wave
v_p	phase velocity of rf wave
v_x, v_y, v_z	coordinates of electron velocity (see figure 31)
W_s	stored energy per unit length
w_1,w_2,w_s	circuit dimensions (see figure 11)
x_o	beam injection position above sole electrode
Z_{dc}	beam impedance (V_o/I_b)
Z_i	interaction impedance at position of beam
Z_o	characteristic impedance
α	circuit attenuation per unit length
α_c, α_p	circuit attenuation per cell or periodic length
α_T	total circuit attenuation
β, β_o	phase shift per unit length (fundamental mode)
ϵ_o	permittivity of free space
ϵ_r	relative permittivity, dielectric constant
λ	wavelength

η	electron charge to mass ratio
η, η_o	overall efficiency
η_c	circuit efficiency
η_e	electronic efficiency
ω, ω_o	radian frequency
ω_c	cyclotron frequency (ηB_o)
μ_o	permeability of free space

7.0 REFERENCES

1. Okress, Ernest C.: Microwave Power Engineering, Volume 1. 1968.

2. Gould, R.S.: Space Charge Effects in Beam Type Magnetrons. J. Appl. Phy., Vol. 28, no. 5, May 1957, pp. 599-605.

3. Pierce, J.R.: Traveling Wave Tubes, D. Van Nostrand, Inc., 1950, pp. 168-181.

4. Fletcher, R.D.: A Broadband Interdigital Circuit for Use in Traveling Wave-Type Amplifiers. Proc. I.R.E., vol. 40, Aug. 1952, pp. 951-958.

5. Walling, J.C.: Interdigital and Other Slow Wave Structures. J. Elec. Control, vol. 3, no. 3, Sept. 1957, pp. 239-258.

6. Warnecke, R., et. al.: The Magnetron Type Traveling Wave Amplifier Tube. Proc. I.R.E., vol. 38, May 1950, pp. 486-495.

7. Wray, F.: An Experimental1KW CW Helix Traveling Wave Tube for C to X Band. Paper presented at 1965 Int. Elec. Dev. Meeting (Washington D.C.) Oct. 1965.

8. Orr, J.E.: Development of Compatible Family of Injected-Beam Crossed-Field Amplifier Tubes. IR-9-684L(III), 1968.

9. Bickford, N.K., et al.: Final Report on Design of an Octave Bandwidth High Power, S-Band Injected - Beam CFA. AFML-TR-66-314, Pt.II, April, 1967.

10. Karp, A: Traveling-Wave Tube Experiments at Millimeter Wavelength with a New Easily Built Space Harmonic Circuit. IRE,vol. 43, no. 1, January, 1955, pp. 41-46.

11. Karp, A.: Backward-Wave Oscillator Experiments at 100 to 200 Kilomegacycles. IRE, vol. 45, no. 4, April, 1957. pp. 496-503.

12. Feinstein, J. and Collier, R.J. : A Class of Waveguide-Coupled Slow-Wave Structures. IRE Transactions on Electron Devices, vol. ED-6,no. 1, January, 1959, pp. 9-17.

13. Millman, S.: A Spatial-Harmonic Traveling-Wave Amplifier for Six-Milliameters Wavelength. Proc. IRE, vol. 39, no. 9, September, 1951, pp. 1035-1043.

14. Froom, J.: Pearson, A.: Ash, E.A.: Ridge-Loaded Ladder Lines. Proc. I.E.E.E., vol. ED-12, July, 1965, pp. 411-421.

15. Pallakoff, O.E.: Electrostatic Focusing Study Program (VA 130). Varian Associates, Contract no. AF 33(615) 6590, July, 1961.

16. Pond, N.H.: Eggers, R.E.: X-Band High Power CW Amplifier and Amplifier Console. Microwave Electronics, Contract DA-38-039-AMC-03334 (E), August, 1967.

APPENDIX A

DESCRIPTION AND LISTING OF THREE COMPUTER PROGRAMS

The following pages list three digital computer programs which were written for solving particular problems associated with this study. Each program is written in a flexible version of Fortran 2 which is compatible with the General Electric 265 Mark I timeshare computer.

KARP CIRCUIT ANALYSIS

The Karp circuit, anti-Karp circuit and ridge-loaded stub-supported meander line were analyzed using the Fletcher[4] method by Froom, et al[14]. The curves of interaction impedance and dispersion were more comprehensive than any others in recent literature. Nevertheless only the special cases of uniform ridge loading and particular bar thicknesses were included.

KARPIE is a computer program which computes and tabulates circuit parameters over any particular region of phase shift for any combination of bar and loading ridge dimensions. Equations are based upon the analysis by Walling[5]. Walling's extension of the bar line analysis by Fletcher[4] predicts dispersion characteristics which agree well with experimental measurements for a wide range of geometric configurations. Predicted values of interaction impedance are generally higher than measured

values, primarily because the analysis neglects transverse field variations.

Input data include actual circuit dimensions as defined in figure 7. Program output is tabulated for increasing values of normalized phase shift from a minimum to a maximum specified value. Output variables are: symmetric mode frequencies (MHz) in the fundamental and second passband, normalized fundamental symmetric mode frequency (kl), equivalent velocity voltage (V_o in eV), fundamental mode interaction impedance at the circuit (K_o), delay ratio (c/v_p) and circuit match impedance (Z_o).

REDUCTION OF COLD TEST CIRCUIT DATA

Cold test determination of interaction circuit parameters involves measurement of particular frequencies and changes in frequency as a function of phase shift. Manual calculation of circuit parameters is quite time-consuming when many circuit variations are studied.

CTDATA is a short program which converts experimental data into useful quantities. The methods of obtaining data and determining interaction impedance are outlined in Appendix B.

Input data include circuit dimensions, the number of cells in the cold test structure, resonant fre-

quencies, dimensions of the particular dielectric perturbation element, its dielectric constant, and frequency shifts which resulted from the perturbations. The program output is a tabulation of the following quantities: normalized phase shift ($\beta p/\pi$), the corresponding frequency, normalized frequency (kl), interaction impedance at the circuit (K_o), the ratio of phase velocity to group velocity (v_p/v_g) and phase shift per unit length.

CALCULATION OF SMALL SIGNAL INTERACTION PARAMETERS

The computer program SSCFA is useful for examining a wide range of CFA design parameters. Certain quantities are held constant while others are treated as incremental variables. In addition, the program includes certain constraints which avoid computation of useless parametric combinations.

Input data include: frequency, dc input power, phase shift, circuit impedance and attenuation, beam width in the direction of magnetic field, and the range of each incremental variable. Output data are: cathode potential, magnetic field, beam velocity voltage, sole to circuit gap, circuit pitch, gain and space charge parameters, sole potential with respect to cathode, circuit length required for DN=0.5, circuit attenuation per unit length and interaction impedance at the position of the input beam.

```
100     REAL  KL, KL0S, KL1S, KL2S, KM1S, K0S, KN1A, KN1S, KN0VERZ
105     REAL L1,L2,K1S,K0A,KN0A,KN0S
107     COMMON L1,L2,AN,PHIN,P,PI,WB1,WB2,WS,PHI,M,A
109 NEW DATA: PRINT,!!"CPU SEC=",3600*TIME(-1); PRINT,!
110     READ, Q,P,D1,D2,WS,WB1,WB2,L1,L2, M,IPRINT
111 +   ,BPOVER PI MIN, BP OVER PI MAX, BP OVER PI INCR
120     PRINT 11, Q,P,D1,D2,L1,L2,WB1,WB2,WS,M,IPRINT
130 11: FORMAT("GAP = ",F6.1,3X,"PITCH = ",F6.1,3X,"D1 = ",F6.1,
132    +3X,"D2 = ",F6.1,/
133    +" L1 = ",F6.0,3X,"L2 = ",F6.0,3X,
134 +  "WB1 = ",F6.1,3X,"WB2 = ",F6.1,/ 1X,"WS = ",F6.1,3X,
136 +  "M = ",I2,6X,"PRINT INTERVAL =",I2//)
140 140:
150     Y10=Y20=PHI0=0.; I=-1
152     X0=0.
160     PI=3.14159; Q=Q*2.54E-5; P=P*2.54E-5; D1=D1*2.54E-5
162     D2=D2*2.54E-5; WS=WS*2.54E-5; WB1=WB1*2.54E-5;
164 +   WB2=WB2*2.54E-5; L1=L1*2.54E-5; L2=L2*2.54E-5
170     A=Q/P
175     EVK=2./1.76E11*(PI*P)!2
180     XT=BPOVERPIMAX; XI=BPOVERPIINCR
182     XB=BPOVERPIMIN
200     PRINT" BP/PI     FS(0)    FS(1)    KLS(0)    V0        ZIS(0)
201 +   C/VP  ZOS " ; PRINT,!
300     DO 91 X=XB,XT,XI
305     XN=X
320     PHI0=PHIN
330     PHIN=X*PI
335     PHI=PHIN
340     S1A=S(WB1) 'S1A IS S IN REGION---BAR END TO BACKWALL
360     S2A=S(WB2)'---BAR CENTER TO BACKWALL'
380     S12S =S(WS)'---TOTAL BAR TO SOLE
420     Y1N=((4*D1/Q)*SIN(PHI/2)!2+2*(1-A)*SIN(PHI/2)*(S1A+S12S))/376.7
440     Y2N=((4*D2/Q)*SIN(PHI/2)!2+2*(1-A)*SIN(PHI/2)*(S2A+S12S))/376.7
460     AN=Y1N/Y2N
470     XL=0.01; XH=0.98*PI/2/(L1+L2)
475     XHIGH=XH
480     CALL ROOTSYM(XL,XH,XKS)
490     K0S=XKS
500     F0S=(K0S*3$8)/(2*PI)
520     XL=XHIGH; XH=1.3*XL
540     V0=EVK*(F0S/PHI)!2+1.
560     COVP=3.E8/5.93E5/SQRT(V0)
580     CALL ROOTSYM(XL,XH,XKS)
590     K1S=XKS
600     F1S=(K1S*3E8)/2/PI
```

```
630 630:
640     I=I+1   'ASSUME DY/DPHI = 1 FOR FIRST STEP
660     IF(I) 12,12,22
680  12:  YY=1.
690     GOTO 13
720 22: YY=(Y1N-Y10)/(XN-X0) - (Y1N/Y2N)*(Y2N-Y20)/(XN-X0)
730 13: CONTINUE
740     N=0
750     Y10LD=Y10=Y1N; Y20LD=Y20=Y2N; X0LD=X0=XN
760     Z0S=SIN(K0S*L1)/(COS(K0S*L2)↑2*COS(K0S*L1)*YY+1E-8)
780     Z1S=SIN(K1S*L1)/(COS(K1S*L2)↑2*COS(K1S*L1)*YY+1E-8)
800     RADANG=PHIN/2 +N*PI
820     KNOVERZ=(SIN(PHIN/2)/RADANG↑2*SIN(A*RADANG)/A)↑2
840     Z1OS=Z0S*KNOVERZ 'FUND MODE INTERACTION IMPEDANCE AT SWS FACE'
860     Z11S=Z1S*KNOVERZ 'FIRST SPACE HARMONIC ZI'
920 91: PRINT 41, X,F0S*1E-6,F1S*1E-6,K0S*(L1+L2),V0,ABS(Z1OS),
925 +   COVP,ABS(Z0S)
940 41:FORMAT(F6.3,2I8,F8.2,I8)
950     GO TO NEW DATA
7000     SUBROUTINE ROOTSYM(XL,XH,XKS)
7020     REAL L1,L2,KS
7040     COMMON L1,L2,AN
7060     IX=0; EPS=.0001
7070     XHSTORE=XH
7080     VAL(KS)=SIN(KS*L1)/COS(KS*L1)*SIN(KS*L2)/COS(KS*L2) - AN
7100     GOTO CHK
7120 SHIFT: IX=IX+1
7140     XL=1.02*XHSTORE; XH=1.3*XL
7150     XHSTORE=XH
7160     IF(IX-5) CHK,NOROOT,NOROOT
7180..... IS THERE A SOLN BETWEEN XL AND XH////////???????????/
7200 CHK: IF(VAL(XL)*VAL(XH)) SKIP,SHIFT,SHIFT
7220 SKIP: ITN=0; XRANGE=ABS(XH-XL); XLSTORE=XL; XHSTORE=XH
7260 AGAIN: IF(ITN-4*0.434*LOG(XRANGE/EPS)) EVAL, EVAL, SHIFT
7280 EVAL: VAL1=VAL((XL+XH)/2); VAL2=VAL(XL); ITN=ITN+1
7320 COMPARE: IF(ABS(VAL1)-EPS) ROOT1,ROOT1,ROOT2
7340 CHKSIGN: IF(VAL1*VAL2) SIGNCHANGE, NOSIGNCHANGE,NOSIGNCHANGE
7360 SIGNCHANGE: XH=(XH+XL)/2
7380     GOTO AGAIN
7400 NOSIGNCHANGE: XL=(XL+XH)/2
7420     GOTO AGAIN
7440 ROOT1: XKS=(XL+XH)/2; RETURN
7460 ROOT2: IF(ABS(VAL2)-EPS) ROOT3, ROOT3, CHKSIGN
7480 ROOT3: XKS=XL; RETURN
7500 NOROOT: XKS=0
7520 RET: RETURN; END
7720 SKIP: ITN=0; XRANGE=ABS(XH-XL)
```

```
8000     FUNCTION S(W)
8004     REAL L1, L2
8005     COMMON L1,L2,AN,PHIN,P,PI,WB1,WB2,WS,PHI,M,A
8010     SM=0
8020     S=0
8030     M2=2*M
8040     DO 119 I=0,M2
8050     M1=I-M
8060     X1=(PHIN/2)+M1*PI
8070     X2=W*(PHIN+2*M1*PI)/P
8072     IF(ABS(X2)-170) OK,OK,BAD
8074 BAD: IF(X2) LOW,LOW,HIGH
8076 LOW: X2=-175.
8077     GOTO OK
8078 HIGH: X2=175.
8079 OK: CONTINUE
8080     COTHX=(EXP(X2)+EXP(-X2))/(EXP(X2)-EXP(-X2))
8090     SM=((-1)**M1)*COTHX*SIN((1-A)*X1)*SIN(A*X1)/(A*(1-A)*X1**2)
8100     S=S+SM
8110 119: CONTINUE
8120     RETURN; END
9900     $DATA
9910     47  94   62   62  132  50
9920     30  500  938
9930     2   1   .1   1.   .1
```

```
100  DIMENSION XKL(99),XKZERO(99),XN(99),F(99),DELTAF(99),DELAY
110 +RATIO(99),VPHASE(99),VGROUP(99),BETA(99)
120  REAL L1,L2
125 NEW DATA:
127  READ F2,
130  READ, NL,NH,XNCELLS,A,B,EPS,P,L1,L2
135  DO 1 I=NL,NH
136 1: XN(I)=I
140  READ, (F(I),I=NL,NH)
145 NEW DELTAF VALUES: READ, (DELTAF(I),I=NL,NH)
150  L1=L1*2.54E-5; L2=L2*2.54E-5; P=P*2.54E-5
155  A=A*2.54E-5; B=B*2.54E-5
160  PI=3.14159; DELTAEPS=EPS-1
170  DO ALL, I=NL,NH
175  DELTAF(I)=DELTAF(I)*1E6
178  F(I)=F(I)*1E6
180  BETA(I)=XN(I)/XNCELLS*PI/P
190  XKL(I)=2*PI*F(I)*(L1+L2)/3E8
200  DELAY RATIO(I)=3E8*BETA(I)/2/PI/F(I)
210  VPHASE(I)=3E8/DELAY RATIO(I)
212 ALL:
215  DO WHY, I=NL,NH
220  IF(I-NL) FIRST,FIRST,CHECK
230 CHECK: IF(I-NH) MID,LAST,LAST
240 MID: VGROUP(I)=2*PI*(F(I+1)-F(I-1))/(BETA(I+1)-BETA(I-1))
250  GOTO COMPUTE KZERO
260 FIRST: VGROUP(I)=2*PI*(F(I+1)-F(I))/(BETA(I+1)-BETA(I))
270  GOTO COMPUTE KZERO
280 LAST: VGROUP(I)=2*PI*(F(I)-F(I-1))/(BETA(I)-BETA(I-1))
285 COMPUTE KZERO:
292  XKZERO(I)=240*PI*DELTAF(I)*3E8*(2+DELTAEPS)/A/B/DELTAEPS/F(I)
293 +  /VGROUP(I)/(4+DELTAEPS)/(BETA(I)**2)
300 WHY:
315  PRINT F2,
320  PRINT,:"  BP/PI   MHZ     KL      OHMS   VP/VG   C/VP   BETA(R/M)"
321  PRINT,::
340  PRINT F1, (BETA(I)*P/PI,F(I)*1E-6,XKL(I),XKZERO(I),VPHASE(I)
342 +  /VGROUP(I),3E8/VPHASE(I),BETA(I), I=NL,NH)
350 F1: FORMAT (F6.3,I6,F7.2,I7,F7.2,F7.3,F9.1)
355 F2: FORMAT(72H
356 +                          )
380  GO TO NEW DATA
```

CTDATA LIST

```
90     REAL IK, KO, H, L
92     REAL LCATH,LKINO
94     J=1E4  'LIMIT CATHODE CURRENT DENSITY TO 1 A/CM↑2'
100 ND1:  READ, F,VKIK,VKL,VKH,VKI, BL,BH,BI, RL,RH,RI
110 ND2:  READ,BPOVPI,DBPERPITCH,H,KO
120 ND3:  READ, POS '(=XO/A) ALL INPUT PARAMETERS IN MKS UNITS'
125 ND4:
130    READ, ND
140    PRINT FA, F,VKIK,POS,BPOVPI,DBPERPITCH,KO,H/2.54E-2
150    PI=3.14159; COSH(X)=(EXP(X)+EXP(-X))/2; SINH(X)=(EXP(X)-EXP(-X)
151 +  )/2
152.
160    PRINT,↑"VK(KV) B(G)  VO(V) A(MILS) P(MILS)  DSS  VS(KV)
162    +L(IN) DB/IN    S    ZI"
180    DO LOOP, VK=VKL,VKH,VKI
190    PRINT FC, VK,VKIK/VK
200    DO LOOP, B=BL,BH,BI
201.    KINO RESTRICTION---IS CATHODE LESS THAN XN=10?
202    LCATH=VKIK/VK/H/J
206    IF(LCATH-LKINO) OK4,OK4,LOOP
208 OK4:
204    LKINO=J/8.85E-12/1.76E11↑2/B↑3
210    PRINT FD, B
220    DO LOOP, RATIO '=VK/VO' =RL,RH,RI
230    VO=VK/RATIO; VP=SQRT(2*1.76E11*VO)
240    BETA=2*PI*F/(SQRT(2*1.76E11*VO))  'RADIANS/METER'
250    P=BPOVPI*PI/BETA
260    DB PER INCH=DB PER PITCH/P*2.54E-2
270    IK=VKIK/VK; VS=(VK*POS-VO)/(1-POS)
275    A=(VS+VK)/B/VP
280    BETAA=BETA*A;  BETAX=BETAA*POS

300    D=SQRT(PI/2*F*IK*KO*SINH(2*BETAX)/1.76E11/B/VO)/SINH(BETAA)
310    S=IK/4/8.85E-12/1.76E11/B/H/VO/D
320    L=PI/BETA/D/2.54E-2  'L CORRESPONDING TO DN=0.5, IN INCHES'
325    ZI=KO/2*SINH(2*BETAX)/(SINH(BETAA))↑2
326    IF(((VS+VK)/A*2.54E-5)-500) OK1,OK1,LOOP
327 OK1: IF(L-20) OK2,OK2,LOOP
328 OK2: IF(S-4) OK3,OK3,LOOP
329 OK3: IF(KO/ZI -300)OK,OK,LOOP
330 OK:  PRINT FE, VO,A/2.54E-5,P/2.54E-5,D,VS,L,DBPERINCH,S,ZI
335 LOOP:
340    GOTO (ND1,ND2,ND3,ND4) ND
350 FA:  FORMAT("F=",-6PF6.0,"MHZ  PDC=",0PF6.0,"W  XO/A=",F4.3,
355 +     "  BP/PI=",F4.2,/
360 +     "ATTEN=",F6.3," DB/PITCH  KO=",I4," OHMS  H=",F6.3," IN")
370 FC:  FORMAT(/-3PF6.4,10X,"IK =",0PF6.3)
380 FD:  FORMAT(6X,4PF6.0)
400 FE:  FORMAT(11X,0PF6.0,F7.1,F8.1,F7.5,-3PF7.3,0PF6.2,F6.3,F6.3,
401 +            F5.1)
```

SSCFA* LIST

APPENDIX B

MEASUREMENT TECHNIQUES FOR INTERACTION CIRCUITS

Cold testing of interaction circuits involves the measurement of dispersion (ω-β diagram), interaction impedance, electric field distribution and circuit attenuation. Various techniques are known for these measurements, many of which are described in this Appendix.

A cold test circuit is generally made several times as long as the structure periodic length. If each end is shorted at a plane of symmetry, the structure becomes a resonant cavity. A swept frequency source and a fixed or movable detector probe will indicate resonant frequencies if rf energy is loosly coupled into the structure with a similar probe. Resonant frequencies correspond to lengths equal to an integral number of half-wavelengths calculated with the fundamental phase constant β_o.

The particular resonance number can be identified by any of several techniques. For this program we generally measured the distance between adjacent minima with a traveling detector probe, or perturbed the resonant frequency with a small moving dielectric bead attached to a strip chart recorder drive mechanism. As the traveling probe or perturbation detects adjacent minima separated by a distance x, the fundamental phase constant can be calculated from the relation

$$\beta_o = m\pi/(nx)$$

where n is the total number of periodic lengths (cells) in the circuit under test and m is a positive integer. These resonant frequencies with the corresponding values of phase shift can be plotted in various ways as an ω-β diagram or dispersion curve.

Interaction impedance at any frequency is determined by measuring the shift in resonant frequency due to a known perturbation. The ratio ($\Delta f/f$) is used in the following equation to obtain the interaction impedance at the circuit beam face for a thin dielectric slab as wide as the anticipated electron beam[15].

$$K_o = \frac{240}{\beta o^2} \frac{\Delta f}{f} \frac{c}{v_g} \frac{\pi}{A} \frac{2+\Delta\epsilon}{\Delta\epsilon(4+\Delta\epsilon)}$$

where

A = cross sectional area of dielectric perturbation

f = unperturbed resonant frequency

Δf= frequency shift due to perturbing dielectric

$\Delta\epsilon$= change in dielectric constant between perturbed and unperturbed conditions

c = velocity of light in vacuum

v_g= group velocity of unperturbed wave

β_o= fundamental phase constant

Appendix A includes a description and list of CTDATA, a

computer program which determines K_o, as well as other electrical parameters, at each measured frequency. Group velocity is normally estimated as the tangent to the ω-β curve at each frequency of interest; however CTDATA computes this quantity by linear interpolation from quantized input data.

Many interaction circuits, including the Karp structure, exhibit a transverse variation in K_o. Since normal impedance measurements are performed with a dielectric slab as wide as the anticipated electron beam, measured values of K_o are average values. In certain instances it is desirable to measure the transverse impedance variation. For these measurements a narrow dielectric slab or a small diameter dielectric rod is used as the perturbing element. Successive measurements at different locations across the circuit provide the information needed to plot K_o as a function of transverse dimension at a given frequency.

Circuit attenuation can be determined by simple substitution techniques or by measuring return loss of a shorted structure. The former method generally results in more repeatable results, particularly if the circuit under test contains twenty or more cells.

Electric field distribution and mode determination measurements can be rather involved, depending upon the problem under consideration. One type of measurement

which is often of interest is the determination of the type of propagating mode:

1. symmetric, with maximum electric field midway between the side walls, or
2. antisymmetric, with zero electric field in the center and two maxima, opposite in phase, each located between a side wall and center plane of the circuit.

For these measurements a dielectric perturbation or electric field probe-detector combination is moved across the circuit by a micrometer head (i.e., a depth micrometer with the spindle replaced by a low dielectric constant rod). Data are recorded as a function of micrometer position.

Another technique which requires accurate determination of distance is the measurement of field decay as a perturbing dielectric is moved away from the circuit. With a sole element spaced a distance 'a' from the circuit, the fundamental mode impedance should decrease as $\sinh 2\beta(a-x_o) / \sinh^2 \beta a$ where $(a-x_o)$ is the distance from the circuit to dielectric. Deviation from the theoretical relationship can indicate the relative magnitude of higher order field components.

DISTRIBUTION LIST FOR

FINAL REPORT
NAS3-11513

	No. of Copies
National Aeronautics and Space Administration Headquarters Washington, D. C. 20546	
Attention: SA/L. Jaffe	1
SAC/A.M.G. Andrus	10
National Aeronautics and Space Administration Lewis Research Center 21000 Brookpark Road Cleveland, Ohio 44135	
Attention: C. C. Conger, MS 54-1	1
R. E. Alexovich, MS 54-3	1
Dr. H. G. Kosmahl, MS 54-3	1
Technology Utilization Officer, MS 3-19	1
Spacecraft Technology Procurement Sec., MS 54-2	1
Library, MS 60-3	2
Report Control Office, MS 5-5	1
N. T. Musial, MS 501-3	1
Peter Ramins, MS 54-3	50
Communication Systems, Inc. 5817 Columbia Pike Falls Church, Virginia 22046	
Attention: J. Bisaga	1
Rand Corporation 1700 Main Street Santa Monica, California 90404	
Attention: Dr. J. Holt	1
National Aeronautics and Space Administration Electronics Research Center 575 Technology Square Cambridge, Massachusetts 02139	
Attention: E/Dr. L. Vanatta	1
EM/C. Veronda	1
Library	1

National Aeronautics and Space Administration
George C. Marshall Space Flight Center
Huntsville, Alabama 35812
Attention: RASTR-A/E. C. Hamilton 1
Library 1

National Aeronautics and Space Administration
Goddard Space Flight Center
Greenbelt, Maryland 20771
Attention: 733/R. Pickard 1
Library 1

National Aeronautics and Space Administration
Ames Research Center
Moffett Field, California 94035
Attention: 0ART-MA0/E. Van Vleck, MS 202-6 1
Library 1

National Aeronautics and Space Administration
Langley Station
Hampton, Virginia 23365
Attention: B. Kendall, MS 173 1
Library, MS 185 1

National Aeronautics and Space Administration
Manned Spacecraft Center
Houston, Texas 77001
Attention: Library 1

Jet Propulsion Laboratory
4800 Oak Grove Drive
Pasadena, California 91103
Attention: L. Derr 1
Library 1

National Aeronautics and Space Administration
Scientific and Technical Information Facility
P. O. Box 5700
Bethesda, Maryland
Attention: NASA Representative 3

Radio Corporation of America
Astro-Electronics Division
Princeton, New Jersey 08540
Attention: R. B. Marstin 1

TRW Systems
One Space Park
Redondo Beach, California 90278
Attention: W. A. Finley/Space Vehicle Division 1

General Dynamics
Convair Division
P. O. Box 1128
San Diego, California 92112
Attention: F. J. Dore/Advanced Programs 1

Hughes Aircraft Company
Space Systems Division
1194 West Jefferson Boulevard
Culver City, California 90230
Attention: H. A. Rosen/Satellite Systems Laboratory 1

General Electric Company
Missile and Space Division
Valley Forge Space Technology Center
P. O. Box 8555
Philadelphia, Pennsylvania 19101
Attention: H. Collins 1
P. Nadler 1

Federal Communications Commission
521 Twelfth Street
Washington, D. C. 20554
Attention: H. Fine 1

U.S. Information Agency
25 M Street S.W.
Washington, D. C. 20547
Attention: IBS/EF/G.Jacobs 1

General Electric Company
Tube Department
Microwave Tube Business Section
Schenectady, New York
Attention: R. Dehn 1

S-F-D Laboratories, Inc.
800 Rahway Avenue
Union, New Jersey 07083
Attention: Dr. G. Farney 1

Hughes Aircraft Company
Electron Dynamics Division
P. O. Box 2999
Torrence, California 90509
Attention: Dr. J. Mendel 1

Watkins Johnson Company
333 Hillview Avenue
Palo Alto, California 94304
Attention: Dr. D. Watkins 1

Varian Associates
611 Hansen Way
Palo Alto, California 94303
Attention: F. Melzer 1

Radio Corporation of America
Industrial Tube Division
Lancaster, Pennsylvania
Attention: W. P. Bennett 1

Radio Corporation of America
Electronic Components
New Holland Avenue
Lancaster, Pennsylvania 17604
Attention: Mr. F. S. Keith 1